MANCHESTER
1824
The University of Manchester

Optimal Coordination of District-Scale Multi-Energy Systems using Multi-Agent Control Architecture

A thesis submitted to the University of Manchester for the degree of
Doctor of Philosophy
in the Faculty of Science and Engineering

2022

Michael Taylor
Department of Electrical and Electronic Engineering

Contents

Word Count: 40,126

List of Figures

List of Tables

List of Publications

Research outputs which have been generated in relation to this thesis and which have either been published or submitted for publishing, are as follows:

M. Taylor, S. Long, O. Marjanovic, and A. Parisio, 'Model Predictive Control of Smart Districts with Fifth Generation Heating and Cooling Networks,' *IEEE Trans. Energy Convers.*, 2021.

M. Taylor, O. Marjanovic, and A. Parisio, 'Decentralised Predictive Control of Multi-Energy Resources in Buildings,' *Proceedings - IEEE 29th Mediterranean Conference on Control and Automation (MED)*, 2021, pp. 39–44.

Nomenclature

Abbreviations

4GDH	Fourth Generation District Heating
CO_2	Carbon Dioxide
H_2O	Water
AC	Alternating Current
ASHP	Air-Source Heat Pump
CHP	Combined Heat and Power Plant
CM	Classic Momentum Acceleration
COP	Coefficient of Performance
DC	Direct Current
EER	Energy Efficiency Ratio
HP	Heat Pump
LP	Linear Programming
MILP	Mixed-Integer Linear Programming
MINLP	Mixed-Integer Non-Linear Programming
MIP	Mixed-Integer Programming
MIQP	Mixed-Integer Quadratic Progrmming
MISOCP	Mixed-Integer Second Order Cone Programming
MLD	Mixed-Logical Dynamical Systems

MPC	Model Predictive Control
NAG	Nesterov's Accelerated Gradient
NLP	Non-Linear Programming
PV	Photovoltaic
QP	Quadratic Programming
RBC	Rule Based Control
SOCP	Second Order Cone Programming
TC	Thermal Collector
ULTDH	Ultra-Low-Temperature District Heating
ULTDHC	Ultra-Low-Temperature District Heating and Cooling
WSHP	Water-Source Heat Pump

Greek Letters

α	Dual Multiplier Update Step Length
β	Momentum Tuning Parameter
$\boldsymbol{\mu}$	Momentum Variable
$\boldsymbol{\rho}$	Contraction Vector
ΔH	Pressure Head Loss / Gain
Δt	Sampling Interval Length
δ	Discrete Auxiliary Variable
ℓ	Magnitude of Current Squared
η_i	Efficiency of Device i
γ_{ij}	Conversion Constant for Connection between Source i and Sink j
λ	Price Associated with a Variable or Variables
ν	Magnitude of Voltage Squared

σ	Binary Indication Vector
τ	Index Set of Sampling Intervals
$L_{\text{batt}},\ L_{\text{thm}}$	Storage Standby Loss Factor

Latin Letters

$\boldsymbol{C}_{\text{shift}}$	Circular Shift Matrix
$\hat{k}$	Current Sampling Instance
$\mathcal{A}^n$	Arcs in a Directed Graph of Energy Type n
$\mathcal{F}$	Set of Decision Variables
$\mathcal{G}^n$	Directed for Energy Type n
$\mathcal{N}$	Nodes in a Directed Graph of Type n
$\nabla \boldsymbol{g}$	Vector of Subgradients
A	Coefficient Matrix
$a_{\text{fsp,on}}$	Constant Standby Power for Fixed Speed Circulation Pump
b	Resource Vector
b_{fsp}	Power Coefficient for Fixed Speed Circulation Pump
C	Head Loss Coefficient
c	Cost Function
cH	Cold Side Nodal Pressure Head
D	Pipe Diameter
E	Nominal Energy Amount for Flexible Demand
f	Darcy Pipe Friction Factor
H	Prediction Horizon Length
h	Scheduling Instance Index
i, j, l, n	Indexes

I	Complex Current
J	Cost Objective
k	Sampling Instance Index
L_{pipe}	Pipe Length
m	Set of Aggregated Component Modules
$m_i,\ m_{ij}$	Mass Flow
N	Dimension of Vector or Matrix / Cardinality of a Set
P	Arc Power Flow
p	Nodal Power Flow
Q	Arc Reactive Power Flow
q	Nodal Reactive Power Flow
R	Line Resistance
r	Reference Value
T	Specified Number of Sampling Intervals
u	Control Variable
V	Complex Voltage
v	Generic Decision Variable
w	Disturbance Variable
wH	Warm Side Nodal Pressure Head
X	Line Reactance
x	State Variable
y	Output Variable
z	Continuous Auxiliary Variable

Physics Constants

ρ^{water}	Density of Water, $998\,\mathrm{kg\,m^{-3}}$
C_p^{water}	Specific Heat Capacity of Water, $4.18\,\mathrm{kJ\,kg^{-1}\,K^{-1}}$
g	Gravitational Acceleration, $9.81\,\mathrm{ms^{-2}}$

Symbols

$[\cdot]_+$	Projection onto Non-Negative Orthant
$\overline{v}$	Upper Limit of Variable v
$\underline{v}$	Lower Limit of Variable v
$\underset{\sim}{v}$	Preferred Lower Limit of Variable v
$\widetilde{v}$	Preferred Upper Limit of Variable v

Abstract

A major challenge in the transition to a net-zero energy system is how to decarbonise energy use for heating, cooling and transport via electrification, whilst simultaneously ensuring the security of a power system with high penetration of renewable energy generation. One possible way to address this challenge is to implement a multi-energy systems approach, in which traditionally separate energy systems for the delivery of electricity, gas, heating and cooling are co-optimised as an integrated whole. A major benefit of this approach is that flexible distributed energy resources in non-electrical systems can be exploited in support of the power grid.

This thesis presents a novel multi-energy system optimisation modelling framework, capable of quickly generating large-scale optimisation problems. These problems are readily integrated into model predictive control (MPC) schemes, providing a method for online energy management of a continuously evolving system. Such schemes can optimally manage distributed energy resources at district-scales, ensuring that all energy demands are met, networks are operated within acceptable limits and costs savings are delivered to both customers and network operators.

Given the potentially large size of the resulting control problem, a multi-agent control architecture and associated coordination algorithms are also presented. These ensure that near-optimal, feasible control actions can be determined within timescales that are suitable for online energy management. In an exemplary case study, considering a 15 minute sampling interval for a district comprising 84 buildings and multiple energy supply networks, a maximum computation time of around 55 minutes for a single controller is reduced to just over 1 second using the novel multi-agent MPC scheme, demonstrating the substantial benefit of the proposed approach.

Declaration of originality

I hereby confirm that no portion of the work referred to in the thesis has been submitted in support of an application for another degree or qualification of this or any other university or other institute of learning.

Copyright statement

i The author of this thesis (including any appendices and/or schedules to this thesis) owns certain copyright or related rights in it (the "Copyright") and s/he has given The University of Manchester certain rights to use such Copyright, including for administrative purposes.

ii Copies of this thesis, either in full or in extracts and whether in hard or electronic copy, may be made *only* in accordance with the Copyright, Designs and Patents Act 1988 (as amended) and regulations issued under it or, where appropriate, in accordance with licensing agreements which the University has from time to time. This page must form part of any such copies made.

iii The ownership of certain Copyright, patents, designs, trademarks and other intellectual property (the "Intellectual Property") and any reproductions of copyright works in the thesis, for example graphs and tables ("Reproductions"), which may be described in this thesis, may not be owned by the author and may be owned by third parties. Such Intellectual Property and Reproductions cannot and must not be made available for use without the prior written permission of the owner(s) of the relevant Intellectual Property and/or Reproductions.

iv Further information on the conditions under which disclosure, publication and commercialisation of this thesis, the Copyright and any Intellectual Property and/or Reproductions described in it may take place is available in the University IP Policy (see `http://documents.manchester.ac.uk/DocuInfo.aspx?DocID=24420`), in any relevant Thesis restriction declarations deposited in the University Library, The University Library's regulations (see `http://www.library.manchester.ac.uk/about/regulations/`) and in The University's policy on Presentation of Theses.

Acknowledgements

I would like to start by thanking my supervisors Dr Ognjen Marjanovic and Dr Alessandra Parisio for all their help and support throughout my PhD programme. Dr Ogi for guiding me through life as an academic, keeping me on track and giving up so much of his time to talk, whatever the subject matter, and Dr Alessandra for her attention to detail, generous feedback and for always challenging me to improve my work. A special thank you also to Seb Long for paving the way and helping me to understand his software, which was an invaluable starting point.

Next, I'd like thank my friends who have helped me along the way: Anita who faced the same problems and kept me sane; fellow CDTers Sam and Timna for the entertainment and support; Tom for inspiring me to do the PhD and for sharing his wisdom; Bally and Dicko, for still finding the time with newborns to look after; Sean and Adam for getting me through the lockdowns; and Kate for being an awesome friend, always a phone call away.

Finally, I'd like to thank all of my family, who showed an interest and kept me going. Paula, Cliff, Helena and Sam for their kindness and for unwittingly providing the writing retreats that were a massive help. My brother Paul, Nic, Elsie and Theo who could always remind me that there's more to life than work. My Nanna Doreen for being an inspiration. My mum and dad for their care, generosity, love, cheerleading and for always listening. Most of all I'd like to thank Hannah, for her boundless patience, understanding, encouragement and companionship - for always telling me I could do it.

Chapter 1

Introduction

1.1 Background and Motivation

1.1.1 The Transition to Net Zero

The Intergovernmental Panel on Climate Change continues to report changes in the Earth's climate that are unprecedented in thousands of years, many of which are irreversible over hundreds to thousands of years to come [1]. The rate of global warming is accelerating and, unless large-scale reductions in greenhouse gas emissions commence immediately, limiting warming close to 1.5°C or even 2°C will not be possible [2]. The consequences of increased warming to these levels include increased frequency and intensity of hot extremes, marine heatwaves, heavy precipitation and flooding, droughts, tropical cyclones and sea level rises. Mitigation against these consequences requires the reduction of cumulative CO_2 emissions in the coming decades, reaching at least net zero CO_2 [2].

It is against this backdrop that many governments around the world have committed to significant decarbonisation plans up to 2040 and beyond, aiming to fulfil their contributions to global emissions reductions as part of the Paris Agreement [3]. The drive for decarbonisation has already caused significant changes to national electricity supply systems and will continue to do so as the transition is made to net zero. In a scenario in which all governments' national decarbonisation policies are implemented by 2040, the following changes are also expected (see Fig. 1.1):

- the recent global expansion in gas based generation is set to slow down and generation from coal should finally start to decline by 2025 [4];
- renewable generation from wind and solar photovoltaics (PV) is anticipated to expand rapidly, with solar PV likely to become the dominant generation technology; and
- nuclear generation is also expected to significantly expand compared to the previous two decades.

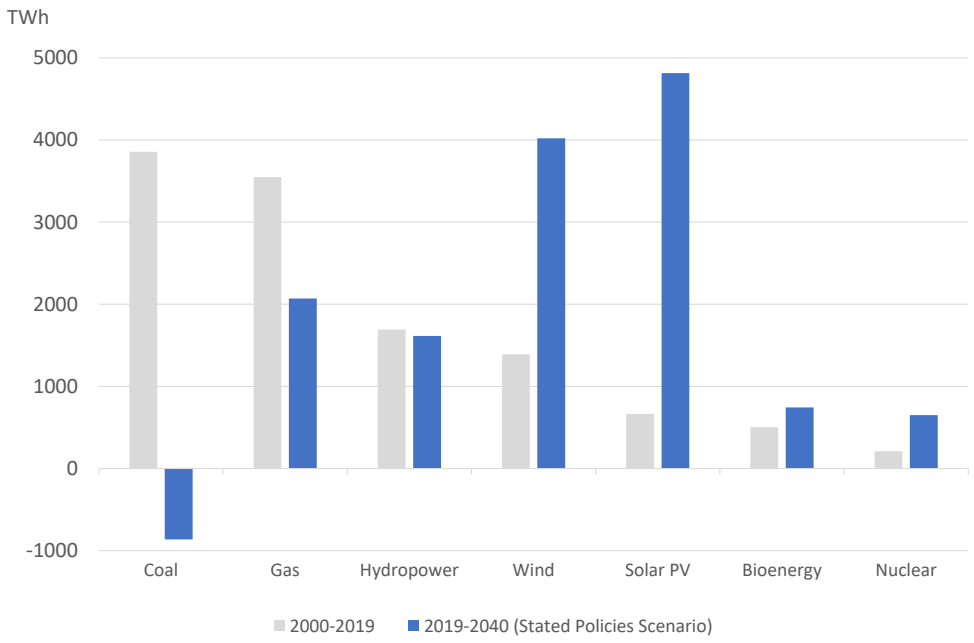

Figure 1.1: Change in global electricity generation by source in the IEA Stated Policies Scenario, 2000-2040 (Source: [4]).

The decarbonisation agenda will also have an impact on electricity demand, both in terms of the amount consumed and the pattern of consumption [5]. Transport and heating sectors, traditionally reliant on fossil fuels, contribute more than half of all greenhouse gas emissions in the UK and these have reduced far more slowly than those produced by the electricity sector [6]. Direct electrification of these sectors is a potential strategy for their decarbonisation; however, in addition to an overall increase in electricity consumption, this will also yield disproportionately higher demand peaks, based on current transport and heating patterns [5], [7]. Such changes could not be accommodated with the current UK power system infrastructure.

All of these changes will have far-reaching consequences in terms of energy security, the growth of power system ancillary service markets and the way in which energy systems are operated.

1.1.2 Power System Operation

Power systems must operate within strict ranges of frequency and voltage in order to maintain stability. In the UK, for example, the nominal frequency is equal to 50 Hz and variations within 1% of this value are permitted; on low voltage distribution networks the nominal voltage is 230 V with permitted variations of -6%/+10%. The challenge for power system operators is to deliver generation output that is equal to the instantaneous system load, whilst maintaining frequency and voltage within these ranges.

The system load is inherently uncertain and must be predicted ahead of time, based on historical trends and weather forecasts. Power generation capacity is then allocated to cover the base load, with additional *spinning reserve* capacity (generators operating below maximum output) allocated to cover peaks in the load. At any given time, the output from system generators is unlikely to exactly equal the load and this is reflected in the frequency. When output exceeds the load, generators spin faster, which increases the system frequency, and vice versa. Variation within the permitted frequency range is normal and often of little consequence; for small excursions below the lower limit, the headroom of spinning reserve can be used to restore the frequency to its nominal value. However, if the total capacity of generation (both scheduled and in reserve) is insufficient and frequency falls by more than around 1 Hz, loads may need to be continually disconnected until frequency is restored, a process known as load shedding, to avoid a full system blackout [8].

Traditionally, system operators have had limited control over the system load and would rely on the generation capacity of large, nuclear or fossil fuel driven synchronous generators (operating at nominal frequency) to balance the system. However, as coal and gas fired power plants are phased out as part of the transition to net zero, system operators will no longer have this large amount of controllable capacity at their disposal. Instead, the supply mix will become dominated by unscheduled wind and solar PV, greatly reducing supply side flexibility to match changes in demand; currently, intermittent renewable generation must be backed up by expensive

gas-fuelled spinning reserve to provide flexibility, known as renewable energy *firming* [9]. The loss of large synchronised generators also reduces system inertia, which is the effect of kinetic energy in the system resisting changes in frequency. Inertia provides vital time to respond in the event of a sudden loss of generation or a network fault.

Voltage stability is also impacted by greater penetration of generation from wind and solar PV, which are connected to the grid using power electronic inverters. These non-synchronous generators, whilst able to provide some voltage regulation, cannot do so over as wide a range as synchronous machines [10]. Therefore, when voltage rises or falls due to active and reactive power imbalances in the power system, there is limited capability to restore voltage to a stable operating point. In fact, the intermittency of distributed renewable generation, coupled with weak connections to the main grid via congested power lines, is a major cause of voltage instability in the first place [11].

1.1.3 Demand-Side Flexibility

To address the inflexibility of generation in a net zero scenario, power system operators and researchers are increasingly looking at how flexibility can be sourced from the demand side - through *demand-side response*. This refers to the various ways in which power consumption can be managed at the customer side of the meter, which can be broadly defined under three categories [12]:

- reduction of energy consumption through load curtailment;
- demand shifting between time periods; and
- use of onsite generation capacity to vary consumption from the main grid.

The various demand-side assets which can fulfil these criteria are known as *distributed energy resources*, comprising flexible loads, energy storage and distributed generation:

- Flexible loads capable of temporary interruption or adjustment can be used for load curtailment, e.g. building lighting or ventilation fans;

- temporal demand shifting can be provided by storage devices and shiftable or pliable loads, e.g. electric vehicle batteries, smart washing machines or heat pumps (HPs)
- small scale generators, e.g. combined heat and power plants (CHPs), by supplying power to local loads, can effectively reduce consumption from the main grid; and
- curtailment of distributed generation output would increase consumption from the main grid and this is a form of flexibility which is also available for small scale generators, e.g. wind and PV installations.

Demand response from transport, heating and cooling loads is especially important, not only because of their potential impact on power system utilisation, but also because of the energy storage opportunities associated with these sectors [9], [13]. Electric vehicles with smart charging or vehicle-to-grid capability [14], [15] could provide a vast reserve of fast-response electrical energy storage with which to accommodate large amounts of renewable generation. Similarly, buildings heated or cooled by electric HPs or air-conditioning units have inherent thermal storage capability due to their thermal inertia, meaning that these loads can be shifted in time without compromising building user comfort [16], [17]. Moreover, the advent of ultra-low-temperature district heating and cooling (ULTDHC) networks (see Section 2.2.4) provides the opportunity for large amounts of thermal energy storage to be leveraged for power system demand shifting [18]. These networks are operated through the use of electrically driven HPs and water circulation pumps, which means that the use of thermal energy storage capacity, e.g. from water tanks in buildings or larger centralised storage such as aquifers and borehole fields, has direct impacts on power system load [19].

1.1.4 Flexibility in Energy Markets

The value of flexibility from distributed energy resources is significant, both in terms of reduced capital investments in power system infrastructure and reduced operating costs. The potential cost saving due to decentralised flexibility in the Great Britain system has been estimated to be £3.8-8.1 billion/year in 2030, if target emissions of 50-100 gCO_2/kWh are to be reached by then [20]. More recently, flexibility

managed across heat, transport, industry and power sectors in Great Britain was estimated to potentially save £9.6-16.7 billion/year for a net zero scenario in 2050 [6]. However, the full benefits of flexibility from distributed energy resources are not currently recognised in European energy retail markets; most small customers are still presented with flat tariffs which do not reflect time-varying system operating conditions [5]. To unlock flexibility from whole-energy systems, customers with the capacity to provide demand response must be transformed from passive consumers into active *prosumers*. The use of dynamic rates in retail markets, which reflects the time-varying components of energy system operation costs, is one way to incentivise prosumers [21]; when exposed to hourly or sub-hourly pricing, flexible customers can shift their consumption from periods of high prices, normally occurring during demand peaks, to periods of lower prices and make significant savings on their electricity bills [5].

The use of dynamic pricing in energy retail markets is an indirect type of flexibility management, since prosumers may or may not respond to these price changes [21]. Explicit demand response, on the other hand, refers to the trading of flexibility services in wholesale markets, whereby commitments to provide consumption reductions are made to preserve the reliability of the power system [12]. The value and price of these services is expected to undergo significant growth in a system with large-scale integration of renewable generation [5]. However, small prosumers are currently prevented from participating in wholesale markets, owing to their size and, in the case of commercial or residential customers, also their time-varying ability to provide flexibility. This has led to the establishment of *aggregators*, commercial entities which act as mediators between the system operator and a portfolio of prosumers providing flexibility services [22]. By amassing a large and diverse portfolio of distributed energy resources, aggregators can provide demand response services with a higher level of certainty than is possible from individual prosumers.

Although aggregation does not need to take place over a specific geographical location, commercial aggregation at the district scale is beneficial and convenient for customers that are already physically aggregated by shared infrastructure, e.g. an electrical feeder or district heating and cooling network. Not only are the benefits of cumulative size and diversity of prosumers obtained within a district, coordination at this scale can also provide distribution of system management tasks [21]. As an example, if an aggregator detects a potential voltage instability event on the local

distribution network, it could unilaterally procure load reductions from prosumers, without necessarily having to involve the power system operator. In addition, an aggregator with knowledge of district power, gas, heating and cooling networks would be able to coordinate resources so that network performance and reliability objectives are satisfied individually, whilst also recognising operational constraints and the inherent interdependencies between these systems.

1.1.5 Coordination of Multi-Energy Districts

Optimisation of independent power systems enables operators to determine optimal set points of controllable generators, i.e. such that performance objectives are optimised, whilst satisfying operational, security and demand related constraints [23]. Generators each have an associated fixed cost and marginal cost per MWh of energy used in each scheduling period, hence optimisation involves minimising the power provided from more expensive generators. For power system operators, single period optimisation, known as optimal power flow, and multi-period scheduling, known as unit commitment, are routine computational tasks. However, implementation of global scheduling and control of an aggregated, multi-energy system district presents significant technical challenges [24]. Difficulties arise due to several factors:

- the large number of decision variables in the combined system;
- the non-linear equations used to describe the flow physics in multiple, interconnected energy networks; and
- the non-convex, mixed-integer modelling formulations commonly used to represent hybrid dynamical energy resources, e.g. battery storage systems or multimode energy conversion devices [25], [26].

The combination of these factors increases the likelihood that a global optimisation problem for on-line district management will be intractable, i.e. not solvable in the timescales required, particularly as the system size and scheduling horizon are increased [24].

An attractive method to address the high computational burden of complex optimisation problems is to decompose the global problem into smaller sub-problems which can be solved in parallel by multiple independent agents. In the context of district

coordination, the role of an independent agent could be fulfilled by an automated building energy management control system, which manages demand response at the individual building level [12], in communication with a district energy aggregator. For such methods to gain acceptance, the agents must exhibit guaranteed convergence to solutions which are feasible for the original global problem; these solutions would ideally be globally optimal too, although sub-optimality is generally accepted due to the challenges involved [24]. However, for non-convex mixed-integer formulations, convergence of decomposition approaches can prove difficult and even converged solutions may not actually be feasible [27]. Decentralised approaches to mixed-integer linear optimisation have recently been developed [27], [28], but they have not been applied to the problem of non-linear multi-energy system optimisation.

In light of the above issues and given the potential for huge cost savings, improved reliability and emissions reductions enabled by flexible multi-energy districts, the authors in [24] recently concluded that:

'*...it is critical to represent multi-energy system and network models as relevant optimisation and control tasks and uncover intrinsic convexity structures that lead to computationally efficient distributed solutions*'.

This critical need for improved modelling representations and efficient optimisation approaches, which can turn the ambitious vision of multi-energy districts into a practical reality, is the central motivation for this research.

1.2 Project Aim and Objectives

The research reported in this thesis is part of a project whose aim was to develop a modelling and control framework which would enable a commercial multi-energy district aggregator to manage energy flows from distributed energy resources, providing ancillary service brokering between prosumers and power system operators. The energy management control framework proposed in the thesis supports this aim by:

- being capable of on-line implementation, providing regular control actions which take into account sub-hourly retail price updates in the energy market;

- minimising customer costs whilst avoiding problematic demand response synchronisation;
- ensuring customer comfort levels and inflexible loads are not compromised by the provision of demand response;
- supporting energy system security by restricting operation to within acceptable limits; and
- maintaining privacy between different stakeholders through a decentralised implementation.

The following development objectives were initially identified to represent progressive milestones towards the final modelling and control tool that would satisfy the project aim:

1. Establish a general multi-energy system optimisation modelling framework and develop an object-oriented programming software implementation.
2. Adopt or develop computationally efficient models of relevant distributed energy resources.
3. Adopt or develop computationally efficient models of relevant energy transportation networks.
4. Adopt or develop a multi-agent control architecture for district energy system management.

The satisfaction of these objectives required the development of novel modelling formulations, optimisation algorithms and control schemes. These are described as contributions in the following section.

1.3 Contributions

In the course of this research, several contributions to the body of knowledge on multi-energy district modelling and coordination have been made. The contributions of this thesis are summarised as follows:

- The extension of existing multi-energy system mixed-integer linear programming (MILP) frameworks to a mixed-integer second-order cone programming (MISOCP) framework that can be readily integrated into model predictive control (MPC) schemes.
- Model development for key distributed energy resources which couple electricity and heat networks, namely reversible variable-speed water circulation pumps and reversible water-source heat pumps.
- The development of a bi-directional ULTDHC MISOCP model, which is convex after integer relaxation, ensuring efficient computation using mixed integer programming (MIP) solvers.
- The development of a multi-agent optimisation algorithm for MILP problems, using dual decomposition with constraint tightening and convergence acceleration using Nesterov's Accelerated Gradient method.
- A control scheme implementation of the multi-agent optimisation algorithm in which an aggregator coordinates distributed energy resources, described by MILP models, to maintain security in energy networks, described by MISOCP models.

It should be noted that the development of a computationally efficient ULTDHC model could also be applied in energy system design and planning applications where computational efficiency may also be of value. Similarly, the applications of the multi-agent optimisation algorithm extend beyond energy management control, indeed this method could be applied to any MILP problem of suitable structure.

1.4 Published Research

Research outputs from the project, which are described in Chapter 4, have also been published as a journal article:

[29] M. Taylor, S. Long, O. Marjanovic, and A. Parisio, 'Model Predictive Control of Smart Districts with Fifth Generation Heating and Cooling Networks,' *IEEE Trans. Energy Convers.*, 2021.

However, it should be noted that the method of generating model constraints used in Chapter 4 is different from that detailed in the published article. The modelling framework used in the article follows that of [30], which was initially adopted for use in the project. After publication, a decision was subsequently taken to adopt and develop a different modelling framework, that of [26], owing to the following drawbacks of [30]:

- the approach of defining particular node types with connecting arcs, to generalise modelling of energy conversion devices, was not intuitive;
- the generality of the framework did not extend to modelling water circulation pumps and required modification to accommodate these devices;
- another node type had to be introduced to model all incoming and outgoing flows of thermodynamic cycle devices; and
- device operational constraints, such as minimum up and downtime constraints, could not be readily accommodated in the original framework.

By contrast, the modelling framework of [26], based on the established Mixed-Logical Dynamical (MLD) framework [31] (see Chapter 3), is both intuitive and can readily incorporate the above elements within the original generalised description, without modification. These reasons of clarity and greater generalisation motivated the decision to switch methods during the project, as well as the decision to only describe the framework of [26] in this thesis. However, whilst the methods of generating constraints differ between the published article and Chapter 4, the actual constraints passed to the optimisation solver were the same in each case (after simplification) and therefore the results are also the same.

Some preliminary results of Chapter 6 have also been published in conference proceedings:

[32] M. Taylor, O. Marjanovic, and A. Parisio, 'Decentralised Predictive Control of Multi-Energy Resources in Buildings,' *Proceedings - IEEE 29th Mediterranean Conference on Control and Automation (MED)*, 2021, pp. 39–44.

To the authors' knowledge, the research presented at the conference was the first implementation of a decentralised iterative solution algorithm for multi-agent MILP

problems from [27] within an MPC scheme (see Algorithm 8 of Chapter 6). However, as elaborated in Chapter 6, conditions were subsequently found for which the algorithm in [27] encountered convergence issues, making it unattractive for a MPC scheme in certain cases. Hence, novel algorithms are described in Chapter 6 which address these issues and are therefore suitable for MPC.

Finally, a journal article is in preparation which presents the combined outcomes of Chapters 5, 6 and 7:

[33] M. Taylor, O. Marjanovic, and A. Parisio, 'Decentralised Supervisory Control of Networked Multi-Energy Buildings,' *Manuscript in preparation*, 2023.

1.5 Thesis Outline

The remainder of the thesis consists of the following topics by chapter:

- A literature review covering multi-energy system modelling concepts, energy coordination methods and techniques to address computational efficiency in district-scale optimisation problems (Chapter 2).
- An introduction to the optimisation modelling methodology used, documenting any existing models adopted from the literature and proposed models developed for this work (Chapter 3).
- Application to buildings in a small multi-energy district, without detailed network energy flow modelling, examining the performance of MPC versus a rule-based control scheme to optimally integrate electricity, gas and ULTDHC systems (Chapter 4).
- Assessment of centralised MPC performance for a large multi-energy district, considering detailed electricity and ULTDHC energy-flow models (Chapter 5).
- Development and implementation of a multi-agent optimisation algorithm within an MPC scheme, with application to control a large number of buildings in a district, without detailed energy-flow modelling (Chapter 6).
- Implementation of the multi-agent optimisation algorithm within an MPC scheme capable of managing a district whilst considering detailed electricity and ULTDHC energy-flow models (Chapter 7).

- Final conclusions and discussion of several research challenges, highlighted by this work, which could be addressed in future (Chapter 8).

Chapter 2

Literature Review

This chapter begins with a brief introduction in Section 2.1, discussing the two main types of multi-energy system coordination which are encountered in the literature. Following this, various modelling frameworks for multi-energy system optimisation are discussed in Section 2.2, together with an introduction to Ultra-Low-Temperature District Heating Networks, which cannot be modelled with sufficient accuracy using the available frameworks. Finally, examples of multi-energy system coordination from the literature are reviewed in Section 2.3.

2.1 Introduction

As mentioned in Chapter 1, coordination of multi-energy systems involves the prioritisation of some performance objective(s) whilst satisfying operational, security and demand related constraints. This may be achieved through operational planning ahead of time, e.g. days or hours ahead, or through online control, which regularly imposes actions at intervals in the order of minutes or seconds. There are clear advantages to each approach and they are often used in unison: operational planning facilitates participation in day-ahead markets and can be used for more complex problems, since the time taken to reach a solution is less critical; whereas online control offers the opportunity to address deviations from imperfect forecasts that are used when planning, such as price or demand forecasts.

This literature review explores various approaches to energy system management in relation to operational planning and online control, for which the trade-off between

model accuracy and computation time must be managed differently. The scope is limited to multi-energy system applications, except in circumstances where background knowledge from another relevant topic is required. The definition of a multi-energy system that was used to guide the literature search is taken from [13], in which the concept of *multi-energy* refers to:

'*considering a whole-system approach to optimisation and evaluation of the specific case under study (for instance, a building or a country). In particular, the analysis approach refers to explicitly expanding the system boundary beyond one specific sector of interest (for instance, beyond electricity only or beyond heat only, as typical study cases).*'

In addition, works concerned with optimal infrastructure planning in multi-energy systems are not within the scope of this review, only strategies and modelling approaches that are concerned with optimal system operation.

Most multi-energy management schemes proposed in the literature involve solving a mathematical optimisation problem at some point. The following sections assume an understanding of mixed-integer mathematical programming problems, problem structure, convexity and the implications for optimisation solvers. For the unfamiliar reader, some basic concepts and terminology frequently used in relation to mathematical optimisation are provided in Appendix A.

2.2 Multi-Energy System Modelling

For optimisation problems in multi-energy system management, equality and inequality constraints are used to describe the physical or operational limits of undetermined system variables, as well as the physical relationships between them; the constraints provide a representative mathematical model of the system. A convenient level of detail at which to model resources in large, complex energy systems is to focus on steady-state energy flows. These are the quantities for which there may be limited capacity at various points within a system and which strongly correlate to overall operating costs, since commodities such as electricity and gas are priced per unit of energy. Models therefore typically describe the production, consumption, conversion, storage and loss of energy during operation. However, these processes in real, dynamic systems are inherently non-linear and often involve discrete states of operation, i.e, they are *hybrid dynamical* systems. Therefore, the main challenge for

multi-energy system modelling is to formulate constraints that represent real systems relatively accurately, whilst also ensuring that the problem can be solved efficiently and remain tractable.

2.2.1 Mixed Logical Dynamical Systems

In the majority of articles reviewed, mixed-integer linear programming (MILP) was used to model and optimise the energy system of interest [25], [26], [30], [34]–[49]. This stems from the fact that non-linear and hybrid system behaviour can be approximated by transforming logical statements into mixed-integer linear equality and inequality constraints. For prediction of hybrid dynamical systems, this method has been formalised using a compact representation known as the mixed-logical dynamical (MLD) approach [31]. This method introduces additional continuous and discrete auxiliary variables, $\boldsymbol{z}$ and $\boldsymbol{\delta}$, to the well-known discrete state-space representation of a system:

$$\boldsymbol{x}_{k+1} = \boldsymbol{A}\boldsymbol{x}_k + \boldsymbol{B}_u\boldsymbol{u}_k + \boldsymbol{B}_d\boldsymbol{\delta}_k + \boldsymbol{B}_z\boldsymbol{z}_k \tag{2.1}$$

$$\boldsymbol{y}_k = \boldsymbol{C}\boldsymbol{x}_k + \boldsymbol{D}_u\boldsymbol{u}_k + \boldsymbol{D}_d\boldsymbol{\delta}_k + \boldsymbol{D}_z\boldsymbol{z}_k \tag{2.2}$$

$$\boldsymbol{E}_d\boldsymbol{\delta}_k + \boldsymbol{E}_z\boldsymbol{z}_k \leq \boldsymbol{E}_u\boldsymbol{u}_k + \boldsymbol{E}_x\boldsymbol{x}_k + \boldsymbol{E} \tag{2.3}$$

However, the casting of logical constraints into inequalities in (2.3) can be non-intuitive and this can hinder the generation of MLD models [26]. One option is to use HYSDEL parser software [50], yet the reliance on another layer of software with rigid functionality is restrictive when designing an energy management scheme. This highlights another challenge in multi-energy system modelling - the development of frameworks which enable rapid generation of the required optimisation constraints for potentially large systems.

2.2.2 Energy Hub Framework

The *energy hub* framework [51], [52] was intended to address the issue of optimisation model constraint generation, providing a matrix-based formulation to model co-located energy conversion devices within a 'hub', which could be a building, a building complex or even a district [52]. In this framework, static input-output models are used to represent any number of connected conversion devices within a hub,

using conversion coefficients, $c_{\alpha\beta}$, to describe energy flow between a hub input, P_{β}^{in} of energy type β, and a hub output, P_{α}^{out} of energy type α. The matrix formulation for an energy hub is given as follows:

$$\begin{bmatrix} P_{\alpha}^{out} \\ P_{\beta}^{out} \\ \vdots \\ P_{\omega}^{out} \end{bmatrix} = \begin{bmatrix} c_{\alpha\alpha} & c_{\alpha\beta} & \dots & c_{\alpha\omega} \\ c_{\beta\alpha} & c_{\beta\beta} & \dots & c_{\beta\omega} \\ \vdots & \vdots & \ddots & \vdots \\ c_{\omega\alpha} & c_{\omega\beta} & \dots & c_{\omega\omega} \end{bmatrix} \begin{bmatrix} P_{\alpha}^{in} \\ P_{\beta}^{in} \\ \vdots \\ P_{\omega}^{in} \end{bmatrix} \tag{2.4}$$

The fact that this approach is straightforward to formulate, easily scalable and can represent many hub topologies has made it popular amongst researchers, e.g. [34], [53]–[56], and the term 'energy hub' has become synonymous with multi-energy systems. However, there are well documented drawbacks to this approach:

- The use of 'dispatch factors' to describe multi-output devices leads to a non-linear formulation [13], [34];
- bi-directional energy flows can not be accommodated [30], [57];
- a converter which connects hub outputs, e.g. an absorption chiller, cannot be modelled [57]; and
- the use of a conversion coefficient matrix only permits very basic modelling of devices in comparison to the MLD approach - for example, affine functions, which are commonly used to represent thermal generators such as CHP units, cannot be modelled using the energy hub formulation.

There have been various developments reported in the literature to improve the energy hub framework, such as linearising the constraints and adding the functionality to either include logical conditions for hybrid systems [30], [34] or to accommodate more complex topologies [30], [55], [57]. Unfortunately, these improvements detract from the simplicity and ease of the original formulation, whilst failing to address the issue of affine function representation.

2.2.3 Modular Multi-Energy Management Framework

The multi-energy management framework presented in [26] presents arguably the most computationally efficient and straightforward approach for modelling hybrid

systems. This framework consists of individual sub-system modules using the following generic representation:

$$\boldsymbol{x}_{k+1} = \boldsymbol{A}\boldsymbol{x}_k + \boldsymbol{B}_u\boldsymbol{u}_k + \boldsymbol{B}_d\boldsymbol{\delta}_k + \boldsymbol{B}_z\boldsymbol{z}_k + \boldsymbol{B}_w\boldsymbol{w}_k \tag{2.5}$$

$$\boldsymbol{y}_k = \boldsymbol{C}\boldsymbol{x}_k + \boldsymbol{D}_u\boldsymbol{u}_k + \boldsymbol{D}_d\boldsymbol{\delta}_k + \boldsymbol{D}_z\boldsymbol{z}_k + \boldsymbol{D}_w\boldsymbol{w}_k \tag{2.6}$$

$$\boldsymbol{E}_d\boldsymbol{\delta}_k + \boldsymbol{E}_z\boldsymbol{z}_k \leq \boldsymbol{E}_u\boldsymbol{u}_k + \boldsymbol{E}_x\boldsymbol{x}_k + \boldsymbol{E}_w\boldsymbol{w}_k + \boldsymbol{E} \tag{2.7}$$

It therefore extends the original MLD method to account for predictable disturbance forecasts, $\boldsymbol{w}_k$, and, because it is intended specifically for multi-energy systems, the difficulty in generating constraints is avoided by having a set of predefined modules with which to model distributed energy resources. Modules may be connected up in any configuration and a general cost function is provided which allows a user to encourage desirable operational behaviour, e.g. to minimise the rate of change in the value of a given decision variable. The set of predefined modules includes energy conversion devices, controllable energy sources and sinks, predictable (uncontrollable) energy sources and sinks, simple energy balances and storage devices, only. Hence, a key disadvantage with this, and all the other frameworks mentioned thus far, is the lack of support for detailed, computationally efficient modelling of physical network flows in conjunction with distributed energy resources. The framework is therefore limited to applications with relatively small systems or situations where network conditions might justifiably be ignored.

2.2.4 Network Modelling and Analysis

Network conditions are not usually ignored in practice and modelling is typically carried out using:

- alternating current (AC) power flow models of voltage, current, active and reactive power in electricity networks [23];
- gas flow models of mass and pressure in gas networks [58]; and
- thermal models relating mass, pressure and temperature in district thermal networks [59].

Each of these flow models, which are herein collectively referred to as *energy flow* models, involves highly non-linear, non-convex relationships.

Power flow models include the *bus injection model* and the less common *branch flow model*, which are used to represent steady-state, balanced, single-phase networks [23]. The branch flow model is of particular interest for optimisation because it can be relaxed to a convex second-order cone programming (SOCP) form for which solutions are considered to be *exact*, i.e. feasible for the original problem, under mild conditions [60].

The gas flow model, typically based on the popular steady-state Weymouth equation to determine pressure drop [58], can also be relaxed to a mixed-integer conic form which has been shown to be exact for radial gas networks that have one fixed pressure node [61].

Finally, district thermal networks require both a hydraulic model and a thermal model, each based on steady-state conservation of mass and energy [54], [59]. Both of these models are non-convex and attempts to provide a convex formulation have either involved a conic relaxation of the hydraulic model and linearisation of the thermal model, by ignoring thermal losses [62], or linearisation of both models by assuming fixed mass flow rates [63]–[66]. However, district heating networks with constant mass flow rates have worse performance than for variable flows [59] and the assumption of negligible thermal losses to the surroundings would only be valid for networks operating at close to ambient temperatures, known as *Ultra-Low-Temperature District Heating (ULTDH)* [67].

Ultra-Low-Temperature District Heating and Cooling Networks

District heating has evolved over the last 140 years via a series of distinct technological generations, from the 1st to the current 4th generation of district heating (4GDH) (see Fig. 2.1). The 1st generation is identified by the use of centrally generated pressurised steam as the heating medium, relying on coal combustion for the production of heat. In each subsequent generation, operating temperatures have decreased incrementally, motivated by some socio-economic change [68]. The 2nd generation was introduced in the 1930s to maximise the use of efficient, fossil fuel-based combined heat and power plants, necessarily lowering the supply temperature, whilst the 3rd generation was driven by a desire to improve efficiency and reduce costs, following two international oil crises in the 1970s. The 3rd generation is typified by a lowering of temperatures, the use of pre-insulated pipes to reduce thermal losses, and greater

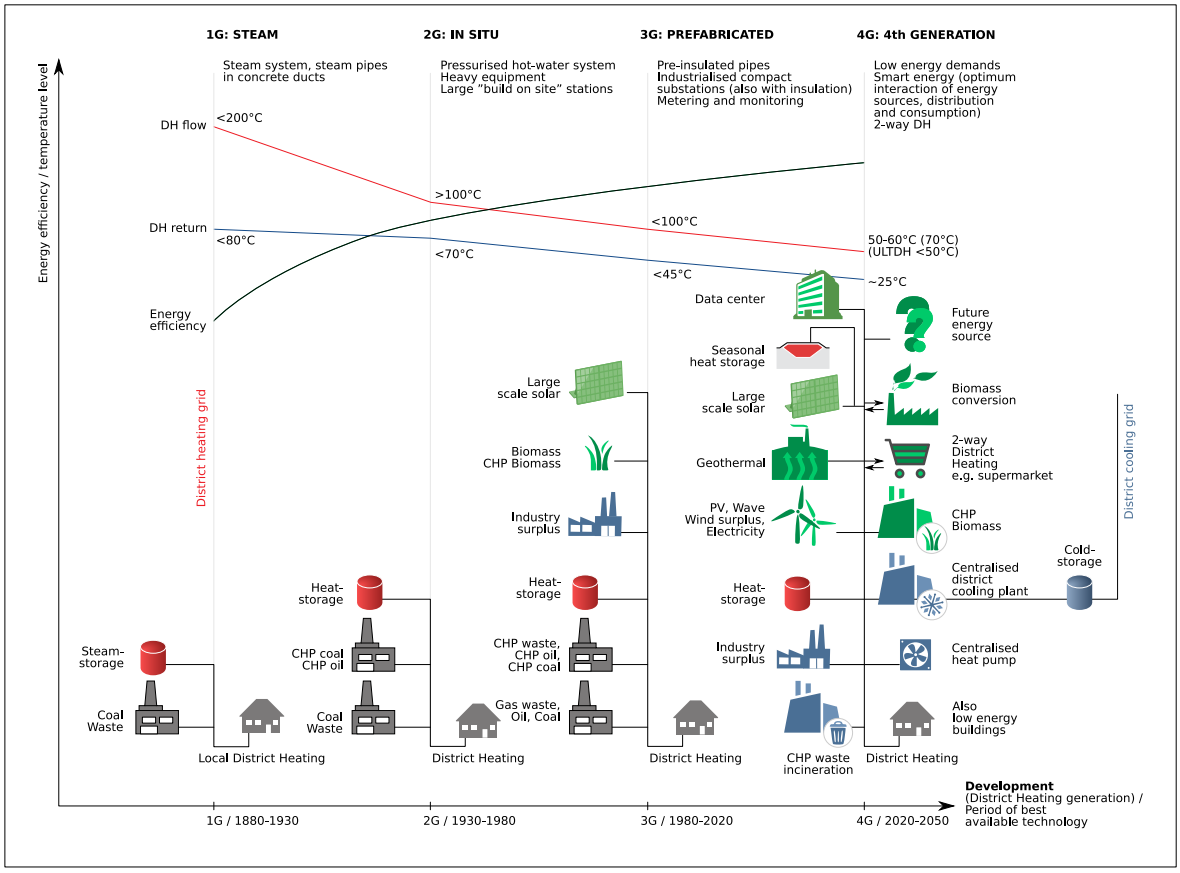

Figure 2.1: The evolution of district heating by generation, based on [68]. Sourced from [69].

use of cheaper alternatives to oil, such as natural gas, biomass and waste incineration [67].

Now, in recognition of the need to decarbonise the supply of energy, the 4GDH concept has been developed [68] to continue the trend of lower operating temperatures, increased efficiency and alternative heat sources, with the aim to completely displace fossil fuels for heating. An additional stipulation of 4GDH is that it can be operated flexibly in a smart multi-energy system, making use of cheap thermal storage and coupling to the power system, via electrically powered heating, to support the integration of electrical and thermal energy from renewable sources.

Ultra-Low-Temperature District Heating (ULTDH) is a specific configuration of 4GDH which operates at temperatures closer to the ground (below 50°C) and is therefore not suitable for direct heating (Fig. 2.2). As a result, each substation connecting the network to a given building is equipped with a water-source heat pump (WSHP) able to supply heated water at the required delivery temperature. It is also possible for substations to operate in reverse, to provide building cooling by means of a WSHP or direct cooling (if network operating temperatures are sufficiently low), to form an

Ultra-Low-Temperature District Heating and Cooling (ULTDHC) network. This is a unique advantage not shared with other, higher temperature 4GDH configurations, which deliver heat from heat producers to end-users by a series of uni-directional supply and return pipes (Fig. 2.3). When using such uni-directional configurations, the provision of cooling would have to be delivered by a separate cooling network [67], [68]. Heating is supplied from ULTDHC networks by drawing water from a warm pipe, extracting the heat using a WSHP and discharging the cooled water to a cooler pipe (Fig. 2.4). The reverse is true for a cooling demand. Thus both heating and cooling can be supplied simultaneously by a single two-pipe network, reducing installation cost and complexity.

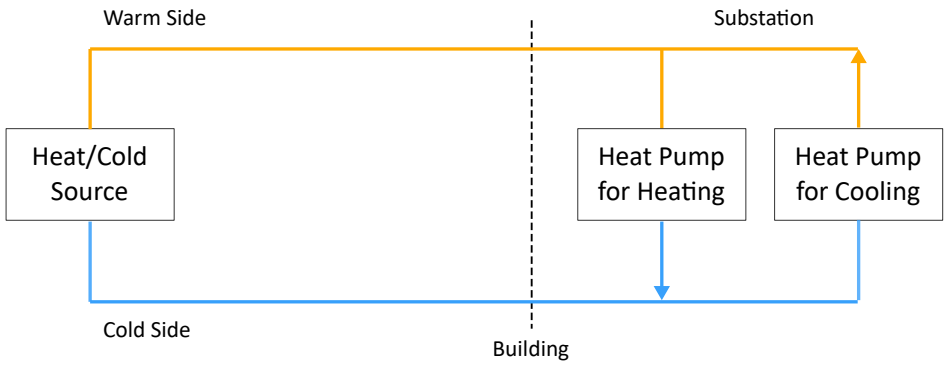

Figure 2.2: Schematic of the 'ULTDH combined heating and cooling (ULTDHC)' 4GDH configuration, based on [67].

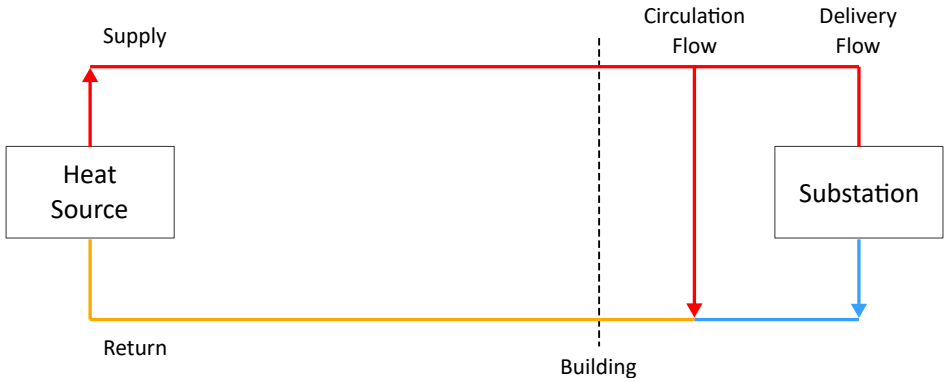

Figure 2.3: Schematic of the 'Classic' 4GDH configuration, based on [67].

ULTDHC networks may have a centralised pumping station, with some users demanding heating and others cooling (*bi-directional energy flow*), or have decentralised pumps located at each substation (Fig. 2.4), with users able to switch between demand for heating or cooling at different times (*bi-directional mass and energy flow*), enabling them to become heat prosumers [19]. Heating and cooling demands from

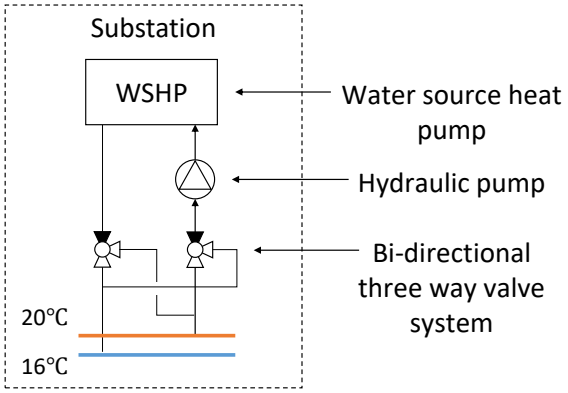

Figure 2.4: Schematic of an example ULTDHC substation, capable of bi-directional operation using a reversible WSHP, based on [19].

buildings are partly balanced in real time by the district network. However, seasonal variations will cause either heating or cooling demands to dominate at different times. Therefore, some form of large thermal storage to manage seasonal balancing is needed, e.g. aquifer or borehole storage. If cumulative heating and cooling demands are not balanced in a given year then an external supply of heating or cooling is also needed.

ULTDHC networks can provide additional benefits to those gained in other 4GDH networks: increased interchange of heat between buildings, negligible thermal losses, fewer pipelines and increased operational flexibility so that large thermal storage capacity can be leveraged to support the power system. Due to the differences in design and operation of ULTDHC compared to other 4GDH configurations, such networks are often referred to *5th Generation District Heating and Cooling* [19], including by this author [29]. However, given that 4GDH is still in the early adoption phase [67] and that generations are defined over several decades [68], it is more accurate to describe these networks as a configuration of 4GDH [70].

An analysis of levelised cost of heat apparently showed that 'Classic' 4GDH was more cost effective than UTLDH [71], yet the analysis did not take into consideration any cooling demands, the cost of a separate cooling network or the additional revenue for prosumers providing ancillary services. It may also be noted that whilst the improved thermal efficiency of ULTDHC networks is slightly offset by increased circulation pumping requirements [19], ULTDHC networks still offer emissions and energy consumption reductions in comparison to traditional district heating and separate cooling [72]. Many successful examples of bi-directional ULTDHC networks exist [19], including the 'Mijnwater Grid' in Heerlen, The Netherlands [73], the 'Surstoffi

District' in Rotkreuz, Switzerland [74] and the 'Anergy Grid' in ETH Zurich, Switzerland [75].

In order to exploit the flexibility of bi-directional ULTDHC networks for optimal integration with other energy systems, an advanced control strategy is required [18]. Not only is it needed to effectively dispatch energy resources that can provide support to the power system, it is also necessary to provide supervisory level dispatch of circulation pumps in a network with bi-directional mass flows. Otherwise, pump-to-pump interactions in bi-directional networks can cause pump feedback control loops to become unstable, with pumps continuously adjusting their speed [76]. However, of the few examples of bi-directional ULTDHC models in the literature, [77] does not include pressure drop modelling and therefore uses linearised pump models, whilst [78] and [72] each present models from a simulation environment which are not suitable for optimisation. There is therefore a research opportunity to develop a computationally efficient, bi-directional ULTDHC network flow model, including variable flow circulation pumps, which could be utilised in an energy management scheme.

To summarise, multi-energy system modelling and ULTDHC network concepts have been introduced in this section and two gaps in the literature have been identified thus far: the lack of support for detailed network analysis in multi-energy system optimisation modelling frameworks and the lack of computationally efficient modelling approaches for bi-directional ULTDHC networks with decentralised circulation pumps. The following sections review existing approaches to multi-energy system management in both the operational planning and online control domains.

2.3 Multi-Energy System Management

In this section, numerous examples of operational planning and of online control for multi-energy systems are assessed. As discussed in the introduction to this chapter, the relevant aspects when distinguishing between these problem classifications are the time available for computation, the accuracy of problem inputs and the overarching objective, from energy market participation to minimisation of resource consumption. The general approach taken when discussing examples of each is to start with the most basic problem formulations, which may exhibit good computational

performance but do not provide the most accurate reflection of the real system, before moving on to other examples with gradually increasing size and complexity.

2.3.1 Operational Planning

Several approaches to multi-energy resource management in the literature use operational planning to facilitate strategic bidding in day-ahead markets, including retail [34], [39], [43], [45], [46], [55], [62], [63], [65], [66], [79], [80], peer-to-peer [44], ancillary service [43], [45], [81] and carbon trading markets [45], [55]. These range from solving relatively simple problems, e.g. deterministic resource scheduling of a small system, to large, complex problems, e.g. robust scheduling of a district whilst accounting for network energy flows (see Table 2.1).

Ref.	Year	Prediction Horizon	Sampling Interval	Connected Systems	Networks Modelled	Uncertainty Handling	Method
Problems without Network Energy Flow Constraints:							
[55]	2019	24 hr	1 hr	1	n/a	Deterministic	MILP
[44]	2020	24 hr	1 hr	2	None	Deterministic	MILP
[46]	2021	24 hr	1 hr	5	None	Deterministic	MIQP
[34]	2012	24 hr	1 hr	1	n/a	RO	MILP
[81]	2021	1 hr	5 min	6	None	RO	MINLP
[43]	2019	24 hr	0.5 hr	50	None	RO	MILP
[79]	2020	24 hr	1 hr	1	n/a	RO	MILP
Problems involving Network Energy Flow Constraints:							
[54]	2018	n/a	n/a	5	Power & HTDH	n/a	NR
[82]	2016	n/a	n/a	32	Power & HTDH	n/a	NR
[83]	2016	n/a	n/a	11	Power, Gas & HTDH	n/a	NR
[84]	2014	n/a	n/a	11	Power & Gas	n/a	EA
[85]	2017	n/a	n/a	118	Power & Gas	n/a	MILP
[80]	2018	n/a	n/a	13	Power & Gas	n/a	SOCP
[65]	2018	n/a	n/a	33	Power & HTDH	n/a	SOCP
[86]	2018	n/a	n/a	24	Power & Gas	n/a	MISOCP
[87]	2015	24 hr	1 hr	30	Power, Gas & HTDH	Deterministic	EA
[62]	2019	24 hr	1 hr	5	Power & HTDH	Deterministic	MISOCP
[66]	2021	24 hr	1 hr	6	Power & HTDH	Deterministic	MISOCP
[63]	2020	24 hr	1 hr	4	Power, Gas & HTDH	Deterministic	MISOCP
[45]	2021	24 hr	1 hr	26	Power, Gas & HTDH	Deterministic	MIQP + NLP
[64]	2020	24 hr	1 hr	32	Power & HTDH	RO	MISOCP
[39]	2018	24 hr	0.5 hr	26	Power, Gas & HTDH	RO	NR + MILP

Table 2.1: Overview of operational planning studies reviewed in this section. EA = Evolutionary Algorithm; HTDH = High-Temperature District Heating; NR = Newton-Raphson; RO = Robust Optimisation.

Problems without Network Energy Flow Constraints

The most basic example of resource scheduling is presented in [55], in which a day-ahead optimisation is used to minimise the operating costs of a single energy hub, considering carbon pricing and time-of-use electricity and gas prices. The method

uses a modified energy hub modelling approach to determine optimisation constraints, resulting in an MILP problem, although converters are only represented by static models.

Prices for electricity and heat are determined in [44] using a peer-to-peer market between a residential and a commercial prosumer, for which an MILP is also solved. The centralised optimisation seeks to maximise fairness between the two prosumers based on an uncooperative game, exploiting the demand flexibility from their respective distributed energy resources. The outputs of the optimisation are fixed prices for electricity and heat over the next 24 hours, together with an operating schedule for demand response.

A more complicated scheme in [46] attempts to implement dynamic pricing for a collection of four integrated energy systems connected to a power supplier. The scheme uses an MIQP optimisation to allow the power supplier to determine real-time pricing which maximises supplier profits and reduces the costs for each energy system. Demand response from the energy systems is determined using a rule-based strategy and all information regarding the operation of the energy systems must be available to the power supplier carrying out the centralised optimisation.

In each of these schemes, economic and operational decisions are made based on an operating schedule without any method for mitigation against uncertainty in system models and forecast data. Robust scheduling may be used to address this by considering worst-case bounds on parameter uncertainty during optimisation, as demonstrated in [34], [43], [79], [81].

The uncertainty of conversion coefficients, production and load for an energy hub is captured in a robust MILP formulation in [34]. The work demonstrates that robustness against uncertainty can be ensured for a small ($\sim$10%) increase in the cost of purchased energy for a relatively small system.

Multiple district energy systems are coordinated using robust scheduling in [81], enabling an amount of 'certain' capacity to be traded in the electricity reserve market. However, the problem is formulated using mixed-integer non-linear programming (MINLP) and solved by particle swarm optimisation, which may or may not converge to a globally optimal solution.

In [43], a similar objective to provide reserve capacity from flexible resources in a smart district, without compromising thermal building comfort, is demonstrated using stochastic, robust MILP optimisation. For the case studied, the response to reserve calls from the power system operator, by manipulating indoor building temperatures, proved to be effective in maximising revenue.

An *affine adjustable* robust optimisation, formulated as a MILP problem, is presented in [79], using a hospital and a university campus as case studies. The approach performs comparably to an 'omniscient' optimisation, in terms of cost and satisfaction of demands, and also significantly outperforms a deterministic counterpart with imperfect forecasts. One downside, as noted by the authors, is that the size of the robust MILP problem grows rapidly with an increase in the system scale. A further weakness in each of these methods is the lack of detailed network analysis when scheduling resources, since these resources ultimately affect network operation.

Problems involving Network Energy Flow Constraints

Before submitting bids on behalf of prosumers in a district, for energy supply or purchase in retail or flexibility service markets, a multi-energy aggregator must first check that their bidding strategy is feasible and will not violate district network constraints. Otherwise the aggregator's bids may be rejected or they may face fines by the energy system operator for failure to deliver [40], [45]. This requires integrated multi-energy network analysis to be carried out, to determine whether submitted bids for energy production and consumption violate network constraints in any given time period. Checks could either be carried out as:

- an energy flow problem, in which all production and consumption variables have already been determined (except for slack nodes) [54], [82], [83], [86];
- as an optimal energy flow problem, which optimises resources subject to network constraints in a single period [65], [80], [84], [85]; or
- as a network constrained unit commitment or scheduling problem, in which the temporal constraints of distributed energy resources at the district [62]–[64], [66], [87] or building level [39], [45] are taken into consideration.

Since energy flow problems simply involve solving a set of simultaneous equations, coupled non-linear energy flow models for power and heat [54], [82] or power, heat and gas [83] can be solved relatively easily using the iterative Newton-Raphson method. However, as is discussed in Appendix A, optimisation problems with non-linear constraints are not so easily solved. Hence, integrated optimal energy flow problems based on the same non-linear models must be solved using heuristic algorithms [84], [87], which cannot guarantee convergence to the optimal solution.

To avoid non-linear solution methods, the same general problem from [84] is reformulated as a MILP problem in [85], linearising the gas flow constraints and using the linear DC power flow model (which assumes negligible line resistance, constant voltage and small voltage angles). This can be solved much more easily and the error introduced by linearising the gas network constraints is reduced through further MILP optimisations in an iterative algorithm. However, the inaccuracy introduced by use of the DC flow model for an AC power network is not addressed. The linearised AC DistFlow model is utilised in [63], [64], which incorporates reactive power and voltage magnitudes, but is still inaccurate when power losses and voltage drop are significant.

The energy flow problem in [86] and optimisation problems in [62], [65], [66], [80] accommodate AC power flow behaviour by adopting a convexified branch flow model [60]. For integrated power and gas networks, the gas flow problem may be transformed into a mixed-integer second-order cone programming (MISOCP) problem, by relaxing non-convex quadratic equalities to convex inequalities and introducing binary variables to indicate gas flow directions [86], or solved as a SOCP problem in successive iterations [63], [80]. However, for integrated power and heat networks in [62]–[66], the heat flow problem is transformed into a convex one by assuming fixed mass flows in supply and return lines which, as previously mentioned, is not the preferred operating mode due to their inefficiency when compared to variable mass flow operation.

Network-secure scheduling of buildings' energy systems in a smart district is considered in [39] and [45]. In each case, the problem of optimally scheduling resources in buildings is separated from the integrated network analysis problem. In [39], the non-linear integrated power, gas and heat energy flow problem is solved using the Newton-Raphson method from [83], enabling the identification of network violations produced by the optimal building operation schedule. If there are any violations, ad-

ditional linear constraints are added to the optimal scheduling problem and it is resolved in an iterative process until a feasible operation schedule is determined.

Similarly, separate non-linear energy flow models are solved for power, gas and heat networks using a non-linear solver in [45]. Power, gas and heat system operators interact with an aggregator, responsible for optimal scheduling of energy resources in buildings and submitting market bids, via an alternating method of multipliers algorithm. Whilst the computational performance of the two approaches reported in [39], [45] is shown to be sufficiently quick for day-ahead bidding, the use of non-linear network models and centralised optimisation for all buildings are weaknesses in each case. Privacy of building users is not preserved with this structure and, given that each also considers mixed-integer modelling of energy resources, increasing the size or complexity of the system is likely to cause exponential increases in computation time.

The various methods discussed in this section may offer some advantage in operational planning for their intended application, particularly those which are based on robust optimisations and/or consider network energy flow constraints. However, this approach of 'open-loop' scheduling, without any recourse to address forecast or modelling errors, is unsuitable for online dispatch of controllable system resources. This is the role for online control, as discussed in the following section.

2.3.2 Online Control

Online control strategies reported in the literature either assume that a schedule for a set of aggregated resources has already been determined via day-ahead scheduling, and that there are economic incentives or penalties for tracking this schedule, or that resources are dispatched in online based on known and forecasted price signals. The dominant online control strategy, *model predictive control* (MPC), is well suited to handling either scenario and is discussed first.

Model Predictive Control

Many of the techniques in optimal scheduling can be repurposed for online control by implementing a MPC or *receding horizon* strategy. It is important to note that MPC

does not designate a specific control formulation, rather a wide range of methods with the following common features [88]:

- explicit use of a model to predict system outputs over a time horizon;
- calculation of a control signal by minimising an objective function; and
- receding horizon updates (see Fig. 2.5) in which the first instance of the control signal is applied before the time horizon is displaced one time step towards the future and a new control signal is recalculated.

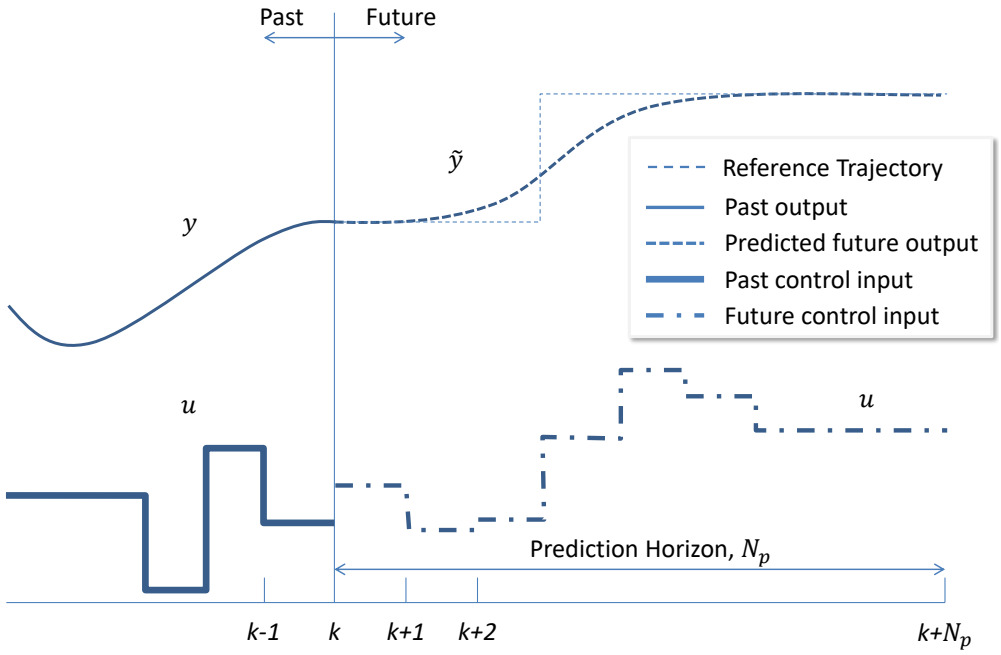

Figure 2.5: Illustration of receding horizon strategy from [89]. At each sampling instance, k, system states are updated and new future trajectories determined.

A MPC scheme is a multi-variable strategy integrating online optimisation of a prediction model with a feedback mechanism which can compensate for forecast and modelling errors [88]–[91]. All of these features make MPC ideal for energy management applications which generally involve a large number of variables, dynamic models, operational constraints and a degree of uncertainty in forecasted variables [25]. Whether explicitly stated or not, many optimisation based methods in real-time control of multi-energy systems satisfy this generic definition of MPC [26], [30], [36], [37], [40]–[42], [47], [48], [56], [92]–[94].

Computation time is a critical factor in optimal online control. If a feasible, optimal (or at least near-optimal) control action cannot be provided within a limited period after a system state measurement or estimate is obtained, then this action will be based on out of date information and may no longer be optimal or even feasible. Furthermore, if the worst-case computation time is longer than the sampling interval length, an even more problematic situation may arise in which no control action is provided at all. As a result, there is typically a compromise made regarding either the modelling accuracy, system scale, scheduling horizon length or sampling frequency when designing online energy management control schemes (see Table 2.2).

Ref.	Year	Prediction Horizon	Sampling Interval	Connected Systems	Networks Modelled	Uncertainty Handling	Method	Control Structure
Model Predictive Control:								
[37]	2017	4 hr	15 mins	1	n/a	Deterministic	MILP	Single Controller
[30]	2019	24 hr	30 mins	1	n/a	Deterministic	MIQP	Single Controller
[26]	2020	24 hr	15 mins	1	n/a	Deterministic	MILP	Single Controller
[48]	2021	3-7 days	7.5-15 mins	1-12	HTDH & DC	Deterministic	MILP	Single Controller
[94]	2019	24 hr	1 hr	6	None	ANN	NLP	Single Controller
[95]	2017	150 secs	30 secs	1	n/a	SO	QP	Single Controller
[93]	2016	10 secs	1 sec	1	n/a	SO	QP	Hierarchical
[40]	2019	24 hr	30 mins	1000	None	SO	MILP + RBC	Hierarchical
[42]	2019	3-24 hr	0.5-1 hr	1	n/a	Deterministic	MILP + RBC $\rightarrow$ LP	Single Controller
[41]	2019	24 hr	10 mins	1	n/a	Deterministic	LP	Single Controller
[92]	2018	24 hr	15 mins	3690	Power	Deterministic	MILP	Multi-Agent
[63]	2020	24 hr	1 hr	4	Power, Gas & HTDH	Deterministic	MISOCP	Multi-Agent
[36]	2017	24 hr	10 mins	5-15	None	Deterministic	MILP	Multi-Agent

Table 2.2: Overview of model predictive control studies reviewed in this section. ANN = Artificial Neural Network; DC = District Cooling; HTDH = High-Temperature District Heating; RBC = Rule-Based Control; SO = Stochastic Optimisation.

For example, an MPC scheme for a microgrid with a combined cooling, heat and power system is presented in [37]. The scheme aims to minimise energy production costs by solving an MILP problem every 15 minutes, using short-term error prediction and static optimisation based feedback correction every 5 minutes. The computation times of the rolling optimisation and feedback correction are sufficiently small, averaging 2.2 and 1.1 seconds, respectively. However, the prediction horizon length of 4 hours is relatively short and the size of the system is also relatively small, with only two storage systems and four controllable energy conversion devices, therefore the resulting MILP problem is small and easily solved.

The scale and complexity of the system under consideration is increased in [30], in which an energy hub supplies three university campus buildings. One of the buildings can consume heat flexibly, whilst another can consume electricity flexibly, providing additional demand response capacity. The controller optimises an economic objective

to minimise costs and changes to flexible loads, resulting in an MIQP problem, for a prediction horizon of 24 hours which is discretised into 48 half hourly periods. Although the reported computation time for the control problem of 32 seconds is appropriate given the sampling frequency, if the system scale were increased to the district scale then the problem could become intractable.

A similarly sized system was studied in [26] which utilised more detailed device modelling by virtue of the adopted MLD modelling formulation, although it did not include flexible loads. A very similar MPC scheme to that of [30] was presented, solving a single MILP problem every 15 minutes with a prediction horizon of 48 hours. The computation time was surprisingly fast at approximately 1.3 seconds, which may be attributed to the use of a high performance server to run the computation and possibly fewer binary variables in comparison to [30]. However, no networks were modelled in detail in either study and the problem of scalability for MILP problems remains.

The problem of scalability is well demonstrated by [48], for which an MILP problem is designed to manage the thermal comfort of up to twelve buildings, connected by a high temperature district heating network and separate cooling network. Due to the slow thermal dynamics considered, a prediction horizon of three days to one week is considered, for which the resulting computational times are given in Table 2.3.

No. of Buildings	Prediction Horizon	Sampling Interval	Computation Time
1	7 days	15 mins	$<$ 5 mins
12	7 days	7.5 mins	5 hrs
12	3 days	7.5 mins	20 mins

Table 2.3: Computational time for case studies of varying problem size reported in [48]

Clearly the scheme would require amendment if it were to be used in a receding horizon implementation, as is suggested by the authors, since the computation time for twelve buildings exceeds the sampling interval. Moreover, the network modelling is arguably already over-simplified since fixed mass flows and uniform supply temperatures are considered in the thermal networks.

The approach proposed in [94] avoids MILP optimisation altogether, favouring a combination of non-linear modelling and an artificial neural network. The reason given for avoiding MILP is that it cannot accommodate the non-linear functions used

to represent devices operating at part-load, although these can be approximated using MILP, as discussed in [26]. The artificial neural network is used to predict the indoor temperature of an office building in response to a controllable set-point temperature. This office temperature prediction model and non-linear models for a heat pump, gas boiler and CHP are incorporated into a genetic algorithm optimisation solver, implemented every hour with a 24 hour prediction horizon. Despite having relatively few controllable resources and only four fixed heating loads from other buildings, the non-linear optimisation takes 143 seconds to compute a control action, which is slow for a system of this size.

At the other end of the spectrum of modelling complexity, stochastic optimisation schemes for a hydrogen based microgrid in [95] make use of models which have been linearised around an operating point. The increased computational burden encountered with scenario based stochastic MPC methods is offset by a very short prediction horizon of 150 seconds and very small system size, enabling a sampling interval of 30 seconds. These examples highlight the compromises made in centralised single-controller MPC architecture in order to maintain tractability.

Hierarchical MPC schemes offer one route to decompose the control problem into simpler sub-problems at different timescales. The stochastic MPC controller from [95] is split into two management layers in [93], an optimal generation scheduling layer and an MPC layer. Stochastic scenario generation optimisation is undertaken every hour and provides a reference value to be tracked by the MPC layer. Still using linearised modelling for a small system, the MPC optimisation is undertaken every second, a considerable increase in sampling frequency, and uses a prediction horizon of 10 seconds.

A much larger system consisting of 1000 prosumers is also managed by a hierarchical MPC scheme in [40]. An aggregator first submits bids in day-ahead energy and reserve markets on behalf of the prosumers, based on a stochastic optimisation model [96], providing a schedule of energy demand and reserve capacity which must be satisfied. The MPC controller then attempts to minimise the cost of delivering this schedule, updating the state of the prosumers' resources and solving a MILP optimisation every half an hour, whilst a lower level rule-based controller dispatches resources with higher frequency, i.e. every 10 seconds, in response to an automatic generation control signal from a power system operator. The scheme leaves the responsibility for congestion analysis with the system operator and it should be noted

that a heating network is not considered. Furthermore, whilst the computational performance of the MPC controller is impressive, considering there are 1000 prosumers each with three flexible resources, i.e. an electric vehicle, battery and controllable thermal load, the execution time of nearly 20 minutes is far from ideal for half hourly sampling.

Other innovative ways to address computation time include methods which reduce the number of optimisation variables in the control problem. For example, rule-based MPC is proposed for an electricity-only microgrid in [42], in which binary variables are fixed prior to optimisation. This method, which uses a set of rules related to dynamic prices and output from renewable energy sources to fix binary values, can reduce the computation time of the original MILP by 65-80%, with only a marginal increase in microgrid operating costs. However, when the method is applied to more complex systems with greater degrees of freedom for demand satisfaction, the derivation of if-then-else rules for fixing integer variables becomes too complicated.

Alternatively, variable reduction can be achieved through multi-rate MPC, which involves using two different time steps in the control problem - a short time step for the prediction model and a longer time step for applying control inputs. The technique is demonstrated in [41] to schedule operation of a chiller which is used to regulate the indoor temperature of an office building. A prediction model time step of 10 minutes is considered with control actions determined at time steps of between 10 minutes and 8 hours. Computation time in comparison to the single-rate case is reduced by around two thirds for all control intervals tested, with little increase in overall costs up to a control interval of 2 hours. Whilst this may be useful for a specific problem with high computational burden, the fact that no further reduction in computation time is achieved for longer control intervals suggests this approach has a limit to its effectiveness.

A proven method to aid tractability is to decompose the global optimisation into a set of smaller sub-problems which can be solved in parallel by individual agents [97]. A secondary advantage of these *multi-agent* schemes for energy system management is that a greater degree of privacy can be maintained between different parts of a multi-stakeholder system. There are numerous examples of decentralised energy management schemes which are based on Lagrangian dual decomposition of convex system models [56], [98]–[102]. However, there are fewer examples that

optimise mixed-integer model formulations, since convergence of Lagrangian-based decomposition methods is affected by convexity.

There are at least two algorithms enabling multi-agent, mixed-integer optimisation using Lagrangian-based methods, either by solving decomposed sub-problems successively [92] or in parallel but with an additional iterative sequential stage involving integer relaxation [63]. Another, non-Lagrangian, cooperative algorithm involving an energy aggregator was presented in [36] and used to coordinate flexibility services amongst network connected microgrids. Optimal microgrid power profiles were coordinated in a series of phases involving parallel computations and a final power redistribution phase which required sequential sub-problem solving. Therefore, none of these methods allow agents to solve the mixed-integer problem in parallel, using a single iterative algorithm.

Recently the use of dual decomposition and constraint tightening has been demonstrated for decentralised optimisation of up to 10,000 modelled electric vehicles, each subject to shared resource constraints [27], [28]. The proposed algorithms allow parallel computation of sub-problems and require only one iterative stage to achieve finite-time convergence to a feasible solution [27]. Whereas a commercial solver was unable to provide an adequate solution to the centralised MILP problem if the number of vehicles exceeded 700, the decomposition method provides solutions in 30 mins for 10,000 vehicles. Furthermore, the optimality gap diminishes as the size of the system increases, whilst privacy is also maintained between local agents and a central coordinator. Despite these attractive features, the method has not been incorporated into an online control scheme. Moreover, the method has not been demonstrated for the more complex application to flexible multi-energy systems, which typically requires greater computational effort due to additional constraints used to model energy system interactions.

Model Predictive Control Alternatives

Aside from MPC schemes, several other online energy management approaches are reported in the literature. An auction mechanism for day-ahead and online energy trading between system stakeholders is presented in [103]. Trades are made between end-users, a distributed multi-energy generation plant and supplier network operators, with penalties for users who deviate from their agreed schedule. Whilst

this mechanism is shown to be fair for participants, it does not consider a prosumer's ability to sell energy, nor are networks accurately modelled.

Alternatively, a greedy algorithm is discussed in [35] which provides very efficient computation in comparison to a comparable optimisation. The algorithm ranks resources in order of flexibility and prioritises allocation to inflexible resources during dispatch. However, this does not allow energy arbitrage to be carried out, since future control actions are not considered, resulting in solutions that are far from optimal.

Another interesting method is the use of deep reinforcement learning to achieve real-time control [104], [105]. These are 'model-free' approaches, since a control policy based in Markov decision processes is constructed using training data, with the advantage that uncertainty is captured during the learning process. Such methods do not require forecasts, only current state information, and control actions for a residential system in [105] are computed in seconds, with comparable optimality to a MILP solution. However, despite strong performance for a relatively small system with operation which does not deviate significantly from normal operating conditions, it is difficult to predict the controller response in extreme situations not captured by the training data set. Furthermore, a period of retraining would be needed for every change made to the energy system, which requires expertise to select training algorithm parameters and to avoid under- or over-fitting to the training data. For these reasons model based optimal control still holds some advantages.

2.4 Summary

This review has covered a cross section of the literature on multi-energy systems, focusing on modelling approaches and energy management strategies. The two main areas which have not yet been fully addressed in the literature are: the lack of computationally efficient integrated energy network modelling approaches and poor scalability in optimisation based control methods for which computation time must be minimised. These can be broken down more specifically as:

1. Available multi-energy system optimisation modelling frameworks do not sufficiently accurately model, in a computationally efficient manner, the non-linear flow physics of multiple interconnected energy networks.

2. None of the surveyed case studies for online control considered bi-directional ULTDHC networks in an integrated multi-energy system.

3. There are no available methods to model mass and energy flows in bi-directional ULTDHC networks such that they are suitable for optimisation and can therefore be used for network pump dispatching.

4. No MPC strategies have been demonstrated for online management of large hybrid multi-energy systems, modelled using MILP, which allow sub-problems to be solved in parallel via a single iterative algorithm.

5. Novel dual decomposition and constraint tightening methods for MILP problems have not been applied either in an MPC strategy, in a multi-energy systems context or for MISOCP problems.

In the following chapters these gaps are addressed and demonstrated via a series of case studies. In Chapter 3 a multi-energy system optimisation modelling framework is presented which can be used to generate MISOCP problems. It is therefore capable of incorporating network energy flow models. For rapid generation of problems for integration into MPC schemes, an extensive library of pre-defined system component modules are also presented, together with device modifiers to allow modelling of specific device characteristics. Cost modifiers are also included in the framework, allowing for customisation of the control objective associated with a given problem, such that actual economic costs and other penalties to encourage specific system behaviours can be considered.

Newly proposed component modules are then integrated into a control scheme for coordinating a small-scale multi-energy district framework in Chapter 4. These are reversible WSHP and fixed speed circulation pump components which permit a ULTDHC substation to be added to the control problem. A simple network power balance module is also used so that exchange between buildings can be modelled, based on a directed graph representation of a given network. A case study then demonstrates control of three buildings within a small district, each connected to power, gas and a bi-directional ULTDHC network.

Since simple network power balances cannot be used to avoid voltage or pressure violations, in Chapter 5 modules for detailed AC networks and ULTDHC networks are

utilised in the control scheme instead. A module for modelling variable speed circulation pumps, which are more efficient than fixed speed pumps, is then also included, made possible by the ability to model ULTDHC network pressures. The case study of a large multi-energy district which is presented in this chapter demonstrates that these modules can be used to ensure feasible network operation whilst pursuing economic objectives. Set points can also be obtained for decentralised circulation pumps to avoid pump-to-pump interactions, which may otherwise occur if controlled only by feedback control loops based on network sensors. However, the computational performance of the scheme in this chapter is very poor as the employed centralised control approach is not scalable.

To address this, in chapter 6 more scalable optimisation methods are introduced which use dual decomposition to enable parallelised solution of a global problem. Two novel multi-agent algorithms are proposed to address convergence issues when existing approaches from literature are applied in a MPC scheme. The multi-agent algorithms are compared in two case studies, one involving an EV charging optimisation problem and one for control of a multi-energy district with basic network capacity constraints.

The results of Chapters 5 and 6 are combined in Chapter 7, in which a MPC scheme is proposed that is both scalable and capable of considering detailed multi-energy network constraints. Case study results are then presented for online control of a large-scale multi-energy district, demonstrating improved economical performance over a centralised alternative and computational times which would be appropriate for real world applications.

Chapter 3

Multi-Energy System Optimisation Modelling Framework

3.1 Introduction

A general multi-energy system optimisation modelling framework is defined in this chapter. The framework takes inspiration from several MILP based multi-energy system modelling approaches [25], [26], [30], though the hybrid MLD system representation described in [26], specifically, is adopted and extended throughout the thesis. All of the different approaches can be followed to generate the same underlying constraints, after simplification, for a given system and produce the same results. In fact, each of them has been followed to generate material for publication at the various stages of this research project. However, the general representation in [26] is perhaps the easiest to understand in a multi-energy system context and should be familiar to control practitioners, being an extension to the original MLD modelling formulation [31].

The purpose of the framework is to enable an end-user to generate an optimisation problem which can then be readily integrated into a MPC scheme. Therefore, the framework should facilitate the generation of constraints and a cost function for multi-energy systems of arbitrary configuration, and also be amenable to software implementation. As in [26], this is achieved by defining a set of individual modules which represent the component parts of a multi-energy system, which can then be connected to one another in any desired configuration. Individual modules may

represent conversion devices, system loads, storage or connecting networks and, as a minimum, each pre-defined module contains a set of modelling constraints to describe the basic physical characteristics of that component part. An end-user can also modify modules, through the addition of pre-defined constraint sets which alter the operational behaviour of a given component (see Section 3.3.12), and/or via inclusion of pre-defined cost function terms to define how the component is optimised (see Section 3.7). The framework therefore provides a scalable and versatile means of MPC model development for multi-energy systems.

To facilitate model development, an object-oriented programming solution was created, built upon the open-source optimisation software parser, YALMIP [106]. The newly developed software uses classes, methods and inheritance to enable the rapid development of large system models, by connecting up individual device modules to form larger, aggregated modules. The open-source repository for this software can be found at: `https://github.com/mike280512/COMMES_MLD`.

3.2 Generic Module Representation

The general representation of MILP module constraints is given by [26] as:

$$\boldsymbol{x}_{k+1} = \boldsymbol{A}\boldsymbol{x}_k + \boldsymbol{B}_u\boldsymbol{u}_k + \boldsymbol{B}_d\boldsymbol{\delta}_k + \boldsymbol{B}_z\boldsymbol{z}_k + \boldsymbol{B}_w\boldsymbol{w}_k \tag{3.1}$$

$$\boldsymbol{y}_k = \boldsymbol{C}\boldsymbol{x}_k + \boldsymbol{D}_u\boldsymbol{u}_k + \boldsymbol{D}_d\boldsymbol{\delta}_k + \boldsymbol{D}_z\boldsymbol{z}_k + \boldsymbol{D}_w\boldsymbol{w}_k \tag{3.2}$$

$$\boldsymbol{E}_d\boldsymbol{\delta}_k + \boldsymbol{E}_z\boldsymbol{z}_k \leq \boldsymbol{E}_u\boldsymbol{u}_k + \boldsymbol{E}_x\boldsymbol{x}_k + \boldsymbol{E}_w\boldsymbol{w}_k + \boldsymbol{E} \tag{3.3}$$

where k is the discrete time index, $\boldsymbol{x}_k \in \mathbb{R}^{N_x}$ is the vector of system states, $\boldsymbol{u}_k \in \mathbb{R}^{N_{u_c}} \times \mathbb{Z}^{N_{u_d}}$ is the vector of continuous and discrete control inputs, $\boldsymbol{\delta}_k \in \mathbb{Z}^{N_\delta}$ is the vector of discrete auxiliary variables, $\boldsymbol{z}_k \in \mathbb{R}^{N_z}$ is the vector of continuous auxiliary variables, $\boldsymbol{w}_k \in \mathbb{R}^{N_w}$ is the vector of disturbance forecasts and $\boldsymbol{y}_k \in \mathbb{R}^{N_y}$ is the vector of system outputs. The vector $\boldsymbol{E}$ contains variable upper and lower bounds as well as fixed system inputs. Variable values are held constant during each sampling period, i.e. they are modelled with zero-order hold.

In order to accurately represent non-linear component behaviour, modules may also be defined that feature quadratic inequality constraints. Hence, the general representation of (3.1)-(3.3) is extended with the addition of constraints with the following

form:

$$\frac{1}{2}\boldsymbol{z}_k^\top \boldsymbol{F}_{zz_n}\boldsymbol{z}_k + \boldsymbol{F}_{z_n}^\top \boldsymbol{z}_k \leq F_n, \quad n = 1, ..., m \tag{3.4}$$

in which m is the total number of quadratic constraints per discrete time period, $\boldsymbol{F}_{zz_n}$ is a $N_z \times N_z$ matrix, $\boldsymbol{F}_{z_n}$ is a $N_z \times 1$ vector and F_n is a scalar.

All of the component parts of a generic multi-energy system are represented as distinct modules which may be connected up to form larger aggregate modules. Hence, energy demand, conversion and storage components can be aggregated to represent energy systems in buildings and these in turn can be aggregated to represent building districts (see Fig. 3.1). When components are aggregated, their variable vectors are concatenated, their respective coefficient matrices in (3.1) - (3.3) are combined using block-diagonal concatenation and matrices in (3.4) are padded with zeros to achieve the correct dimensions. For example, if two components are aggregated, their continuous auxiliary variable vectors, $\boldsymbol{z}_{k_1} \in \mathbb{R}^{N_{z_1}}$ and $\boldsymbol{z}_{k_2} \in \mathbb{R}^{N_{z_2}}$, would be concatenated to $\boldsymbol{z}_k \in \mathbb{R}^{N_{z_1}+N_{z_2}}$, matrices $\boldsymbol{B}_{z_1}$and $\boldsymbol{B}_{z_2}$ would be combined to form $\boldsymbol{B}_z = \begin{bmatrix} \boldsymbol{B}_{z_1} & 0 \\ 0 & \boldsymbol{B}_{z_2} \end{bmatrix}$ and new matrix $\boldsymbol{F}_{zz_i}^{N_z \times N_z}$ and vector $\boldsymbol{F}_{z_i}^{N_z \times 1}$ would be generated, for which $N_z = N_{z_1} + N_{z_2}$.

To form connections within aggregations, output variables of each component module, y_k, are designated as either source or sink *ports* for connection to the ports of other components. Connection constraints are added which define the flow of energy between connected ports:

$$y_{k,\text{snk}_j} = \gamma_{ij} \cdot y_{k,\text{src}_i} \tag{3.5}$$

For example, the heat output of a heat pump would be designated as a source port and may be connected to the sink port of a heat demand. By convention, a positively valued output variable at a sink port, y_{k,snk_j}, always represents a physical flow into the component at that port. Unlike in [26], γ_{ij} may take positive or negative values to enforce this convention. Furthermore, γ_{ij} may take values of any magnitude, to represent physical transmission losses ($|\gamma_{ij}| < 1$), to convert between different units of a physical quantity, e.g. between kW and p.u. of electricity, or to convert between different physical quantities of relevance, e.g. conversion between a mass flowrate of water at a given temperature and the amount of heat energy available from the water. A table is provided in Appendix B which gives examples of the various forms of γ_{ij} that may be used to connect different modules.

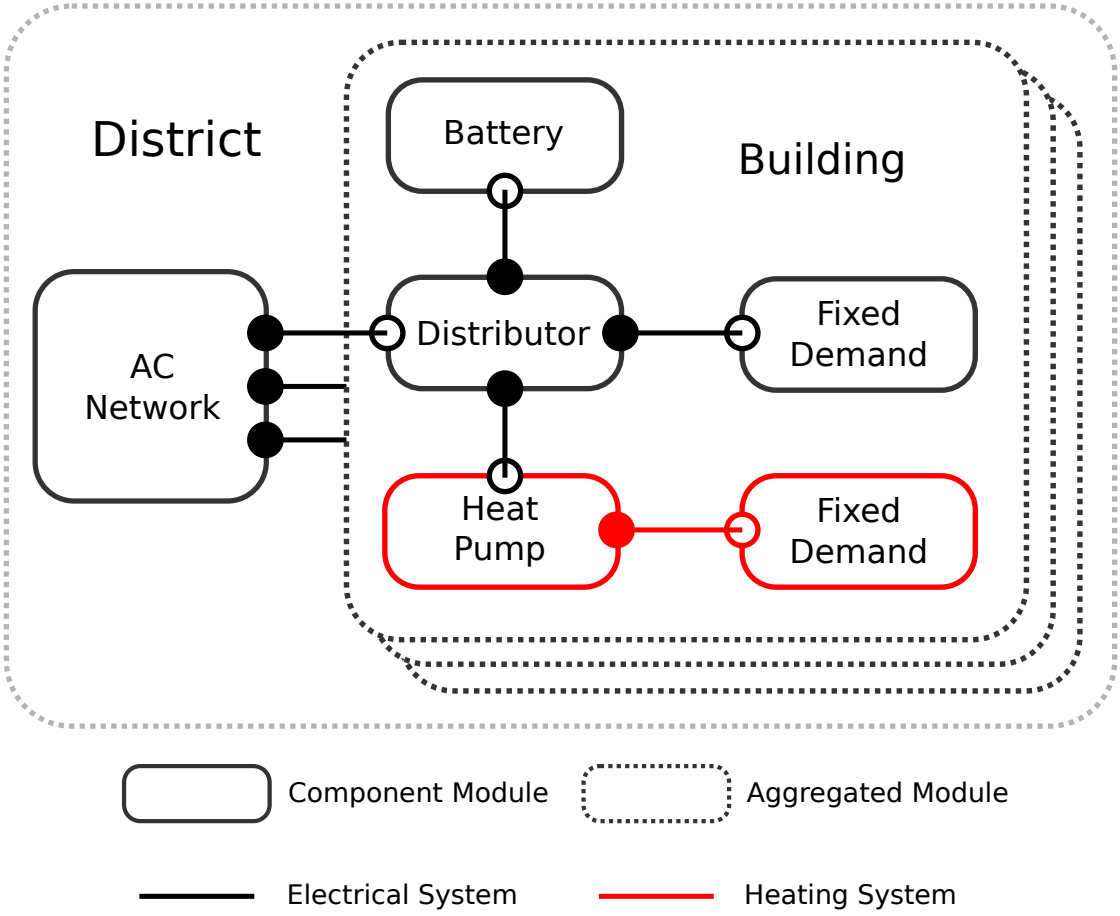

Figure 3.1: Illustration showing the recursive aggregation of connected component modules. Multiple components are aggregated to form a building module and in turn multiple buildings are aggregated to form a district. Filled circles indicate source ports, empty circles indicate sink ports and lines indicate connections.

Whenever there is a need to connect several output ports of the same physical type at a common junction, then a *distributor* module is used with a defined number of source and sink ports:

$$y_{\text{snk}_i} = z_{\text{snk}_i} \tag{3.6}$$

$$y_{\text{src}_j} = z_{\text{src}_j} \tag{3.7}$$

$$\sum_{i=1}^{N_{\text{snk}}} z_{\text{snk}_i} - \sum_{j=1}^{N_{\text{src}}} z_{\text{src}_j} = 0 \tag{3.8}$$

where N_{snk} and N_{src} are the number of sink and source ports of the distributor, respectively. This slightly different representation to [26] ensures positively valued flows into module sink ports can be accommodated. The distributor module may be aggregated and connected via connection constraints like any other module.

The benefits of this aggregation become clear when using an object-oriented software implementation of the framework. It allows optimisation models to be devel-

oped in a logical, bottom-up manner, in which named component objects are first instantiated individually, before being passed as sub-components for the instantiation of aggregation objects. The properties of these aggregation objects comprise the combined properties of the sub-components, alongside a specific 'sub-components' property which stores individual instances of each sub-component object. Since aggregation objects can be created recursively, this makes interrogation of the model to find the properties of specific components easier, as successive aggregations create a hierarchy to facilitate navigation through the model. This is particularly useful for very large optimisation models. It also allows an entire district to be represented by a single, top-level object, one which stores the variable names (sorted by type), constraints and cost function terms of all aggregated sub-components in a single location. This means that the constraint and cost function properties from this single object can be passed to an optimisation solver at run time, reducing the programming effort required to locate and parse this information. Furthermore, when viewing the optimisation results, it is possible to retrieve all variable values of a given type, e.g. all control inputs, by simply referring to the top-level object.

In the following sections, various pre-defined modules and module modifiers are presented which provide useful functionality for the optimisation modelling framework, and which can already be found in the literature regarding multi-energy systems. Newly developed modules which form part of the main contributions of this thesis are highlighted as being 'Proposed' models. The modelling constraints in all pre-defined modules do not provide perfectly accurate descriptions of physical behaviour in each case, since simplifications are often required to obtain tractable problems. However, they are sufficiently accurate to describe steady-state, time-averaged energy flows through the system, the control of which is the primary concern for economic energy management.

3.3 Energy Conversion Device Modules

3.3.1 Boiler Module

Boilers are modelled as single input, single output devices which convert a given fuel input, $y_{k,\mathrm{b,in}}$, into useable heat, $y_{k,\mathrm{b,heat}}$, e.g. via biomethane combustion. The

rate of fuel input is determined by the control input, $u_{k,\mathrm{b}}$ and a constant conversion efficiency η_{b} is assumed. They are described by the following static constraints:

$$y_{k,\mathrm{b,in}} = u_{k,\mathrm{b}} \tag{3.9}$$

$$y_{k,\mathrm{b,heat}} = \eta_{\mathrm{b}} u_{k,\mathrm{b}} \tag{3.10}$$

$$0 \leq u_{k,\mathrm{b}} \leq \overline{u}_{k,\mathrm{b}} \tag{3.11}$$

The boiler module has one designated sink port, $y_{k,\mathrm{b,in}}$, and one source port, $y_{k,\mathrm{b,heat}}$.

3.3.2 Electrical Resistance Heater Module

Electrical resistance heaters are also modelled as single input, single output devices but are even simpler to model, since they convert 100% of the electrical input, $y_{k,\mathrm{rh,elec}}$, into useful heat output, $y_{k,\mathrm{rh,heat}}$, as dictated by the control input $u_{k,\mathrm{rh}}$. They are described by the following static constraints:

$$y_{k,\mathrm{rh,elec}} = u_{k,\mathrm{rh}} \tag{3.12}$$

$$y_{k,\mathrm{rh,heat}} = u_{k,\mathrm{rh}} \tag{3.13}$$

$$0 \leq u_{k,\mathrm{rh}} \leq \overline{u}_{k,\mathrm{rh}} \tag{3.14}$$

The electrical resistance heater module has one designated sink port, $y_{k,\mathrm{rh,elec}}$, and one source port, $y_{k,\mathrm{rh,heat}}$.

3.3.3 Transformer Module

Transformers are found throughout electrical networks and, since they are less than 100% efficient, it is important to model their conversion behaviour. Iron and copper losses may be modelled approximately using a single linear conversion efficiency coefficient η_{tx} relating the input and output [30]. However, a transformer permits electrical power to flow in either direction and is therefore a *bi-directional* device. To account for bi-directional flows, it is necessary to specify differing, reciprocal conversion efficiencies depending on whether the flow is in the forward direction, from $y_{k,\mathrm{tx,in}}$ to $y_{k,\mathrm{tx,out}}$, or in the reverse direction. Following the example of [25], both forward and reverse power flows can be described by the following constraint set:

$$y_{k,\mathrm{tx,in}} = z_{k,\mathrm{tx,in}} \tag{3.15}$$

$$y_{k,\text{tx,out}} = z_{k,\text{tx,out}} \tag{3.16}$$

$$z_{k,\text{tx,out}} = (\eta_{\text{tx}} - \frac{1}{\eta_{\text{tx}}}) z_{k,\text{tx,fwd}} + \frac{1}{\eta_{\text{tx}}} z_{k,\text{tx,in}} \tag{3.17}$$

$$-\overline{z}_{k,\text{tx,in}} \leq z_{k,\text{tx,in}} \leq \overline{z}_{k,\text{tx,in}} \tag{3.18}$$

$$-\overline{z}_{k,\text{tx,out}} \leq z_{k,\text{tx,out}} \leq \overline{z}_{k,\text{tx,out}} \tag{3.19}$$

together with the introduction of binary variable $\delta_{k,\text{tx,fwd}}$ and mixed-integer linear inequalities equivalent to the following logical conditions (see (C.1) and (C.2) in Appendix C):

$$z_{k,\text{tx,in}} \geq 0 \iff \delta_{k,\text{tx,fwd}} = 1 \tag{3.20}$$

$$z_{k,\text{tx,fwd}} = \delta_{k,\text{tx,fwd}} z_{k,\text{tx,in}} \tag{3.21}$$

The transformer output variable $y_{k,\text{tx,in}}$ is designated as a sink port and $y_{k,\text{tx,out}}$ is designated as a source port.

3.3.4 Combined Heat and Power Unit Module

Combined heat and power (CHP) units couple electricity, $y_{k,\text{chp,elec}}$, and heat, $y_{k,\text{chp,heat}}$, energy flows to a given fuel input, $y_{k,\text{chp,in}}$, such as biomethane, the amount of which is determined by the control input, $u_{k,\text{chp}}$. CHP units convert fuel into heat and electricity with differing efficiencies and are described most simply by the following static model constraints [30]:

$$y_{k,\text{chp,in}} = u_{k,\text{chp}} \tag{3.22}$$

$$y_{k,\text{chp,elec}} = \eta_{\text{elec}} u_{k,\text{chp}} \tag{3.23}$$

$$y_{k,\text{chp,heat}} = \eta_{\text{heat}} u_{k,\text{chp}} \tag{3.24}$$

$$0 \leq u_{k,\text{chp}} \leq \overline{u}_{k,\text{chp}} \tag{3.25}$$

The CHP module has one designated sink port, $y_{k,\text{chp,in}}$, and two source ports, $y_{k,\text{chp,elec}}$ and $y_{k,\text{chp,heat}}$.

3.3.5 Air-Source Heat Pump / Electric Chiller Module

Air-source heat pumps (ASHPs), similarly to a CHP, couple a heat energy output flow, $y_{k,\text{ahp,heat}}$, to an electrical input, $y_{k,\text{ahp,elec}}$, with the ratio of useful heating output to

electrical input known as the coefficient of performance, or COP. The operation of an ASHP is governed by the control input, $u_{k,\text{ahp}}$, and described by the following static model constraints [30]:

$$y_{k,\text{ahp,elec}} = u_{k,\text{ahp}} \tag{3.26}$$

$$y_{k,\text{ahp,heat}} = \text{COP} u_{k,\text{ahp}} \tag{3.27}$$

$$0 \leq u_{k,\text{ahp}} \leq \overline{u}_{k,\text{ahp}} \tag{3.28}$$

The output variables $y_{k,\text{ahp,elec}}$ and $y_{k,\text{ahp,heat}}$ are designated as a sink port and a source port, respectively.

A chiller is effectively an ASHP in reverse and can be modelled analogously, with the air acting as a heat sink rather than a heat source. The chiller provides useful heat extraction, $y_{k,\text{ahp,heat}} \leq 0$, from an electrical input, $y_{k,\text{ahp,elec}}$, in a ratio known as the energy efficiency ratio, or EER. Hence, if the COP in (3.41) is replaced by a negatively valued EER, the same module may be used to model an electric chiller.

3.3.6 Reversible Air-Source Heat Pump Module

A reversible ASHP is a multi-mode device which can provide either heating or cooling (heat extraction) using a given electrical input, $y_{k,\text{rahp,elec}}$. Depending on which mode is active, the heat flow, $y_{k,\text{rahp,heat}}$, is determined by multiplying the control input, $u_{k,\text{rahp}}$, by either a COP or EER constant. This is an amalgamation of the ASHP and chiller cases from the previous section, but requires additional logical conditions to determine which mode applies [30]. Following the example of [25], this can be represented with the constraints:

$$y_{k,\text{rahp,elec}} = u_{k,\text{rahp}} \tag{3.29}$$

$$y_{k,\text{rahp,heat}} = z_{k,\text{rahp,heat}} \tag{3.30}$$

$$z_{k,\text{rahp,heat}} = (\text{COP} + \text{EER}) z_{k,\text{rahp,fwd}} - \text{EER} u_{k,\text{rahp}} \tag{3.31}$$

$$0 \leq u_{k,\text{rahp}} \leq \overline{u}_{k,\text{rahp}} \tag{3.32}$$

$$-\overline{z}_{k,\text{rahp,heat}} \leq z_{k,\text{rahp,heat}} \leq \overline{z}_{k,\text{rahp,heat}} \tag{3.33}$$

together with the introduction of binary variable $\delta_{k,\text{rahp,fwd}}$ and mixed-integer linear inequalities equivalent to the following logical conditions ((C.1) and (C.2) in Appendix C):

$$z_{k,\text{rahp,heat}} \geq 0 \iff \delta_{k,\text{rahp,fwd}} = 1 \tag{3.34}$$

$$z_{k,\text{rahp,fwd}} = \delta_{k,\text{rahp,fwd}} u_{k,\text{rahp}} \tag{3.35}$$

The output variables $y_{k,\text{rahp,elec}}$ and $y_{k,\text{rahp,heat}}$ are designated as a sink port and a source port, respectively.

3.3.7 Water-Source Heat Pump Module

A water-source heat pump (WSHP) module is distinguished from an ASHP by an additional system output variable, $y_{k,\text{whp,cool}}$, which represents the flow of water from a heat source. Knowledge of this variable's value might be useful to determine water pumping requirements or to define a capacity limit on this flow. The WSHP is described by the following static model constraints [26]:

$$y_{k,\text{whp,elec}} = u_{k,\text{whp}} \tag{3.36}$$

$$y_{k,\text{whp,heat}} = \text{COP} u_{k,\text{whp}} \tag{3.37}$$

$$y_{k,\text{whp,cool}} = (\text{COP} - 1) u_{k,\text{whp}} \tag{3.38}$$

$$0 \leq u_{k,\text{whp}} \leq \overline{u}_{k,\text{whp}} \tag{3.39}$$

Sink and source ports are the same as for an ASHP, with $y_{k,\text{whp,cool}}$ designated as an additional sink port.

3.3.8 Absorption Chiller

An absorption chiller can be modelled similarly to an electrical chiller, except the EER refers to the ratio of (high temperature) heat input to the ratio of useful (low temperature) heat extraction. The following static model constraints are used to describe an absorption chiller:

$$y_{k,\text{ach,heatHT}} = u_{k,\text{ach}} \tag{3.40}$$

$$y_{k,\text{ach,heatLT}} = \text{EER} u_{k,\text{ach}} \tag{3.41}$$

$$0 \leq u_{k,\text{ach}} \leq \overline{u}_{k,\text{ach}} \tag{3.42}$$

The output variables $y_{k,\text{ach,heatHT}}$ and $y_{k,\text{ach,heatLT}}$ are each designated as sink ports.

3.3.9 Proposed Reversible Water-Source Heat Pump Module

The prosumer-enabled bi-directional ULTDHC concept is predicated on the ability to deliver both heating and cooling to/from the network and therefore individual buildings are able to operate their own reversible WSHPs. The reversible WSHP model described in [29] has been re-written to fit the general optimisation modelling framework used in this thesis, starting with the following equations:

$$y_{k,\text{hp,elec}} = \begin{cases} 1/\text{COP} \cdot y_{k,\text{hp,out}}, & \text{(heating mode)} \\ 1/\text{EER}(-y_{k,\text{hp,in}}), & \text{(cooling mode)} \end{cases} \tag{3.43}$$

$$y_{k,\text{hp,elec}} = |y_{k,\text{hp,out}} - y_{k,\text{hp,in}}| \tag{3.44}$$

$$\text{COP} = \eta_{\text{carnot,h}} \frac{\theta_{load}^{heat}}{\theta_{load}^{heat} - (\theta_w + \theta_c)/2} \tag{3.45}$$

$$\text{EER} = \eta_{\text{carnot,c}} \frac{\theta_{out}^{cool}}{(\theta_w + \theta_c)/2 - \theta_{load}^{cool}} \tag{3.46}$$

which account for the differences between the heating and cooling modes of the heat pump. When in heating mode, the positive heat output $y_{k,\text{hp,out}}$ is the product of the coefficient of performance (COP) and the electrical power input $y_{k,\text{hp,elec}}$. In cooling mode the direction of heat flow is reversed, so that the product of the energy efficiency ratio (EER) and the positive electrical power input must be equal to the negative value of heat flow at the input side, $y_{k,\text{hp,in}}$. Constant COP and EER values are assumed since the optimal temperature set points in the warm and cool pipes of the ULTDHC network, θ_w and θ_c, are fixed. The required temperatures to serve heating and cooling loads are θ_{load}^{heat} and θ_{load}^{cool}, respectively. The Carnot efficiencies $\eta_{\text{carnot,h}}$ and $\eta_{\text{carnot,c}}$ represent reductions from the theoretical maximum, or Carnot, COP and EER.

Following the example of [25], these equations can be expressed as the following constraint set:

$$y_{k,\text{rwhp,elec}} = u_{k,\text{rwhp}} \tag{3.47}$$

$$y_{k,\text{rwhp,in}} = z_{k,\text{rwhp,in}} \tag{3.48}$$

$$y_{k,\text{rwhp,out}} = z_{k,\text{rwhp,out}} \tag{3.49}$$

$$z_{k,\text{rwhp,in}} = ((\text{COP} - 1) + \text{EER}) z_{k,\text{rwhp,fwd}} - \text{EER} u_{k,\text{rwhp}} \tag{3.50}$$

$$z_{k,\text{rwhp,out}} = (\text{COP} + (\text{EER} + 1)) z_{k,\text{rwhp,fwd}} - (\text{EER} + 1) u_{k,\text{rwhp}} \tag{3.51}$$

$$0 \leq u_{k,\text{rwhp}} \leq \overline{u}_{k,\text{rwhp}} \tag{3.52}$$

$$-\overline{z}_{k,\text{rwhp,in}} \leq z_{k,\text{rwhp,in}} \leq \overline{z}_{k,\text{rwhp,in}} \tag{3.53}$$

$$-\overline{z}_{k,\text{rwhp,out}} \leq z_{k,\text{rwhp,out}} \leq \overline{z}_{k,\text{rwhp,out}} \tag{3.54}$$

together with the introduction of binary variable $\delta_{k,\text{rwhp,fwd}}$ and mixed-integer linear inequalities equivalent to the following logical conditions ((C.1) and (C.2) in Appendix C):

$$z_{k,\text{rwhp,in}} \geq 0 \iff \delta_{k,\text{rwhp,fwd}} = 1$$

$$z_{k,\text{rwhp,fwd}} = \delta_{k,\text{rwhp,fwd}} u_{k,\text{rwhp}}$$

The outputs $y_{k,\text{rwhp,elec}}$, $y_{k,\text{rwhp,in}}$ are designated as sink ports whilst $y_{k,\text{rwhp,out}}$ is a source port.

3.3.10 Proposed Bi-directional Fixed Speed Circulation Pump Module

Hydraulic circulation pumps are required to overcome the pressure losses due to friction when transporting liquids via pipes. They are therefore an integral part of district thermal networks and, since they are typically driven by electrical motors, also contribute to overall power consumption during network operation. A fixed-speed, bi-directional circulation pump model is introduced here since network pressure modelling is required to determine the power requirements of more efficient variable speed pumps; a variable speed pump model is introduced in the following chapter. Bi-directional flows at substations are required to switch between heating and cooling provision, enabled by a three-way valve configuration (Fig. 3.2). The fixed-speed, bi-directional circulation pump model introduced in [29] has been re-written to fit the general optimisation modelling framework used in this thesis.

The electrical power, $y_{k,\text{fsp,elec}}$, required by a fixed speed centrifugal pump is a non-linear function of both pressure added to the pumped fluid and the mass flowrate, $y_{k,\text{fsp,in}}$, through the pump. However, a good linear approximation of this relationship can be easily found by fitting a first-order model to manufacturer data over the operational range of $y_{k,\text{fsp,in}}$ [107]–[109]:

$$y_{k,\text{fsp,elec}} = a_{\text{fsp,on}} + b_{\text{fsp}} \cdot y_{k,\text{fsp,in}} \tag{3.55}$$

where the standby power $a_{\text{fsp,on}}$ and coefficient b_{fsp} are constants that can be obtained from characteristic pump curves. Although the flow through a real pump is always

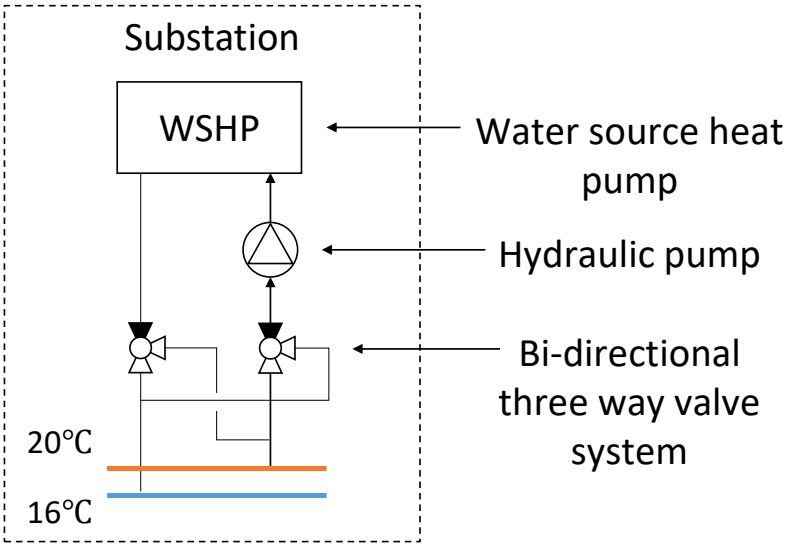

Figure 3.2: Illustration of a bi-directional ULTDHC substation, adapted from [19].

in one direction, for modelling purposes the action of three-way valves is captured within the pump module, such that the sign of output variable $y_{k,\text{fsp,in}}$ can be negative or positive to indicate flow direction. Therefore, the linear approximation for a bi-directional fixed speed circulation pump becomes:

$$y_{k,\text{fsp,elec}} = a_{\text{fsp,on}} + b_{\text{fsp}} \cdot |y_{k,\text{fsp,in}}| \tag{3.56}$$

As this is no longer a linear relationship, this equation is expressed as the following constraint set, using the example of [25]:

$$y_{k,\text{fsp,elec}} = z_{k,\text{fsp,elec}} \tag{3.57}$$

$$y_{k,\text{fsp,in}} = z_{k,\text{fsp,flow}} \tag{3.58}$$

$$y_{k,\text{fsp,out}} = z_{k,\text{fsp,flow}} \tag{3.59}$$

$$z_{k,\text{fsp,elec}} = a_{\text{fsp,on}} + 2b_{\text{fsp}} z_{k,\text{fsp,fwd}} - b_{\text{fsp}} z_{k,\text{fsp,flow}} \tag{3.60}$$

$$0 \leq z_{k,\text{fsp,elec}} \leq \overline{z}_{k,\text{fsp,elec}} \tag{3.61}$$

$$\underline{z}_{k,\text{fsp,flow}} \leq z_{k,\text{fsp,flow}} \leq \overline{z}_{k,\text{fsp,flow}} \tag{3.62}$$

together with the introduction of binary variable $\delta_{k,\text{fsp,fwd}}$ and mixed-integer linear inequalities equivalent to the following logical conditions ((C.1) and (C.2) in Appendix C):

$$z_{k,\text{fsp,flow}} \geq 0 \iff \delta_{k,\text{fsp,fwd}} = 1$$

$$z_{k,\text{fsp,fwd}} = \delta_{k,\text{fsp,fwd}} z_{k,\text{fsp,flow}}$$

The outputs $y_{k,\text{fsp,elec}}$, $y_{k,\text{fsp,in}}$ are designated as sink ports whilst $y_{k,\text{fsp,out}}$ is a source port.

3.3.11 Proposed Bi-Directional Variable Speed Pump Module

As discussed in Section 3.6.3, circulation pumps are required to provide a pressure gain at each substation. Since the pumps are electrically driven, they are also a point of coupling between the electricity and ULTDHC systems. The pressure gain $y_{k,\text{vsp}\Delta H}$ and mass flow into the pump $y_{k,\text{vsp,in}}$ are already determined by the ULTDHC network model, an equation is therefore needed to determine the electrical power, $y_{k,\text{vsp,elec}}$, used at this operating point:

$$y_{k,\text{vsp,elec}} = \frac{\rho \cdot g \left| y_{k,\text{vsp,in}} \right| y_{k,\text{vsp}\Delta H}}{\eta_m \cdot \eta_h} \tag{3.63}$$

where the motor efficiency η_m and hydraulic efficiency η_h are assumed constant [78]. This equation is bilinear and involves a discontinuity because electrical power is consumed whether the pump is acting on a positive or negative valued mass flow. The discontinuity can be hidden by following the example of [25] and introducing the auxiliary variables $\delta_{k,\text{vsp,fwd}}$ and $z_{k,\text{vsp,fwd}}$:

$$y_{k,\text{vsp,elec}} = z_{k,\text{vsp,elec}} \tag{3.64}$$

$$y_{k,\text{vsp,in}} = z_{k,\text{vsp,in}} \tag{3.65}$$

$$y_{k,\text{vsp,out}} = z_{k,\text{vsp,out}} \tag{3.66}$$

$$y_{k,\text{vsp},\Delta H} = z_{k,\text{vsp},\Delta H} \tag{3.67}$$

$$z_{k,\text{vsp,in}} = z_{k,\text{vsp,out}} \tag{3.68}$$

$$z_{k,\text{vsp,elec}} = 2C_{\text{vsp}} z_{k,\text{vsp,fwd}} z_{k,\text{vsp},\Delta H} - C_{\text{vsp}} z_{k,\text{vsp,in}} z_{k,\text{vsp},\Delta H} \tag{3.69}$$

where $C_{\text{vsp}} = \dfrac{\rho \cdot g}{\eta_m \cdot \eta_h}$

together with mixed-integer linear inequalities equivalent to the following logical conditions ((C.1) and (C.2) in Appendix C:

$$z_{k,\text{vsp,in}} \geq 0 \iff \delta_{k,\text{vsp,fwd}} = 1 \tag{3.70}$$

$$z_{k,\text{vsp,fwd}} = \delta_{k,\text{vsp,fwd}} z_{k,\text{vsp,in}} \tag{3.71}$$

This does not address the bilinear term in (3.63). However, an approximate McCormick relaxation can be used to replace bilinear terms and make the model convex. Since this relaxation is automatically carried out on bilinear terms by the mixed-integer solver Gurobi [110], the procedure is not explicitly described here. Moreover, when using the multi-agent approach described in Chapter 7, an iterative procedure is used to avoid the bilinear term altogether, by fixing the value of pump pressure head.

The outputs $y_{k,\text{vsp,elec}}$, $y_{k,\text{vsp,in}}$ are designated as sink ports whilst $y_{k,\text{vsp,out}}$ is a source port.

3.3.12 Conversion Device Operational Behaviour Modifiers

Modules can be selectively modified by adding pre-defined constraints and any necessary auxiliary variables to model more complex operational behaviour, i.e. device on/off states, ramp rates and minimum up and down times. In each case the modification applies to any single given variable, $v_{k,j}$, from the set of all decision variables in the module, $\boldsymbol{v}_k := \left[\boldsymbol{x}_k^\top \ \boldsymbol{u}_k^\top \ \boldsymbol{\delta}_k^\top \ \boldsymbol{z}_k^\top\right]^\top$.

On/Off States

Device on/off states are required to represent the condition that a given device is either off, with $v_{k,j} = 0$, or on, with some minimum value $v_{k,j} > 0$. For any given variable, $v_{k,j,}$ to which this applies, the following constraint may be added, based on the example of [26]:

$$\delta_{k,v_j,\text{on}}\underline{v}_{k,j} \leq v_{k,j} \leq \delta_{k,v_j,\text{on}}\overline{v}_{k,j} \tag{3.72}$$

where $\delta_{k,v_j,\text{on}}$ is a binary auxiliary variable, which takes the value '1' when the device is on, and $\underline{v}_{k,j}$ and $\overline{v}_{k,j}$ are the minimum and maximum values of $v_{k,j}$, respectively.

Ramp Rate Limits

If a device has restrictions on the rate at which a given variable value can be increased or decreased, this can be captured with ramp rate constraints [26]. By introducing a continuous auxiliary variable, $z_{k,v_j,\text{ramp}}$, the following constraints can be added to represent ramp rate restrictions:

$$v_{k,j} = v_{k-1,j} + z_{k,v_j,\text{ramp}} \tag{3.73}$$

$$\underline{z}_{v_j,\text{ramp}} \leq z_{k,v_j,\text{ramp}} \leq \overline{z}_{v_j,\text{ramp}} \tag{3.74}$$

where $\underline{z}_{v_{kj},\text{ramp}}$ and $\overline{z}_{v_j,\text{ramp}}$ are the minimum and maximum possible value changes per discrete sampling interval duration. Note that for the current sampling instance $k = \hat{k}$, the constraint set (3.73) includes a time-varying constraint, since $v_{\hat{k}-1,j}$ is a measured input which is repeatedly updated.

Minimum Up and Down Time Limits

It may be necessary to prevent continuous switching between a device's on and off states, for example to improve efficiency, or prevent wear, by reducing the number of start-up and shut-down events. This can be enforced with minimum up and down time constraints, which specify that a device must be switched on for a minimum number of discrete sampling intervals, T_{up}, or switched off for a given number of intervals, T_{dn}. In addition to the on/off state constraint (3.72), the following constraints are also added [25]:

$$\delta_{k,v_j,\text{on}} - \delta_{k-1,v_j,\text{on}} \leq \delta_{\tau_{\text{up}},v_j,\text{on}}, \quad \forall k \tag{3.75}$$

$$\delta_{k-1,v_j,\text{on}} - \delta_{k,v_j,\text{on}} \leq 1 - \delta_{\tau_{\text{dn}},v_j,\text{on}}, \quad \forall k \tag{3.76}$$

where $\tau_{\text{up}} = k+1, ..., \min\{k+T_{\text{up}}-1, H\}$ is the index of sampling intervals for which a device must remain on after switching on and $\tau_{\text{dn}} = k+1, ..., \min\{k+T_{\text{dn}}-1, H\}$ is the index of sampling intervals for which a device must remain off after switching off. Each index set is limited by the prediction horizon, H. Note that for the current sampling instance $k = \hat{k}$, the constraints (3.75) and (3.76) are time varying, since $\delta_{\hat{k}-1,v_j,\text{on}}$ is a measured input which is repeatedly updated. Furthermore, the control scheme must consider the device's on/off status history to capture device switching which has occurred prior to $\hat{k}-1$:

$$\boldsymbol{\sigma}_{\text{up}} \leq \boldsymbol{\delta}_{\hat{\tau}_{\text{up}},v_j,\text{on}} \tag{3.77}$$

$$\boldsymbol{\sigma}_{\text{dn}} \leq \mathbb{1}^{T_{\text{dn}}-1} - \boldsymbol{\delta}_{\hat{\tau}_{\text{dn}},v_j,\text{on}} \tag{3.78}$$

where $\sigma_{\text{up}} \in \mathbb{Z}^{T_{\text{up}}-1}$ and $\sigma_{\text{dn}} \in \mathbb{Z}^{T_{\text{dn}}-1}$ are repeatedly updated binary vector inputs to the control scheme based on past on/off states. Non-zero elements of these vectors force corresponding on/off status variables indexed by $\hat{\tau}_{\text{up}} = \hat{k}+1, ..., \hat{k}+T_{\text{up}}-2$ or $\hat{\tau}_{\text{dn}} = \hat{k}+1, ..., \hat{k}+T_{\text{dn}}-2$ to take the value 1 or 0, respectively, whereas zero elements have no effect.

3.4 Storage Device Modules

3.4.1 Battery Storage Module

Batteries provide essential storage capability for electrical system flexibility but exhibit losses upon charging and discharging due to internal resistance. Like trans-

formers, losses must be modelled for both the forward and reverse flows through the battery, requiring separate charging and discharging efficiencies. The state-space battery storage model from [25] describes separate charging and discharging efficiencies which apply to mutually exclusive charging and discharging states, represented by the following constraints:

$$x_{k+1,\text{batt}} = (1 - L_{\text{batt}})x_{k,\text{batt}} + (\eta_{\text{chg}} - \frac{1}{\eta_{\text{dchg}}})z_{k,\text{batt,chg}}\Delta t + \frac{1}{\eta_{\text{dchg}}}u_{k,\text{batt,chg}}\Delta t \tag{3.79}$$

$$y_{k,\text{batt,chg}} = u_{k,\text{batt,chg}} \tag{3.80}$$

$$\underline{x}_{k,\text{batt}} \leq x_{k,\text{batt}} \leq \overline{x}_{k,\text{batt}} \tag{3.81}$$

$$\underline{u}_{k,\text{batt,chg}} \leq u_{k,\text{batt,chg}} \leq \overline{u}_{k,\text{batt,chg}} \tag{3.82}$$

with the introduction of binary variable $\delta_{k,\text{batt,chg}}$ and the following logical conditions ((C.1) and (C.2) in Appendix C):

$$u_{k,\text{batt,chg}} \geq 0 \iff \delta_{k,\text{batt,chg}} = 1 \tag{3.83}$$

$$z_{k,\text{batt,chg}} = \delta_{k,\text{batt,chg}} u_{k,\text{batt,chg}} \tag{3.84}$$

where $x_{k,\text{batt}}$ is the amount of energy stored in the battery, $u_{k,\text{batt,chg}}$ is the control input, η_{chg} and η_{dchg} are the efficiencies of charging and discharging, respectively, and L_{batt} is the standby loss factor due to battery self discharge. The output amount of battery charging $y_{k,\text{batt,chg}}$ is designated as a sink port.

3.4.2 Thermal Storage Module

Assuming a perfectly mixed water vessel and well insulated pipes, the only losses considered from thermal storage are due to heat transfer through vessel walls to the surroundings. Therefore a simple state-space model is used for thermal storage modules [26]:

$$x_{k+1,\text{thm}} = (1 - L_{\text{thm}})x_{k,\text{thm}} + u_{k,\text{thm,chg}}\Delta t \tag{3.85}$$

$$y_{k,\text{thm,chg}} = u_{k,\text{thm,chg}} \tag{3.86}$$

$$\underline{x}_{k,\text{thm}} \leq x_{k,\text{thm}} \leq \overline{x}_{k,\text{thm}} \tag{3.87}$$

$$\underline{u}_{k,\text{thm,chg}} \leq u_{k,\text{thm,chg}} \leq \overline{u}_{k,\text{thm,chg}} \tag{3.88}$$

where $x_{k,\text{thm}}$ is the amount of energy stored, $u_{k,\text{thm,chg}}$ is the control input and L_{thm} is the standby loss factor for loss of energy to the surroundings. The output amount of storage charging, $y_{k,\text{thm}}$, is designated as a sink port.

3.5 Prosumer Modules

3.5.1 Fixed Generation / Demand Modules

Fixed energy generation/demand is the term given to system input/output energy flows that cannot be controlled, only forecasted; they are acknowledged, or 'known', disturbances to the system. These are modelled as fixed flows into or out of the system, equivalent to the current (measured) and future (forecasted) values. Such an approach in an MPC setting is known as *certainty-equivalent* MPC [111], in which an uncertain optimisation problem is transformed into a deterministic one by assuming that all future disturbances are equal to deterministic estimates.

All fixed energy generation/demand modules follow the example of [26]. The known disturbance variables $w_{k,\text{fixd},j}$ are the predicted profiles of generation/demand j from a chosen forecasting method; the first element in $\boldsymbol{w}_{\text{fixd},j}$ is the current measured value of the disturbance.

$$y_{k,\text{fixd},j} = w_{k,\text{fixd},j} \tag{3.89}$$

The output $y_{k,\text{fixd},j}$ is designated as a sink port. For a fixed generation flow, the values of $\boldsymbol{w}_{\text{fixd},j}$ are negative.

3.5.2 Flexible Demand Modules

Flexible demands are controllable energy flows out of a system that may be manipulated in some way whilst still delivering a nominal amount of energy. These demands have been formally categorised for a multi-energy system in [30] as being either shiftable, adjustable, pliable or interruptible, or indeed any combination of these categories. The constraints required to model each of these demands are given below; for details on how these flexible demand types might be combined to derive new compound flexibility types, the reader is referred to [30]. The following definitions and general constraints are common to all types of flexible demand.

Each cyclic flexible demand, n, has a cycle duration of N_n^c discrete time periods. The cycle itself is split into N_n^{ph} *phases*, with the length of the i^{th} phase equal to $N_{n,i}^p$ discrete periods. For example, a flexible demand may have a daily cycle length

$N_n^c = 24$ one hour periods and within this cycle the demand may be split into three phases ($N_n^{ph} = 3$) of length $N_{n,1}^p = N_{n,2}^p = N_{n,3}^p = 8$ periods.

During each phase of the cycle, a nominal amount of energy, $E_{n,i}$, is to be consumed. The amount of energy actually consumed by demand n in any given time period, $y_{k,n}$, is given by:

$$y_{k,n} = \sum_{i=1}^{N_n^{ph}} u_{k,n,i}, \quad \forall k, n \tag{3.90}$$

where $\boldsymbol{u}_{k,n} \in \mathbb{R}^{N_n^{ph}}$ is a vector of consumption amounts in each phase of demand at time k. Each element of $\boldsymbol{u}_{k,n}$ is associated with:

- a binary auxiliary variable, $\delta_{k,n,i}^p$, which indicates whether a given phase is being processed in any given time period;
- a second binary variable, $\delta_{k,n,i}^c$, which indicates whether a given phase has already been completed in any given time period; and
- a third binary variable, $\delta_{k,n,i}^w$, which indicates whether a phase is waiting to start in any given time period.

These binary indicator values are defined by the following set of constraints:

$$\underline{u}_{k,n,i}\delta_{k,n,i}^p \leq u_{k,n,i} \leq \overline{u}_{k,n,i}\delta_{k,n,i}^p, \quad \forall k, n, i \tag{3.91}$$

$$\delta_{k,n,i}^p + \delta_{k,n,i}^c \leq 1, \quad \forall k, n, i \tag{3.92}$$

$$\delta_{k-1,n,i}^p - \delta_{k,n,i}^p \leq \delta_{k,n,i}^c, \quad \forall k, n, i \tag{3.93}$$

$$\delta_{k-1,n,i}^c \leq \delta_{k,n,i}^c, \quad \forall k, n, i \tag{3.94}$$

$$\delta_{k,n,i}^p \leq \delta_{k,n,i-1}^c, \quad \forall k, n, i \in \{2 : N_n^{ph}\} \tag{3.95}$$

These constraints ensure that:

- a phase cannot be both processing and complete at once (3.92);
- a phase may only be considered complete once it is no longer processing (3.93);
- once complete, a phase must remain complete for the remainder of the prediction horizon (3.94); and
- the subsequent phase may only begin processing once the previous phase is complete (3.95).

The following section presents the constraint set that defines and differentiates a pliable demand module, which is needed in addition to the common constraints (3.90)-(3.95). The remaining flexible demand modules are not actually employed to generate results referred to in later chapters, therefore these are presented in Appendix D for the interested reader.

Pliable Demand Module

A pliable demand allows consumption within each time period to vary, provided that the nominal energy consumption of each multi-period phase is satisfied before the phase has finished processing. The specific constraints for a pliable demand are as follows:

$$\sum_{k=1}^{H} u_{k,\text{plia},i} = E_{\text{plia},i}, \quad \forall i \tag{3.96}$$

$$\underline{N}^{p}_{\text{plia},i} \leq \sum_{k=1}^{H} \delta^{p}_{k,\text{plia},i} \leq \overline{N}^{p}_{\text{plia},i}, \quad \forall i \tag{3.97}$$

$$\delta^{p}_{k_c,\text{plia},1} = 1 \tag{3.98}$$

$$\delta^{c}_{k,\text{plia},i-1} = \delta^{p}_{k,\text{plia},i} + \delta^{c}_{k,\text{plia},i} \quad \forall k, n, i \in \{2 : N^{ph}_{\text{plia}}\} \tag{3.99}$$

where $\underline{N}^{p}_{\text{plia},i}$ and $\overline{N}^{p}_{\text{plia},i}$ are the minimum and maximum number of periods over which a given phase can be processed. These constraints ensure that:

- the nominal amount of energy is consumed in each phase within the prediction horizon (3.96);
- each phase must be completed within a given range of time periods (3.97);
- the demand commences at a given time period k_c (3.98); and
- each phase starts immediately after the preceding phase (3.99).

In a receding horizon control scheme, the constants $E_{\text{plia},i}, \underline{N}^{p}_{\text{plia},i}$ and $\overline{N}^{p}_{\text{plia},i}$ need to be updated between each call to the optimisation solver. A programmable logic controller (PLC) can fulfil this updating role, performing the following assignments at the end of each time period:

$$E_{\text{plia},i} = E_{\text{plia},i} - u_{k,\text{plia},i}, \quad \forall i \tag{3.100}$$

$$\underline{N}^{p}_{\text{plia},i} = \begin{cases} \underline{N}^{p}_{\text{plia},i}, & \text{if } \delta^{p}_{k,\text{plia},i} = 0 \\ \underline{N}^{p}_{\text{plia},i} - 1, & \text{if } \delta^{p}_{k,\text{plia},i} = 1 \text{ and } \underline{N}^{p}_{\text{plia},i} > 0 \\ 0, & \text{otherwise} \end{cases} \tag{3.101}$$

$$\overline{N}^{p}_{\text{plia},i} = \begin{cases} \overline{N}^{p}_{\text{plia},i}, & \text{if } \delta^{p}_{k,\text{plia},i} = 0 \\ \overline{N}^{p}_{\text{plia},i} - 1, & \text{if } \delta^{p}_{k,\text{plia},i} = 1 \text{ and } \overline{N}^{p}_{\text{plia},i} > 0 \\ 0, & \text{otherwise} \end{cases} \tag{3.102}$$

The PLC would also iterate through the nominal energy consumption profile at the end of each demand cycle.

3.6 Network Modules

3.6.1 Simple Network Power Balance Module

To facilitate modelling of energy exchanges between buildings via AC power, gas and ULTDHC networks, a simple power balance representation of energy networks is presented here. The intention is to avoid modelling of non-linear physical relationships and to therefore ensure a tractable optimisation problem.

The following modelling assumptions are made to avoid introducing non-linearities into the simple network module:

1. Hydraulic circulation pumps are capable of supplying the required pressure head of water at maximum flow conditions;
2. Gas pressure sufficient for maximum flow is provided from an external distribution network, upstream of the district network;
3. ULTDHC substation return temperatures to warm and cold network pipes are maintained at fixed, pre-defined set-points, since the sampling time of the considered control scheme is significantly longer than that imposed by low-level temperature controllers;
4. A single-phase, balanced AC power network is considered; and
5. Nominal voltage is maintained throughout the AC power network and resistive losses are negligible.

Assumptions 1) and 2) should be satisfied when infrastructure is correctly designed to work at maximum flow conditions. With these in place there is no maximum pressure constraint to be considered in either network and therefore pressure changes do not need to be modelled. The assumption of fixed set-point temperatures in 3) is based on [72], in which constant optimal set-point temperatures are identified for thermal networks serving heating and cooling loads; it is shown that the fixed-temperature approach offers comparable performance to varying temperatures, yet is much simpler to implement. If temperatures are assumed fixed, then temperature changes do not need to be modelled. Lastly, assumptions 4) and 5) are commonly used to simplify AC network modelling. Hence, voltage changes do not need to be modelled, only the balance of real power needs to be determined. These assumptions are considered to be valid when modelling a small district with simple structure, since power is transferred over relatively short distances.

Let $\mathcal{G}^n = (\mathcal{N}^n, \mathcal{A}^n)$ be a directed graph representing given network of energy type n, where nodes $\mathcal{N}^n := \left\{0, 1, ..., N^{\text{nodes}}\right\}$ represent buses or substations in the network and each arc $\mathcal{A}^n \subseteq N^n \times N^n$ represents a distribution line or pipe. Denote an arc originating at node i and ending at node j as (i, j), let $z_{k,P_{ij,n}}$ be the power flow along arc (i, j) and $y_{k,p_{j,n}}$ be the power injections at each node j. A generic energy balance at each node may be used to determine energy flows between them:

$$y_{k,p_{j,n}} = \sum_{l:j\to l} z_{k,P_{jl,n}} - \sum_{i:i\to j} z_{k,P_{ij,n}} \tag{3.103}$$

so that power leaving a network at any given node takes a negative value. The output $y_{k,p_{j,n}}$ is designated as a source port.

3.6.2 AC Power Flow Module

An optimal power flow problem using SOCP constraints is used to accurately model internal AC electricity networks, taken from [60]. This problem describes a balanced, radial network with a pre-specified set of bus power injections. The optimal solution determines the required power injection at the slack bus, as well as line powers, currents and bus voltages, which are constrained to be within statutory limits.

Let $\mathcal{G}^E = (\mathcal{N}^E, \mathcal{A}^E)$ be a directed graph representing a radial AC network, where nodes $\mathcal{N}^E := \{0, 1, ..., n\}$ represent buses in the network and each arc $\mathcal{A}^E \subseteq \mathcal{N}^E \times \mathcal{N}^E$ represents a distribution line. Denote an arc originating at node i and ending at node

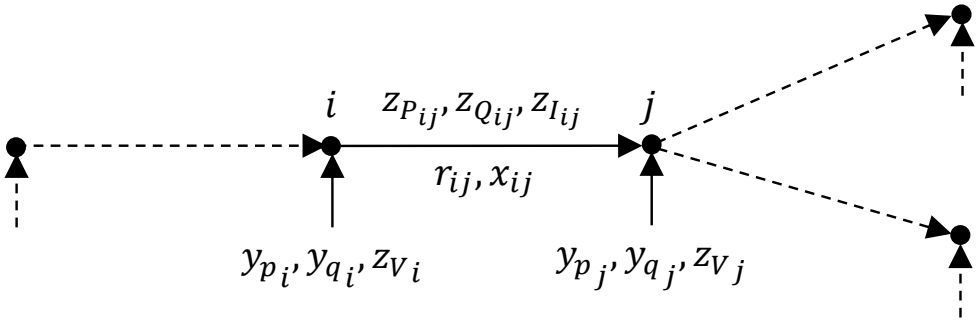

Figure 3.3: Generic representation of AC network section.

j as (i, j) and let R_{ij} and X_{ij} be the resistance and reactance on that line. Let $z_{k,P_{ij}}$ and $z_{k,Q_{ij}}$ be the sending end active and reactive power flows along line (i, j) and let y_{k,p_j} and y_{k,q_j} be the active and reactive power injections at each bus j. Let $z_{k,I_{ij}}$ be the complex current along line (i, j) and $z_{k,\ell_{ij}}$ the magnitude of current squared. Finally, let z_{k,V_j} be the complex voltage at each bus j and z_{k,ν_j} the magnitude of voltage squared. The root of the graph $\mathcal{G}^E$ (node 0) represents the substation bus which is connected to a higher voltage network and is given a reference voltage z_{k,ν_0} of 1 p.u. The orientation of the directed graph is chosen with all arcs directed away from the root node, as shown in Fig. 3.3.

The branch flow model for radial networks is relaxed to form the following convex model (3.104) - (3.106), $\forall j \in \mathcal{N}^E$ and (3.107), $\forall (i, j) \in \mathcal{A}^E$ [60]:

$$y_{k,p_j} = \sum_{l:j\to l} z_{k,P_{jl}} - \sum_{i:i\to j} (z_{k,P_{ij}} - R_{ij} z_{k,\ell_{ij}}) \tag{3.104}$$

$$y_{k,q_j} = \sum_{l:j\to l} z_{k,Q_{jl}} - \sum_{i:i\to j} (z_{k,Q_{ij}} - X_{ij} z_{k,\ell_{ij}}) \tag{3.105}$$

$$z_{k,\nu_i} - z_{k,\nu_j} - 2(R_{ij} z_{k,P_{ij}} + X_{ij} z_{k,Q_{ij}}) + (R_{ij}^2 + X_{ij}^2) z_{k,\ell_{ij}} = 0 \tag{3.106}$$

$$z_{k,P_{ij}}^2 + z_{k,Q_{ij}}^2 - z_{k,\ell_{ij}} z_{k,\nu_i} \leq 0 \tag{3.107}$$

The outputs y_{k,p_j} and y_{k,q_j} are designated as source ports.

Due to the inequality in (3.107), it is necessary to solve the model as a minimisation problem with an objective that is strictly increasing in $z_{k,\ell_{ij}}$ [60]. A value cost modifier (see Section 3.7) associated with $z_{k,\ell_{ij}}$ is therefore added to the AC electrical network module:

$$c_{k,\text{AC}} = \sum_{i\to j \in A^E} \lambda_{\ell_{ij}}^{\text{val}} z_{k,\ell_{ij}} \tag{3.108}$$

with $\lambda_{\ell_{ij}}^{\text{val}} > 0$, which is intended to help recover an *exact*, feasible solution from the model, i.e. when (3.107) is satisfied to equality.

3.6.3 Proposed ULTDHC Network Module

Based on a review of existing operational examples, several classifications of ULTDHC networks can be made [19]. These are whether the network is an open or closed system, the number of pipelines used at differing temperature levels, if the network is radial or in a ring topology and whether energy and mass flows within the network are uni- or bi-directional. Here a closed system of two pipelines is considered, one warm and one cool, with bi-directional flows between them [29]. The model which is proposed can be applied to networks with a radial or ring topology.

The modelled ULTDHC network connects a number of different users which are referred to as *substations*. These are subdivided into *prosumer, plant* and *storage* substations, using the terminology of [78]. Prosumer substations are responsible for covering a fluctuating heating or cooling demand, acting as a thermal producer or consumer, depending on whether they are supplying or extracting heat to/from a building or process. When in heating mode, prosumers draw water from the warm pipe, extract some heat and then discharge the water into the cool pipe. In cooling mode, prosumers withdraw water from the cool pipe, use the water for cooling and discharge into the warm pipe. The direction of mass flow between the two pipes is therefore reversed in each of the two modes, i.e. flows are bi-directional.

Plant substations, on the other hand, must balance the net annual thermal demand of all prosumers in the network, providing a regular service as a heat source (or sink), depending on whether there is a net annual deficit (or surplus) of heat from prosumer substations. Examples of plant substations include sewage plants, combined heat and power plants and solar thermal collectors.

Storage substations are needed to balance the instantaneous demand for heating or cooling in a closed network, since the thermal energy provided by plant substations will not always balance the net demand from prosumer substations. A typical example is the difference between summer and winter seasons, exhibiting a surplus of heat rejected to the network in the summer and a deficit of heat in the winter. Flows through storage substations are bi-directional to accommodate both charging and discharging modes.

Since substations can exchange water with the network pipes bi-directionally, the pressure profile around the network will vary depending on the actions of individual

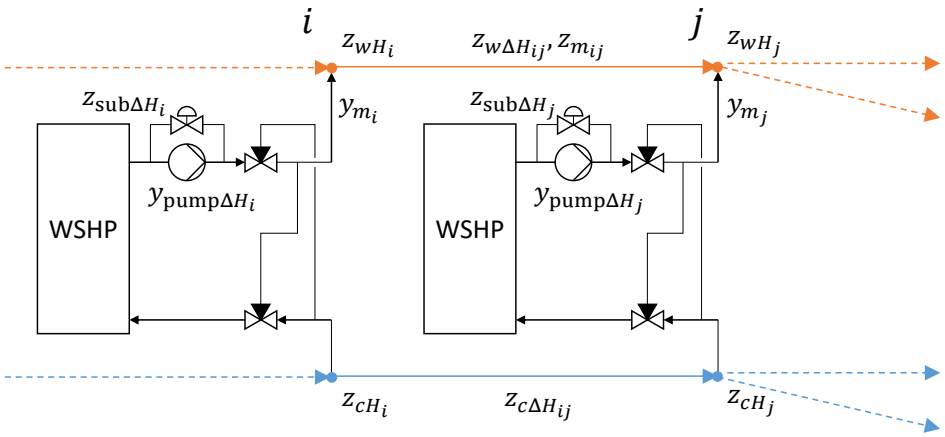

Figure 3.4: Generic representation of ULTDHC network section.

substations. It will sometimes be necessary for a building to withdraw water from a pipe at a lower pressure than that of the intended discharge pipe, therefore each building must operate its own decentralised circulation pump; a pump bypass line with throttling valve is required for the opposite scenario where an building withdraws from the pipe at higher pressure. However, pump-to-pump interactions in bi-directional ULTDHC networks can cause feedback control loops to become unstable, with pumps continuously adjusting their speed [76]. This is a primary benefit of the proposed network model: to be able to determine an optimal pump dispatch at a higher control level so that pump speeds are coordinated throughout the network.

The following modelling assumptions, some of which are carried over from the previous section, are necessary to ensure validity of the proposed ULTDHC module:

1. ULTDHC substation return temperatures to warm and cold network pipes are maintained at fixed, pre-defined set-points, since the sampling time of the considered control scheme is significantly longer than that imposed by low-level temperature controllers; and

2. Large, inter-seasonal thermal storage substations, for example geothermal borehole fields, are able to balance heating and cooling loads annually so that instantaneous prosumer substation demands are always satisfied.

With these assumptions, modelling of the ULTDHC network can be reduced to a water flow problem, determining the mass flows and pressures around the network for a given set of inputs, i.e. exchanges between substations and the network.

Let $\mathcal{G}^W = (\mathcal{N}^W, \mathcal{A}^W)$ be a directed graph representing the warm side of the ULTDHC network, where nodes $\mathcal{N}^W := \{0, 1, ..., n\}$ represent junctions in the network and

each arc $\mathcal{A}^W \subseteq \mathcal{N}^W \times \mathcal{N}^W$ represents a pipe. Denote an arc originating at node i and ending at node j as (i, j). The mass flow of water injected to the warm side at each junction j is y_{k,m_j}, whilst $z_{k,\mathrm{w}H_j}$ is the pressure head of water at that point in $\mathrm{m_{H_2O}}$. Pressure head at the cold side of junction j is denoted $z_{k,\mathrm{c}H_j}$. Let $z_{k,\mathrm{sub}\Delta H_j} \geq 0$ be the head loss that occurs with flow y_{k,m_j} through pressure reducing elements of a substation located at j. The head gain supplied by the substation pump is denoted $z_{k,\mathrm{pump}\Delta H_j} \geq 0$. Let $z_{k,\mathrm{w}\Delta H_{ij}} \geq 0$ be the frictional head loss between the ends of pipe (i, j) for a given mass flow $z_{k,m_{ij}}$. By convention head loss in a pipe is given a positive value, whilst flow $z_{k,m_{ij}}$ is considered positive in the direction from i to j (see Fig. 3.4). Another convention is defined that heating supplied to a substation from a warm pipe is given by a negative flow of warm water y_{k,m_j} at a node j, whereas rejection of heat at a substation is given by a positive nodal flow.

Assuming incompressible flow and constant water properties, the equation for conservation of mass at each node $j \in \mathcal{N}^W$ (3.110) and the Darcy-Weisbach pressure drop equation in all warm pipes $(i, j) \in \mathcal{A}^W$ (3.111) can be defined [54]:

$$y_{k,m_j} = z_{k,m_j} \tag{3.109}$$

$$z_{k,m_j} - \sum_{l:j\to l} z_{k,m_{jl}} + \sum_{l:l\to j} z_{k,m_{lj}} = 0 \tag{3.110}$$

$$C_{ij} z_{k,m_{ij}} \left| z_{k,m_{ij}} \right| - z_{k,\mathrm{w}H_i} + z_{k,\mathrm{w}H_j} = 0 \tag{3.111}$$

$$\text{where } C_{ij} = \frac{8 L_{\mathrm{pipe}} f}{g D^5 \rho^2 \pi^2}$$

where L_{pipe} is the pipe length in m, f is the pipe friction factor (assumed constant), $g = 9.81$ m$/s^2$ is gravitational acceleration, D is the internal diameter of the pipe in m and $\rho = 998$ kg/m^3 is the density of water. Constraint (3.111) is piecewise quadratic due to the bilinear term which accounts for the direction of pressure drop. This can be reformulated in terms of absolute pressure drop:

$$C_{ij} z_{k,m_{ij}}^2 - z_{k,\mathrm{w}\Delta H_{ij}} = 0 \tag{3.112}$$

with the addition of mixed-integer linear inequalities and the binary indicator variable $\delta_{k,m_{ij}}$ to express the following logic (see (C.1) and (C.3) in Appendix C):

$$z_{k,m_{ij}} \geq 0 \iff \delta_{k,m_{ij}} = 1 \tag{3.113}$$

$$z_{k,m_{ij}} \geq 0 \implies z_{k,\mathrm{w}H_i} + z_{k,\mathrm{w}H_j} = z_{k,\mathrm{w}\Delta H_{ij}} \tag{3.114}$$

$$z_{k,m_{ij}} \leq 0 \implies z_{k,\mathrm{w}H_i} + z_{k,\mathrm{w}H_j} = -z_{k,\mathrm{w}\Delta H_{ij}} \tag{3.115}$$

where $z_{k,\mathrm{w}\Delta H_{ij}} \geq 0$ is ensured due to the squared term in (3.112).

Constraint (3.112) is no longer piecewise but is still a non-convex quadratic equality; it must be relaxed to a convex inequality in order to be solved efficiently:

$$C_{ij} z_{k,m_{ij}}^2 - z_{k,\mathrm{w}\Delta H_{ij}} \leq 0 \tag{3.116}$$

This particular reformulation to (3.116) is chosen over comparable approaches [61], [63] because it only requires a single binary indicator variable and a single quadratic constraint to be included per pipe.

The warm and cold side pipes are coupled by mass flows and exhibit symmetry, meaning that known mass flows in the warm side are also known in the cold side [54]. If the warm and cold side pipe networks are assumed to be identical, then it follows that frictional pressure losses are also symmetrical. The following can therefore be defined $\forall (i,j) \in \mathcal{A}^W$:

$$z_{k,\mathrm{w}H_i} - z_{k,\mathrm{w}H_j} + (z_{k,\mathrm{c}H_i} - z_{k,\mathrm{c}H_j}) = 0 \tag{3.117}$$

reducing the number of constraints needed to determine pressures in the cold side.

Similarly to the pipe network, the Darcy-Weisbach equation can also be reformulated for pressure drop through individual substations, $z_{k,\mathrm{sub}\Delta H_j},\ \forall j \in \mathcal{N}^W$:

$$y_{k,\mathrm{pump}\Delta H_j} = z_{k,\mathrm{pump}\Delta H_j} \tag{3.118}$$

$$C_j z_{k,m_j}^2 - z_{k,\mathrm{sub}\Delta H_j} \leq 0 \tag{3.119}$$

with the addition of mixed-integer linear inequalities and the binary indicator variable δ_{k,m_j} used to express the following logical conditions ((C.1) and (C.3) in Appendix C):

$$z_{k,m_j} \geq 0 \iff \delta_{k,m_j} = 1 \tag{3.120}$$

$$z_{k,m_j} \geq 0 \implies z_{k,\mathrm{c}H_j} - z_{k,\mathrm{w}H_j} = z_{k,\mathrm{sub}\Delta H_j} - z_{k,\mathrm{pump}\Delta H_j} \tag{3.121}$$

$$z_{k,m_j} \leq 0 \implies z_{k,\mathrm{c}H_j} - z_{k,\mathrm{w}H_j} = -z_{k,\mathrm{sub}\Delta H_j} + z_{k,\mathrm{pump}\Delta H_j} \tag{3.122}$$

As previously mentioned, a positive mass flow, z_{k,m_j}, is from the cool side to the warm side through the substation. The pump head gain, $z_{k,\mathrm{pump}\Delta H_j}$, is always positive and the pressure drop due to pressure reducing substation elements, $z_{k,\mathrm{sub}\Delta H_j}$, is bounded from below by the quadratic constraint (3.119). The constant C_j is determined for frictional losses which are due to static equipment in the substation, e.g. heat exchangers, fittings, etc. If $z_{k,\mathrm{sub}\Delta H_j}$ exceeds these losses to match the difference between warm and cool side pressure head, this additional pressure drop is

physically interpreted as being due to valve throttling, i.e. variably increasing frictional losses by reducing the pump bypass valve opening. If water is flowing through the substation to discharge into a pipe at greater pressure head than the inlet pipe, then $z_{k,\text{pump}\Delta H_j}$ must take a non-zero value to ensure (3.119) is satisfied. Otherwise, the inequalities describing logical conditions would require $z_{k,\text{sub}\Delta H_j}$ to be negative, violating (3.119).

Outputs y_{k,m_j} and $y_{k,\text{pump}\Delta H_j}$ are designated as source ports for connection to other component modules.

The inclusion of quadratic inequality relaxations (3.116) and (3.119) necessitates minimisation of $z_{k,\text{w}\Delta H_{ij}}$ and $z_{k,\text{sub}\Delta H_j}$ to ensure that feasible solutions are obtained from the model. Another objective is to minimise pumping power throughout the network. Due to the inclusion of pump pressure gain, $z_{k_{\text{pump}\Delta H_j}}$, in logical conditions describing substation pressure drop, minimising $z_{k_{\text{pump}\Delta H_j}}$ ensures that substation pressure drop, $z_{k,\text{sub}\Delta H_j}$, is also minimised. Hence, value cost modifiers (see Section 3.7) associated with only $z_{k,\text{w}\Delta H_{ij}}$ and $z_{k_{\text{pump}\Delta H_j}}$ are added to the ULTDHC module:

$$c_{k,\text{HC}} = \sum_{i \to j \in A^W} \lambda^{\text{val}}_{\Delta H_{ij}} z_{k,\text{w}\Delta H_{ij}} + \sum_{j \in N^W} \lambda^{\text{val}}_{\text{pump}\Delta H_j} z_{k,\text{pump}\Delta H_j} \tag{3.123}$$

A feasible solution is only obtained when (3.116) is satisfied to equality, at which point the model is said to be *exact*. This takes priority over pump energy minimisation and so the penalty prices are determined accordingly, with $\lambda^{\text{val}}_{\Delta H_{ij}} > \lambda^{\text{val}}_{\text{pump}\Delta H_j} > 0$.

When the presented AC power and ULTDHC network component models are used in isolation, the cost functions (3.123) and (3.108) are sufficient to recover an exact, feasible solution (if one exists) in each case. However, when aggregated with other components each with their own cost function, an optimisation solver may only prioritise feasibility if the cost coefficients in (3.123) and (3.108) are given a sufficiently large weighting, which may not produce economically optimal results for the global system. To address this problem, the upper bounds of pipe pressures, $\overline{z}_{k,w\Delta H_{ij}}$, and the upper bounds of line currents, $\overline{z}_{k,\ell_{ij}}$, may be iteratively lowered using an algorithm (see Section 5.2), which is intended to ensure an exact solution regardless of penalty weighting.

3.7 Cost Function Definition

Desirable system objectives, e.g. to minimise purchase of electricity, minimise battery charging cycles or to prevent rapid changes in energy flows, can be achieved by minimising a time-varying cost function, c_k. In any controlled system, at least one module must have an associated cost function which the automated energy management scheme can minimise to determine a rolling optimal schedule.

An end-user may specify cost function modifiers that are associated with any given variable(s), $v_{k,j}$, from the set of all decision variables in a module, $\boldsymbol{v}_k := \left[\boldsymbol{x}_k^\top \; \boldsymbol{u}_k^\top \; \boldsymbol{\delta}_k^\top \; \boldsymbol{z}_k^\top\right]^\top$. These cost function modifiers are added together to create an overall cost function for the module:

$$c_k = c_{k,\text{val}} + c_{k,\text{buy/sell}} + c_{k,\text{abs}} + c_{k,\Delta} + c_{k,\text{slack}} \tag{3.124}$$

where the individual modifiers are explained in the subsequent sections. When modules are aggregated, c_k is a linear combination of all individual module cost functions in the aggregate module.

3.7.1 Cost Function Modifiers

Value Costs

When a unidirectional energy flow is metered with an associated price of purchase, or when a bidirectional energy flow is metered with equal buying and selling prices, a simple value based cost function may be added. Let $\mathcal{F}_{\text{val}}$ represent the set of all variables in a module which have an associated value cost; these costs are given by:

$$c_{k,\text{val}} = \sum\nolimits_{j \in \mathcal{F}_{\text{val}}} \lambda^{\text{val}}_{k,v_j} \cdot v_{k,j} \tag{3.125}$$

where $\lambda^{\text{val}}_{k,v_j}$ is the price associated with the positive or negative value of the variable $v_{k,j}$.

Purchase and Sale Costs

When a metered bidirectional energy flow has differing prices for buying and selling, a simple value based cost function is not suitable. Instead, the different prices must

be applied exclusively, depending on whether the flow is positive or negative. First auxiliary variables $\delta_{k,v_j,\text{buy}}$ and $z_{k,v_j,\text{buy}}$ are introduced and defined by mixed-integer inequalities equivalent the following logical conditions (see (C.1) and (C.2) in Appendix C):

$$v_{k,j} \geq 0 \iff \delta_{k,v_j,\text{buy}} \tag{3.126}$$

$$z_{k,v_j,\text{buy}} = \delta_{k,v_j,\text{buy}} v_{k,j} \tag{3.127}$$

Let $\mathcal{F}_{\text{buy/sell}}$ represent the set of all variables in a module which have associated buying and selling costs; these costs are given by:

$$c_{k,\text{buy/sell}} = \sum\nolimits_{j \in \mathcal{F}_{\text{buy/sell}}} (\lambda^{\text{buy}}_{k,v_j} - \lambda^{\text{sell}}_{k,v_j}) z_{k,v_j,\text{buy}} + \lambda^{\text{sell}}_{k,v_j} \cdot v_{k,j} \tag{3.128}$$

where $\lambda^{\text{buy}}_{k,v_j}$ and $\lambda^{\text{sell}}_{k,v_j}$ are the prices associated with the positive and negative values of the variable $v_{k,j}$, respectively.

Absolute Value Costs

An example where absolute value costs may be required is to account for the degradation costs of a battery, for which there is a positive associated cost every time the battery is charged or discharged. An auxiliary variable is first introduced, $z_{k,v_j,\text{abs}}$, which is defined by mixed-integer inequalities equivalent to the following logical condition (see (C.4) in Appendix C):

$$z_{k,v_j,\text{abs}} = |v_{k,j}| \tag{3.129}$$

Use of the auxiliary variable permits the use of a linear objective function. Let $\mathcal{F}_{\text{abs}}$ represent the set of all variables in a module which have an associated absolute value cost; these costs are given by:

$$c_{k,\text{abs}} = \sum\nolimits_{j \in \mathcal{F}_{\text{abs}}} \lambda^{\text{abs}}_{k,v_j} \cdot z_{k,v_j,\text{abs}} \tag{3.130}$$

where $\lambda^{\text{abs}}_{k,v_j}$ is the price associated with absolute value of the variable $v_{k,j}$.

Absolute Rate of Change Costs

It may sometimes be desirable to reduce the rate of change of a given variable to aid system stability, even if significant changes from one sampling instance to the

next are feasible, i.e. safe and physically possible. In this case it is appropriate to use a cost function to discourage high rates of change where possible. An example might include so called demand smoothing, reducing fluctuations in energy flows to a building in order to reduce peaks in demand [112]. An auxiliary variable is first introduced, $z_{k,v_j,\Delta}$, which is defined by mixed-integer inequalities equivalent to the following logical condition (see (C.4) in Appendix C):

$$z_{k,v_j,\Delta} = |v_{k,j} - v_{k-1,j}| \tag{3.131}$$

Let $\mathcal{F}_\Delta$ represent the set of all variables in a module which have associated rate of change costs; these costs are given by:

$$c_{k,\Delta} = \sum\nolimits_{j \in \mathcal{F}_\Delta} \lambda^{\Delta}_{k,v_j} \cdot z_{k,v_j,\Delta} \tag{3.132}$$

where λ^{Δ}_{k,v_j} is the price associated with absolute rate of change of the variable $v_{k,j}$.

Slack Variable Costs

Slack variables may be included in a module's cost function to penalise deviations from some reference value or to add soft constraints to a model. In the latter case this might be useful to aid feasibility when using storage, by protecting a reserve of storage for use when there is no other option to match fixed generation or demands. The slack variable, $z_{k,v_j,\text{slack}}$ is defined by the following constraints:

$$v_{k,j} \geq \widetilde{v}_{j,\text{slack}} - z_{k,v_j,\text{slack}} \tag{3.133}$$

$$v_{k,j} \leq \underset{\sim}{v}_{j,\text{slack}} + z_{k,v_j,\text{slack}} \tag{3.134}$$

$$z_{k,v_j,\text{slack}} \geq 0 \tag{3.135}$$

where $\underset{\sim}{v}_{j,\text{slack}}$ and $\widetilde{v}_{j,\text{slack}}$ are the preferred upper and lower limits for the variable $v_{k,j}$, respectively. It is then straightforward to define a cost function which penalises non-zero values of the slack variable. Let $\mathcal{F}_{\text{slack}}$ represent the set of all variables in a module which have associated slack variables; the penalty costs are given by:

$$c_{k,\text{slack}} = \sum\nolimits_{j \in \mathcal{F}_{\text{slack}}} \lambda^{\text{slack}}_{k,v_j} \cdot z_{k,v_j,\text{slack}} \tag{3.136}$$

where $\lambda^{\text{slack}}_{k,v_j}$ is the price for using the slack variable associated with $v_{k,j}$. It should be noted that if preferred upper and lower limits are made equal, they serve to provide a reference value for $v_{k,j}$.

3.8 Summary

This chapter has introduced the multi-energy system optimisation modelling framework which will be used throughout the thesis. Existing modular component models from the literature were presented, together with newly proposed models and modifying constraints to alter the behavioural characteristics of individual energy conversion devices. Cost function modifiers have also been introduced, which can be selectively added to fine tune the operational objectives of a controlled system.

The framework provides a flexible tool through which an end-user, e.g. an aggregator or a multi-building site manager, can quickly develop a customised optimisation model of an energy system. The use of modules and standard modifiers, together with recursive aggregation capability, allows systems of significant complexity to be built in manageable stages.

Chapter 4

Centralised Coordination of a Small-Scale Multi-Energy District

4.1 Introduction

The results presented in this chapter concern coordination of several buildings connected by power, gas and bi-directional ULTDHC networks to form a small-scale multi-energy district. A MPC scheme for district-level coordination is first introduced and is then compared to the use of a simple rule-based controller (RBC) to manage each building separately, a common approach for energy system management of a single building in the absence of advanced optimisation-based control [19], [94], [113]. Component modules proposed in Chapter 3 for modelling reversible WSHPs and fixed speed circulation pumps are utilised in the MPC scheme, which are each necessary for considering bi-directional mass and energy flows between buildings and the ULTDHC network.

4.2 Control Scheme

The following scheme enables a single, centralised MPC controller to schedule operation of a district, with the objective of minimising system costs and maximising revenues. Set-points determined by the MPC controller for the current sampling interval are passed to controllable distributed energy resources for implementation (see Fig. 4.1). Actions are then determined by lower-level feedback controllers with higher

frequency in order to track these set-points, responding to deviations in expected demand due to unknown disturbances, incorrect forecasts or modelling inaccuracies.

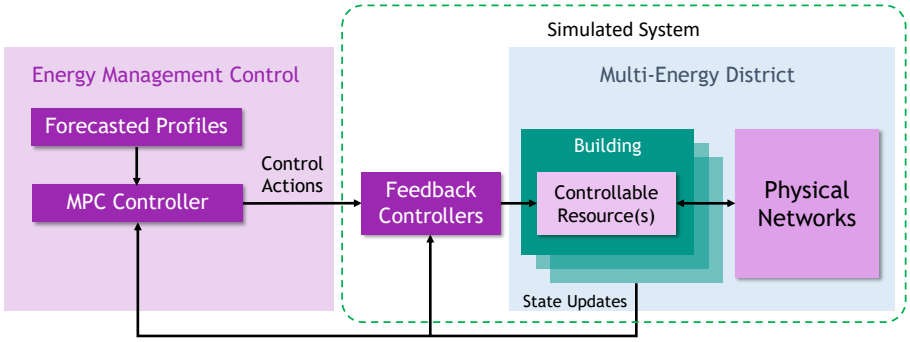

Figure 4.1: Illustration of district control scheme, adapted from [29].

The optimisation performed by the MPC controller is based on the certainty equivalence principle, whereby future values of unknown daily price schedules, energy demand and generation are assumed known and equal to forecasted values. As forecasting methods are not within the scope of this thesis, simple persistence forecasting is adopted which predicts that future disturbances are equal to historical values measured 24 hours previously. If this was substituted for a better forecasting method, then the performance of the MPC controller should improve.

Aggregated component modules, with or without additional modifiers, and the connections between them provide the system model for the MPC controller. The optimisation problem for the MPC controller is to minimise a cost function given in (4.1) at each sampling instance k, subject to the constraints of m aggregated components. The prediction horizon H is a user-defined value that should be long enough to ensure long-term economic optimality.

$$J_k = \sum_{m} \sum_{h=0}^{H-1} c_{k+h,m} \tag{4.1}$$

Solving the controller's optimisation problem provides a solution vector $\boldsymbol{v}_k^*$ from which a set of control actions can be derived, as outlined in Algorithm 1.

It is assumed in this chapter that the district is operated by a single entity, as would be the case for a university, airport or hospital district, for example. This is the basis for (4.1), through which buildings are coordinated for the benefit of the overall district. This objective may also be used to control a district of independent buildings if it is assumed that they are part of a coalition also coordinated by a single entity, e.g. a commercial aggregator. In this case an additional benefit allocation mecha-

Algorithm 1 Generic algorithm for model predictive control scheme

1: $t = 0$, $\Delta t > 0$
2: **for** $k = 0, 1, 2, ...$ **do**
3: Update current system states, $\boldsymbol{x}_k$
4: Update price forecasts, $\boldsymbol{\lambda}_{k+h}$, $h = 0, ..., H-1$
5: Update disturbance forecasts, $\boldsymbol{w}_{k+h}$, $h = 0, ..., H-1$
6: Minimise 4.1 to determine schedule of control actions, $\boldsymbol{u}^*_{k+h}$, $i = 0, ..., H-1$
7: Pass control inputs for next sampling interval, $\boldsymbol{u}^*_k$, to lower-level feedback controllers; discard $\boldsymbol{u}^*_{k+h}$, $h = 1, ..., H-1$
8: **Wait until** $t = (k+1)\Delta t$
9: $k \leftarrow k+1$
10: **end for**

nism would be required to ensure a fair distribution of revenue amongst cooperating buildings (see, for example [114]).

For the simulations reported in Section 4.4, it is assumed that the simulated system shown within the dashed boundary in Fig. 4.1 follows precisely the set-points issued by the MPC controller. The case study in Section 4.3 therefore demonstrates the effectiveness of the MPC controller to continually schedule operation of the district, whilst stability and robustness are ensured by the actions of lower-level controllers.

4.3 Case Study

A multi-energy district shown in Fig. 4.2 is used to exemplify the added capability of the proposed component modules utilised in this chapter, taking inspiration from the case study of [30]. It comprises a commercial office building, a supermarket building and a ULTDHC district heating and cooling (DHC) plant. These are connected by a looped ULTDHC network and by radial electricity and gas networks. Conversion factors associated with devices are provided in Table 4.1 and specific device parameters, such as operational limits and modelling coefficients, are given in Table 4.2. Network modelling parameters are given in Table 4.3. The following paragraphs describe the energy system of each building in detail.

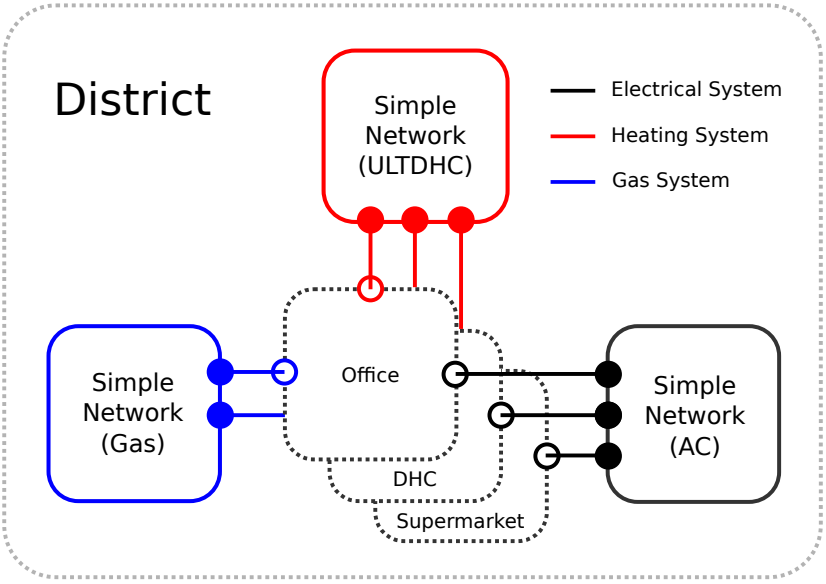

Figure 4.2: Illustration of district modules, adapted from [29].

Table 4.1: Device Conversion Factors

Conversion Factor	Device	Value
η_{tx}	Transformer	0.98
COP/EER_{sc}	Heat Pump (heating/space cooling)	3.40 / 9.50
EER_{ref}	Heat Pump (refrigeration)	3.90
$\eta_{b,heat}$	Auxiliary Boiler	0.80
$\eta_{rh,heat}$	Immersion Heater	1.00
$\eta_{chp,heat}/\eta_{chp,elec}$	CHP (heat/electricity)	0.40 / 0.33
EER_{AC}	Absorption Chiller	1.70
$\eta_{batt,chg}/\eta_{batt,dchg}$	Battery (charging/discharging)	0.90 / 0.85
$\eta_{hthm,chg}/\eta_{hthm,dchg}$	Hot Store (charging/discharging)	0.95 / 0.95
$\eta_{cthm,chg}/\eta_{cthm,dchg}$	Cold Store (charging/discharging)	0.95 / 0.95

A reversible WSHP serves office heating and cooling demands by either importing or exporting heat to the thermal network, via a decentralised circulation pump (see Fig. 4.3). A thermal water storage tank decouples thermal demands from use of the WSHP. An auxiliary gas boiler is also present to ensure sanitary hot water can still be provided when the WSHP is used for space cooling. In addition, local electrical consumption and a solar photovoltaic (PV) array combine to impose a fixed net generation/demand on the building's energy system and a battery is also located within the office.

Table 4.2: Hub Specific Device Modelling Constraints and Coefficients

Building	Office	Supermarket	DHC
Transformer capacity, kW	500	500	500
Battery capacity, kWh	300	400	-
Min./Max. Battery SoC, %	20 / 80	20 / 80	-
Max. Battery charge/disch., kW	225	225	-
Battery loss coefficient	0.001	0.001	-
Hot Store capacity, kWh	200	-	2.40×10^3
Max. Hot Store charge/disch., kW	60.0	-	400
Hot Store loss coefficient	0.01	-	0.001
Cold Store capacity, kWh	-150	-150	-
Max. Cold Store charge/disch., kW	60.0	60.0	-
Cold Store loss coefficient	0.01	0.01	-
HP input capacity, kW	160	160	-
Aux. Boiler input capacity, kW	200	-	-
μ-CHP input capacity, kW	-	-	250
Abs. Chiller input capacity, kW	-	-	300
Pump power constants, Ψ_{on}/b [115]	2.97/0.0355	2.97/0.0355	2.97/0.0355
Max. Pump flowrate, $\mathrm{m^3\,h^{-1}}$	85.0	85.0	85.0

Table 4.3: Network Parameters

Parameter	Description	Value
$\overline{y}_{p_{1,\mathrm{elec}}}$	Main Feeder Capacity Limit	$600\,\mathrm{kW}$
θ_w	Warm Line Temperature	$20.0\,^{\circ}\mathrm{C}$
θ_c	Cool Line Temperature	$16.0\,^{\circ}\mathrm{C}$
C_p^{water}	Heat Capacity of Water	$4.18\,\mathrm{kJ\,kg^{-1}\,K^{-1}}$
ρ^{water}	Density of Water	$998\,\mathrm{kg\,m^{-3}}$

A supermarket refrigeration demand is served by a single mode WSHP whilst a relatively small demand for sanitary hot water is met using an electrical immersion heater (see Fig. 4.4). Similarly to the office, thermal storage is present to decouple operation of the WSHP from demand, in this case a cold storage tank operating at temperatures below ambient. Although no electricity is generated within the supermarket, battery storage is available for energy arbitrage.

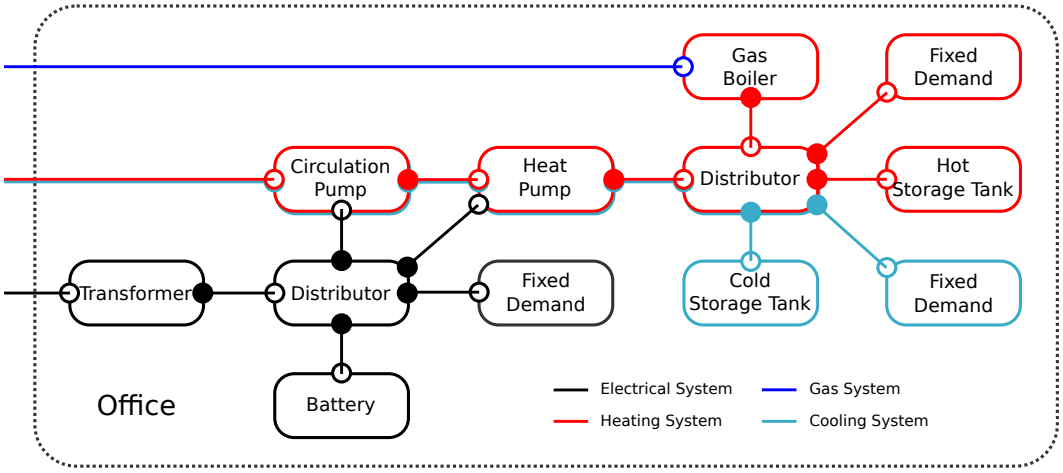

Figure 4.3: Illustration of office modules, adapted from [29].

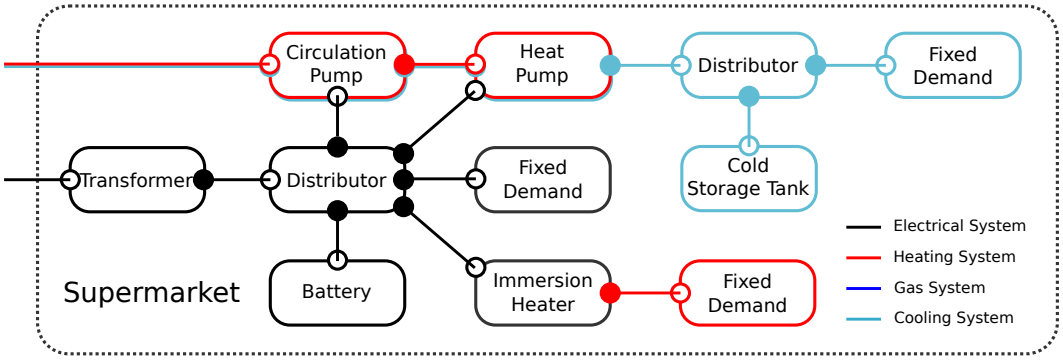

Figure 4.4: Illustration of supermarket modules, adapted from [29].

The district heating and cooling (DHC) plant is needed to provide the balance of thermal demands across the district (see Fig. 4.5). It consists of a tri-generation system with connections to a large solar thermal collector (TC) and seasonal storage. The tri-generation system comprises a microturbine driven CHP (μ-CHP) and an absorption chiller which is able to use heat from the μ-CHP to provide cooling, with the remaining waste heat released to atmosphere via passive cooling. Surplus electricity from the μ-CHP is exported to the district.

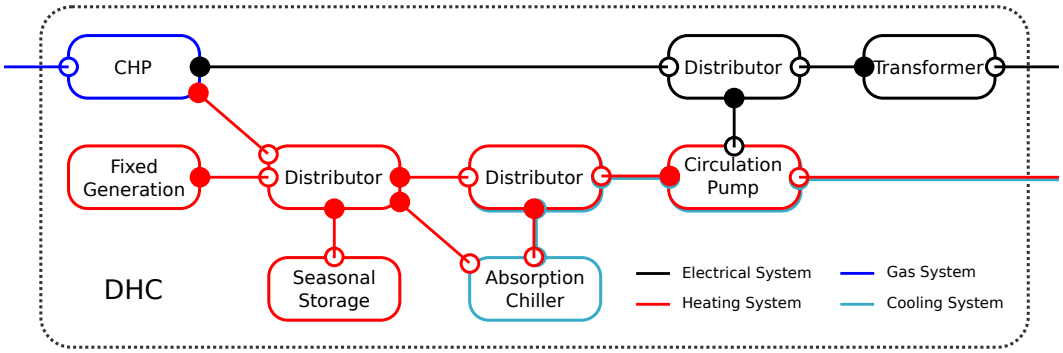

Figure 4.5: Illustration of DHC modules, adapted from [29].

The μ-CHP, due to its small size, is assumed to have greater flexibility than larger CHP units. Hence, the case study does not consider operational constraints on μ-CHP output levels such as minimum up and down-times. Given the considered sampling period, this is unlikely to significantly impact the results. As shown in Chapter 3, these constraints could easily be added to the CHP module using the relevant modifiers provided within the framework. However, at the time of publishing [29], these modifiers had not yet been added to the framework, so were not included in the case study.

4.3.1 Control Problem

The objective function J_k minimised by the controller at each time step consists of the economic cost to the district for importing, and revenue for exporting, energy from/to external networks, as well as the cost associated with battery degradation. A purchase and sale cost modifier is applied to the electricity network output variable, $y_{k,p_1,\text{elec}}$, with associated prices $\lambda^{\text{buy}}_{k,y_{p1,\text{elec}}}$ and $\lambda^{\text{sell}}_{k,y_{p1,\text{elec}}}$. A value cost modifier is applied to the gas network output variable $y_{k,p_1,\text{gas}}$, with associated cost $\lambda^{\text{val}}_{k,y_{p1,\text{gas}}}$. A battery degradation cost coefficient $\lambda^{\text{abs}}_{k,u_{\text{batt}_j,\text{chg}}}$ is applied to all batteries, denoted $batts$, by adding an absolute value cost modifier applied to $u_{k,\text{batt,chg}}$.

$$J_k = \sum_{h=0}^{H-1} c_{k+h} \tag{4.2}$$

$$\begin{aligned} c_{k+h} = {} & (\lambda^{\text{buy}}_{k,y_{p1,\text{elec}}} - \lambda^{\text{sell}}_{k,y_{p1,\text{elec}}}) z_{k,y_{p1,\text{elec}},\text{buy}} + \lambda^{\text{sell}}_{k,y_{p1,\text{elec}}} \cdot y_{k,p_1,\text{elec}} + \lambda^{\text{val}}_{k,y_{p1,\text{gas}}} \cdot y_{k,p_1,\text{gas}} \\ & + \sum_{j \in batts} \lambda^{\text{abs}}_{k,u_{\text{batt}_j,\text{chg}}} \cdot z_{k,u_{\text{batt}_j,\text{chg}},\text{abs}} \end{aligned} \tag{4.3}$$

The control problem is formally stated as:

$$\begin{aligned} \min_{v_i} J_k &= \sum_{h=0}^{H-1} c_{k+h} \\ \text{s.t. } &(3.1)\text{-}(3.4) \ \forall \ m \end{aligned} \tag{4.4}$$

for which the m aggregated components are shown in Figs. 4.2 to 4.5 and the specific constraints for these components are given in Chapter 3.

4.3.2 Simulation Parameters and Inputs

The simulation uses data from February 2018 with a half-hourly sampling interval, totalling 1,344 data points. Half-hourly electricity prices used in the simulation are those set in February 2018 by UK energy supplier Octopus Energy Ltd for customers on its Agile Octopus tariff [116]. Fixed prices are assumed for export of electricity to the external grid and purchasing of gas, at 1 p/kWh and 2.8 p/kWh respectively; the value of $\lambda^{\text{abs}}_{\text{batt,chg}} = 3.15$ p/kWh is determined using the approach in [117]. Historical data recorded for February 2018 in the University of Manchester's building management system were used to obtain representative profiles of energy generation and consumption. For clarity, data profiles are shown for a single weekday only (Figs. 4.6(a)-(d).

4.3.3 Comparative Rule-Based Control Scheme

In order to gauge the performance of the MPC controller, a simple rule based control (RBC) scheme has also been simulated for the same period. This scheme uses simple if-then-else logic to assign priority for the use of resources based on relative costs (see Table 4.4), following the examples of [42], [118], [119]. Renewable generation is always dispatched, whilst batteries and thermal storage tanks are charged or discharged when the electricity buying price passes pre-specified threshold values, i.e. $\lambda^{\text{buy}}_{p_1,\text{elec,low}} = 10$ and $\lambda^{\text{buy}}_{p_1,\text{elec,high}} = 20$. These thresholds have been tuned to achieve the best performance from the RBC controller for the considered system and electricity price profile. After local storage dispatch has been determined, the RBC scheme ensures that local building demands are always met by dispatching remaining available resources. Any surplus energy is exported to internal networks.

4.4 Results

The data described in Section 4.3 were used to run a simulation over 1,296 half-hourly intervals, with prediction horizon $H = 48$. IBM ILOG CPLEX 12.9 [120] with MATLAB [121] API was used to solve the controller MILP problem on an Intel Core i5-6200U CPU @ 2.30 GHz with 8.00 GB of RAM. The default relative MIP gap tolerance of 1×10^{-4} was increased to 1×10^{-3}; this improves the computation time

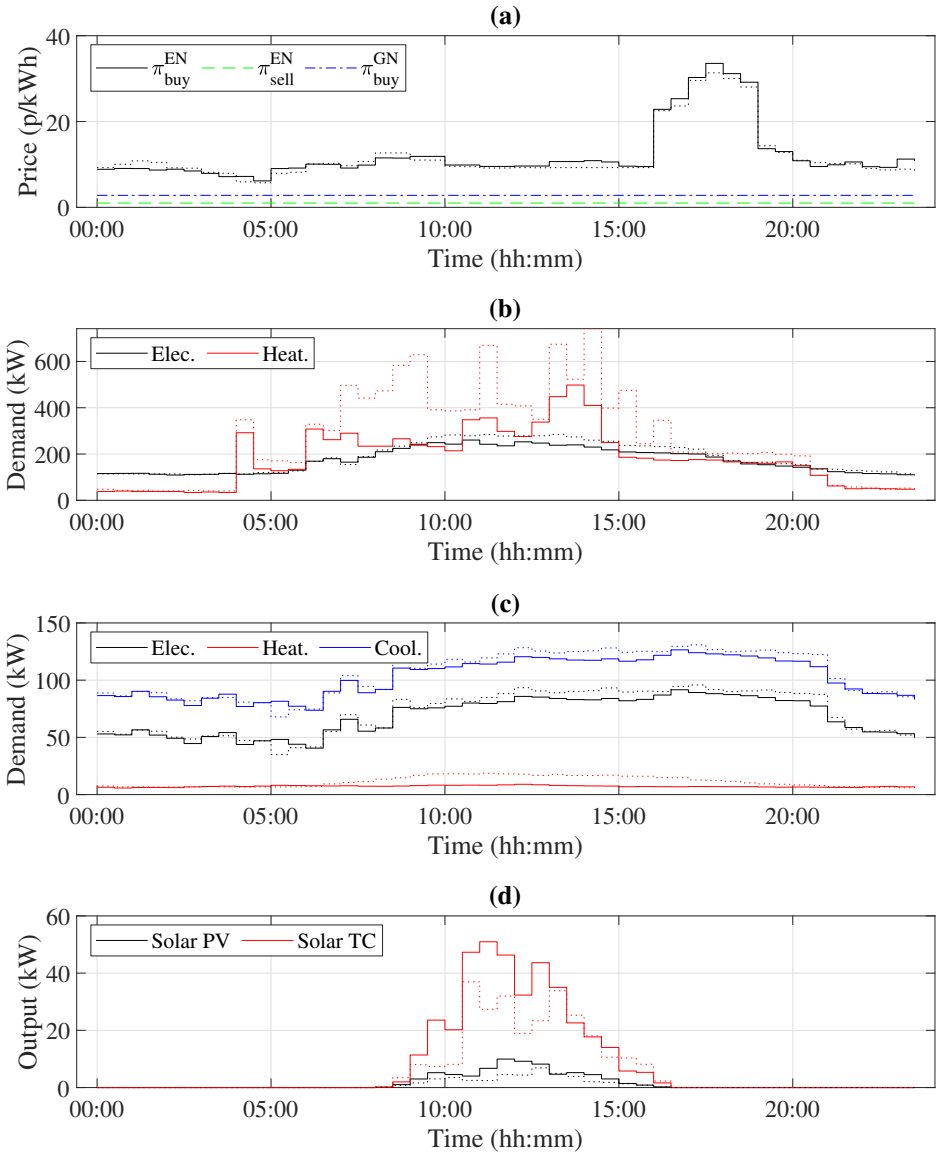

Figure 4.6: (a) Gas and electricity prices; (b) Office half-hourly energy demands; (c) Supermarket half-hourly demands; (d) Half-hourly energy generation from solar PV and solar TC. Profiles are those for 2nd February 2018. Dotted lines in (a)-(d) represent forecasts, recorded on the previous day.

of the controller with only a marginal ($< 0.05\%$) increase in the optimal cost. For clarity, the results are plotted for a single weekday only (Figs. 4.7(a)-(e)).

The amount of energy imported to the district from external gas and electricity networks is shown in Fig. 4.7(a). Import of electricity is minimised by the controller during higher purchase price periods, to the extent that no electricity is imported between 17:00 and 18:30. As shown by the profiles of imported thermal energy in 4.7(b), electricity associated with ULTDHC substation devices is minimised at this time, relying on thermal storage and use of the office gas boiler to reduce use of network pumps. It is worth noting that 19% of the total electrical energy demand of

Table 4.4: Resource Dispatch Priority using Rule-Based Control

Resource	Condition	Dispatch Status
Solar PV	-	Always dispatched
Solar TC	-	Always dispatched
Batteries	**if** $\lambda^{\text{buy}}_{k,p_1,\text{elec}} < \lambda^{\text{buy}}_{p_1,\text{elec,low}}$	Charging state
	else if $\lambda^{\text{buy}}_{k,p_1,\text{elec}} > \lambda^{\text{buy}}_{p_1,\text{elec,high}}$	Discharging state
	else	Standby
Storage Tanks	**if** $\lambda^{\text{buy}}_{k,p_1,\text{elec}} < \lambda^{\text{buy}}_{p_1,\text{elec,low}}$	Charging state
	else if $\lambda^{\text{buy}}_{k,p_1,\text{elec}} > \lambda^{\text{buy}}_{p_1,\text{elec,high}}$	Discharging state
	else	Standby
Heat Pumps	-	Always dispatched
Immersion Heater	-	Always dispatched
Auxiliary Boiler	**if** heat load exceeds heat pump capacity	Dispatched
	else	Standby
Absorption Chiller	**if** cooling is required	Dispatched
	else	Standby
μ-CHP	**if** heat load exceeds solar TC output	Dispatched
	else	Standby
Seasonal Storage	**if** solar TC output exceeds heat load	Charging state
	else if heat load exceeds solar TC output plus μ-CHP capacity	Discharging state
	else	Standby

ULTDHC substation devices over the month is used by the network pumps, substantiating their significance and necessary inclusion in the prediction model.

Thermal and electrical battery storage levels are shown in Figs. 4.7(c) and 4.7(d), respectively, for both the office and supermarket. Fig. 4.7(d) clearly shows that the batteries are operated to take advantage of fluctuating electricity prices, charging at a lower price period and discharging when prices peak. The fact that this behaviour is also observed for the thermal storage in 4.7(c) highlights the coupling between these systems and supports their integrated optimisation. Also apparent from comparison of Figs. 4.7(a) and 4.7(d) is the effect of the electrical network's main feeder

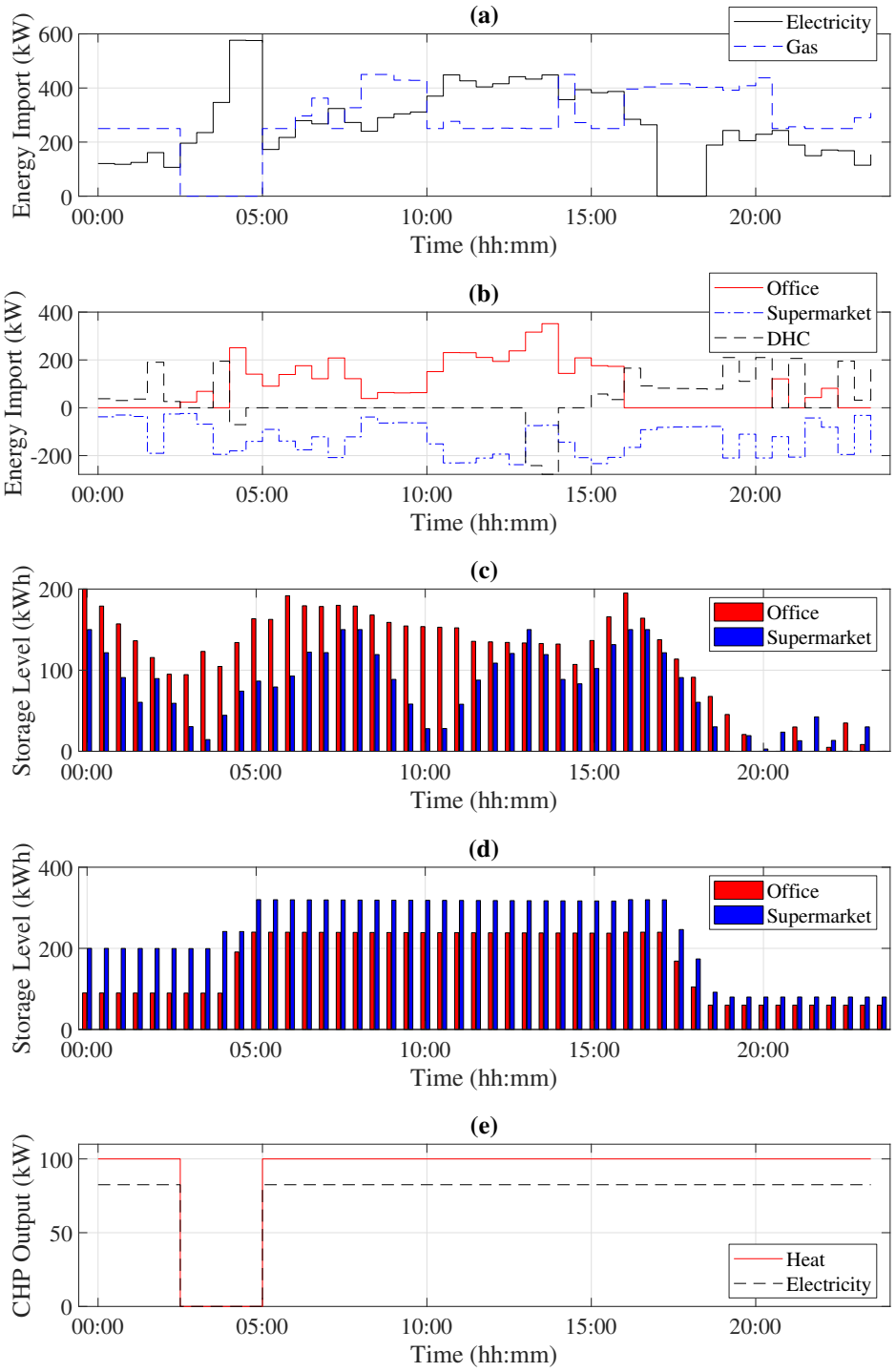

Figure 4.7: (a) District electricity and gas imports; (b) Imports from ULTDHC network; (c) Office hot tank and supermarket cold tank storage levels; (d) Office and supermarket battery storage levels; (e) District μ-CHP output. Results are those for 2nd February 2018.

capacity constraint on simultaneous charging of the batteries. In particular, between 04:00 and 05:00 the controller opts to stagger the rate of charging of each battery so that this constraint is not violated. This scenario shows the importance of including network constraints in the control problem formulation. If, conversely, network capacity constraints were not considered, i.e. if electrical import was only constrained

by transformer capacity, then the main feeder capacity limit could be exceeded by simultaneous charging of the batteries.

The μ-CHP is always operational during periods when the electricity price is at or above approx. 9 p/kWh (Figs. 4.6(a) and 4.7(e)). During these periods it is more economical to supply district electrical loads using local gas-fired generation, even if there are no demands from the ULTDHC network at the time, leading to some charging of the seasonal thermal storage. This again highlights the importance of a multi-energy systems approach; a μ-CHP solely operated to satisfy thermal demands would have reduced output, resulting in higher electricity costs for the district. Fig. 4.7(b) shows that, by discharging seasonal storage, the DHC plant may still provide the balance of energy required by the thermal network when electricity prices are low and the μ-CHP is not operational. Regardless of whether there is an excess or a deficit of heat, the controller is able to schedule operation to balance the ULTDHC network since the DHC plant includes a multi-mode tri-generation plant. This capability relies on the determination of bi-directional power exchanges with the network, enabled by the introduction of reversible fixed speed pump modules to the optimisation modelling framework.

Table 4.5: Comparison of Daily Cost (1 Month Simulation)

Daily Cost (£)	Ave.	Std. Dev.	Min.	Max.
Rule-Based Control	1,115	184	845	1,652
MPC ($H = 48$)	998 (-10.4%)	182	704	1,480

The simulation results using the proposed MPC controller compare favourably with those of the RBC scheme introduced in Section 4.3.3, with an average daily cost that is 10.4% lower than that of the RBC scheme (Table 4.5). The MPC controller is able to achieve this improved economic performance whilst maintaining operation within prescribed limits, unlike the RBC scheme which was found to violate the main electrical feeder capacity limit on several occasions; this is due to the RBC scheme prioritising energy arbitrage and the satisfaction of thermal loads, whilst electricity is left as a degree of freedom to balance energy demands. Hence, the proposed MPC controller performs significantly better than the RBC scheme, both in terms of optimality and operational feasibility.

Table 4.6 shows the impact of increasing prediction horizon length on solver computation time. As expected, there is an increase in average computation time as the

Table 4.6: Effect of Prediction Horizon Length on Computational Performance (1 Month Simulation)

Prediction Horizon Length	12(6h)	24(12h)	36(18h)	48(24h)
Number of Variables	2028	4056	6084	8112
Number of Binary Variables	444	888	1332	1776
Ave. Comp. Time (secs)	0.11	0.25	0.64	0.83
Max. Comp. Time (secs)	0.59	3.25	9.77	2.94
Std. Deviation (secs)	0.05	0.16	0.42	0.27

horizon length is increased from $H = 12$ (6 hrs) to $H = 48$ (24 hrs), although the average computation time of 0.83 secs for $H = 48$ is well within acceptable limits for a control scheme with half-hourly updates. The maximum computation time for the particular case under study can be several seconds longer than the average. This may be explained since in most intervals it was only necessary for the CPLEX solver to explore the route node of the MILP problem before obtaining an optimal solution; longer computation time results from more exhaustive searches by the solver's branch and cut algorithm. With a smaller relative MIP gap tolerance, additional nodes would have to be explored more often, with an associated increase in average computation time.

If the system scale is significantly increased to incorporate a large number of buildings, long computation times could become problematic. However, referring to Fig. 4.8, which shows the effect of increasing horizon length on the overall cost for a single day, it is clear that increasing the prediction horizon length beyond $H = 27$ offers little benefit in this case. Therefore, if computation times are likely to be excessive for larger systems, a similar analysis could be performed in order to determine a minimum horizon length for MPC, thereby significantly reducing the size of the optimisation problem.

4.5 Conclusions

In this chapter, results have been presented to demonstrate that a gap in the research into control of multi-energy districts has been partially addressed; namely, the need for a general model development technique which considers ULTDHC networks and

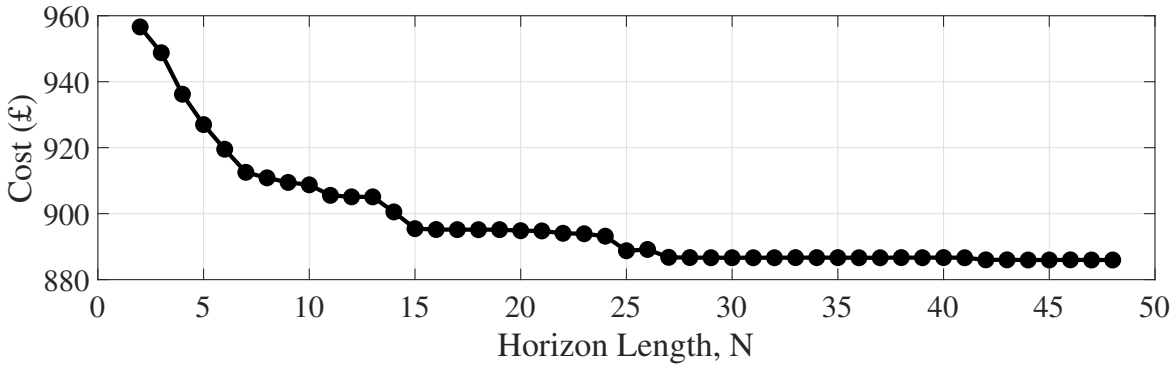

Figure 4.8: Effect of prediction horizon length on overall cost, using data for 2nd February 2018.

which can be readily incorporated into MPC schemes. The modelling contributions utilised in this chapter include the addition of component modules to represent simplified multi-energy networks, fixed speed hydraulic pumps and reversible WSHPs. Using the extended framework, an MPC scheme has also been proposed and analysed by simulation of a district featuring a ULTDHC network. In comparison to a simulation using rule-based control, the proposed scheme exhibits significantly better performance. The results highlight the importance of modelling energy networks and interactions, both to improve optimality and avoid infeasible network operation. Experimentation to vary the MPC prediction horizon length also indicated that there is potential to define a minimum horizon length, thereby minimising the problem size, in order to manage computational burden whilst maintaining optimal economic operation.

A criticism of the method used in this chapter is that the power required from fixed speed circulation pumps is likely to greatly exceed an equivalent network using variable speed pumps. In the following chapter, more detailed multi-energy networks models will be employed for a much larger district, since the assumptions that allow pressures and voltages to be neglected no longer hold for a large district. The use of a reversible variable speed circulation pump module is also used, since it will be possible to determine the necessary pressure head gain required of the pump, based on the modelled network conditions.

Chapter 5

Centralised Coordination of a Large-Scale Multi-Energy District

5.1 Introduction

Modelling formulations of optimal energy flow problems in both ULTDHC and AC electrical networks are incorporated as modules into the multi-energy district control problem in this chapter. The formulation of the ULTDHC optimal flow problem is an original contribution of this thesis, whereas the AC electrical network reformulation is based on the work in [60], adapted for the current framework. An analogous modelling formulation for gas networks based on [122] may also be added to the framework but is not utilised for the case study in this or subsequent chapters. As will become clear from the case study results, the inclusion of just the ULTDHC and AC network types, when modelled in detail and at large scale, is enough to cause the district coordination problem to become intractable. The problem of tractability at large scales is addressed in Chapter 6.

Also utilised in this chapter is a reversible variable speed circulation pump module which relies on the inclusion of the detailed ULTDHC module to function properly. Since the pump is governed by a non-linear relationship, this adds further complexity to the energy management problem, which will similarly be addressed in Chapter 7.

As well as the use of these new component modules, two additional algorithms are presented in the chapter which are used to ensure that the optimal energy flow solu-

tions are feasible and *exact*, i.e. when all second order cone inequalities are satisfied to equality, a concept which was described in Sections 3.6.2 and 3.6.3.

Having introduced the control scheme required for these more detailed network modules, a case study is described to test the functionality of these framework additions when using a single, centralised MPC controller, as in the previous chapter.

5.2 Control Scheme

The control scheme from Chapter 4 is utilised here, with a small amendment to the controller's algorithm to ensure exactness of the ULTDHC and AC network energy solutions. The optimisation problem for the controller remains the same, i.e. to minimise the cost function given in (4.1) at each sampling instance k, subject to the model of m aggregated components. However, the aggregated components now include the ULTDHC and AC network modules. The revised procedure is shown in Algorithms 2 and 3.

The constants $\Delta H_{ij}^{\max}$ and $\ell^{\max}$ in Algorithm 3 are the maximum allowable pipe pressure head loss and line capacity, respectively. The algorithm iteratively replaces these with reduced limits for individual pipes or lines if the optimisation solver returns an inexact solution with respect to the given pipe or line. The solver may return an inexact solution if there is an overall economic benefit for artificially increasing the head loss or line current, an occurrence which is more likely when bi-directional flows are considered and strict limits on voltages and pump capacities apply. The algorithm parameters r^{max} and tol^n are used to balance solution exactness with the time taken to compute a solution and can be adjusted to suit the specific control application; here they are given $r^{max} = 10$, $\text{tol}^W = 1 \times 10^{-3}$ and $\text{tol}^E = 1 \times 10^{-4}$. Since the primary aim of this chapter is to assess the functionality of the additional component modules, uncertainty is not considered; perfect forecasts are provided to the controller.

5.3 Case Study

A case study is presented in this section, in which the operation of a large multi-energy district under centralised control is simulated. The district topology is based

Algorithm 2 Generic algorithm for model predictive control scheme

$t = 0$, $\Delta t > 0$
for $k = 0, 1, 2, ...$ **do**
    Update current system states, $\boldsymbol{x}_k$
    Update price forecasts, $\boldsymbol{\lambda}_{k+h}$, $h = 0, ..., H-1$
    Update disturbance forecasts, $\boldsymbol{w}_{k+h}$, $h = 0, ..., H-1$
    Run Algorithm 3
    Pass control inputs for next sampling interval, $\boldsymbol{u}^*_k$, to lower-level feedback controllers; discard $\boldsymbol{u}^*_{k+h}$, $h = 1, ..., H-1$
    Wait until $t = (k+1)\Delta t$
    $k \leftarrow k + 1$
end for

Algorithm 3 Algorithm to improve inexact energy flow solutions

$\overline{z}_{k,w\Delta H_{ij}} = \Delta H_{ij}^{\max}$
$\overline{z}_{k,\ell_{ij}} = \ell^{\max}$
for $r = 1 : r^{max}$ **do**
    recompute = false
    Minimise 4.1 to determine schedule of control actions, $\boldsymbol{u}^*_{k+h}$, $i = 0, ..., H-1$
    if $C_{ij} z^2_{k,m_{ij}} - z_{k,\mathrm{w}\Delta H_{ij}} \geq \mathrm{tol}^W \ \forall (i,j)$ **then**
        $\overline{z}_{k,w\Delta H_{ij}} = C_{ij} z^2_{k,m_{ij}}$
        recompute = true
    end if
    if $z^2_{k,P_{ij}} + z^2_{k,Q_{ij}} - z_{k,\ell_{ij}} z_{k,v_i} \geq \mathrm{tol}^E \ \forall (i,j)$ **then**
        $\overline{z}_{k,\ell_{ij}} = \left(z^2_{k,P_{ij}} + z^2_{k,Q_{ij}} \right) / z_{k,v_i}$
        recompute = true
    end if
    if recompute = false **then**
        break
    end if
end for

on a MATPOWER test case, 'case85' [123], and the building energy system devices reported for ULTDHC networks in [49], [77]. The district consists of an 85 bus AC distribution network and an 84 node ULTDHC network, connecting $N_B = 84$ large residential and commercial buildings/plants. The topology of the AC network is shown in Fig. 5.1, in which bus 1 represents a connection to a larger network. The topology of the ULTDHC network (also Fig. 5.1) follows that of the AC network but starts at node 2, a plant substation, where a fixed amount of waste heat is contin-

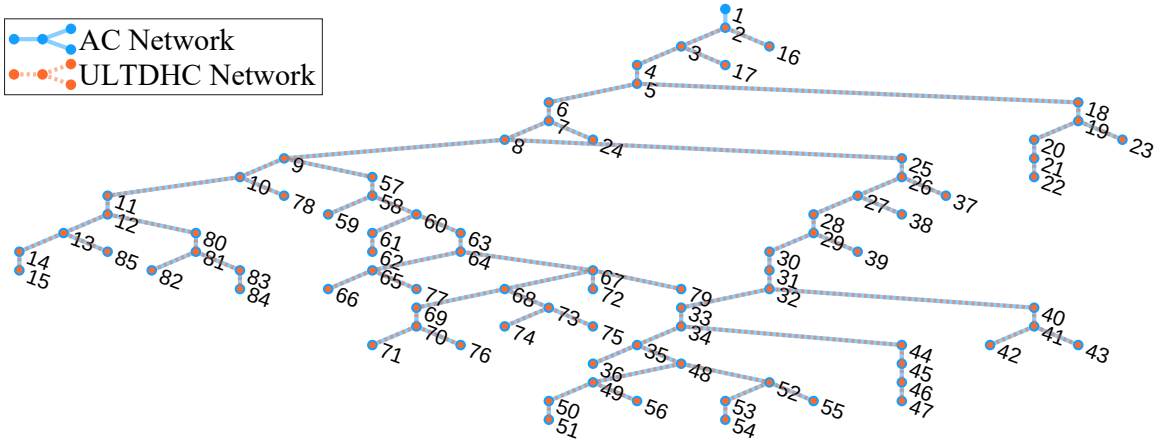

Figure 5.1: Graphs of AC distribution network, based on MATPOWER test case 'case85' [123], and ULTDHC network.

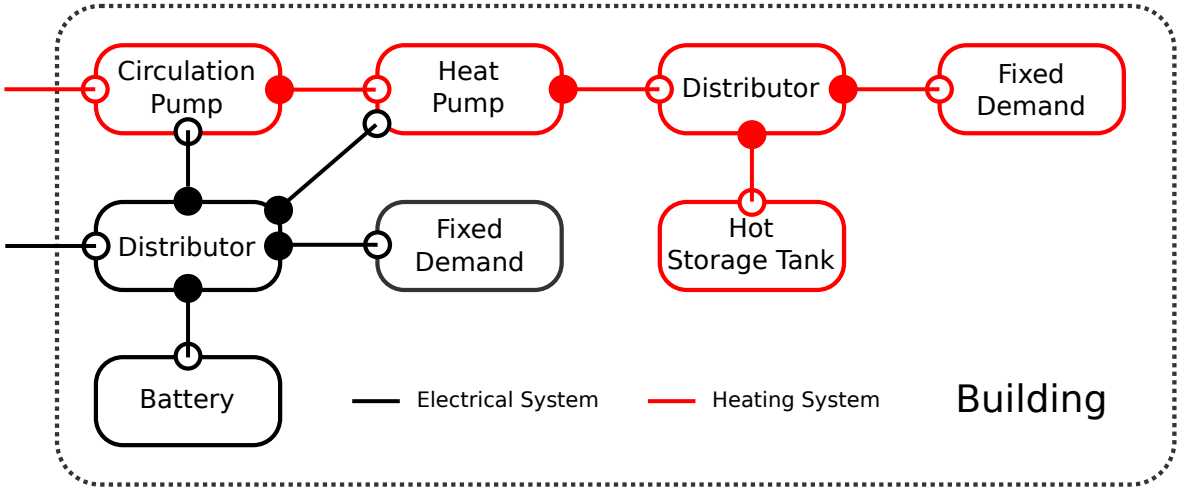

Figure 5.2: Illustration of aggregated building module. Buildings at nodes 31 and 59 utilise a cooling system, with a cold storage tank replacing the hot storage tank shown.

uously supplied by a sewage treatment plant. A large borehole storage field is also located local to the sewage plant at node 2. Nodes 3 to 85 represent buildings, all of which have fixed electricity and heating demands, with the exception of nodes 31 and 59 which both have fixed cooling demands. Every building has the use of a WSHP, circulation pump, battery and thermal storage water tank (Fig. 5.2). Two circulation pumps are located at the plant substation, one for network circulation and one for pumping through the borehole storage field (Fig. 5.3).

5.3.1 Control Problem

The objective function J_k minimised by the controller at each time step consists of the economic cost to each building for importing, and revenue for exporting, power

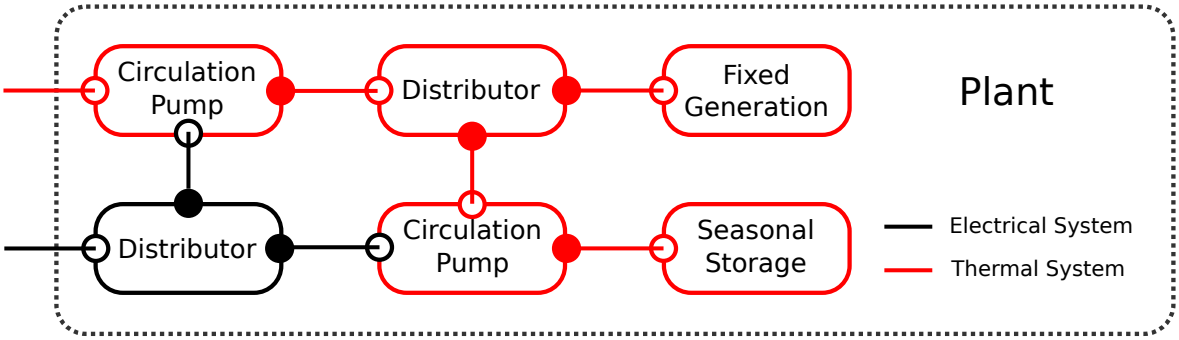

Figure 5.3: Illustration of aggregated plant module.

from/to the AC power network, as well as the cost associated with battery degradation. The controller also considers the cost for purchasing power at the plant substation and the penalty costs associated with each network. A purchase and sale cost modifier is applied to the electricity distributor output variable, $y_{k,\text{snk}_{1,elec}}$, of all N_B buildings, with associated prices $\lambda^{\text{buy}}_{k,y_{\text{snk}_1,\text{elec}}}$ and $\lambda^{\text{sell}}_{k,y_{\text{snk}_1,\text{elec}}}$. A value cost modifier is applied to the electricity distributor output variable, $y_{\text{snk}_{1,elec}}$, of the plant substation, with associated cost $\lambda^{\text{val}}_{k,y_{\text{snk}_1,\text{elec}}}$. A battery degradation cost coefficient $\lambda^{\text{abs}}_{k,u_{\text{batt,chg}}}$ is applied to all batteries by adding an absolute value cost modifier applied to $u_{k,\text{batt,chg}}$.

$$J_k = \sum_{h=0}^{H-1} c_{k+h} \tag{5.1}$$

$$\begin{aligned} c_{k+h} = \sum_{j}^{N_B} \Big[&(\lambda^{\text{buy}}_{k,y_{j,\text{snk}_1,\text{elec}}} - \lambda^{\text{sell}}_{k,y_{j,\text{snk}_1,\text{elec}}}) z_{k,y_{j,\text{snk}_1,\text{elec}},\text{buy}} + \lambda^{\text{sell}}_{k,y_{j,\text{snk}_1,\text{elec}}} \cdot y_{k,j,\text{snk}_1,\text{elec}} \\ &+ \lambda^{\text{abs}}_{k,u_{\text{batt}_j,\text{chg}}} \cdot z_{k,u_{\text{batt}_j,\text{chg}},\text{abs}} \Big] + \lambda^{\text{val}}_{k,y_{\text{plant,snk}_{1,elec}}} \cdot y_{\text{plant,snk}_{1,elec}} + c_{k,\text{AC}} + c_{k,\text{HC}} \end{aligned} \tag{5.2}$$

where the cost functions $c_{k,\text{AC}}$ and $c_{k,\text{HC}}$ are given in Sections 3.6.2 and 3.6.3.

The control problem is formally stated as:

$$\min_{v_i} J_k = \sum_{h=0}^{H-1} c_{k+h} \tag{5.3}$$

$$\text{s.t. (3.1)-(3.4)} \ \forall \ m$$

for which the m aggregated components are shown in Figs. 5.1 to 5.3 and the specific constraints for these components are given in Chapter 3.

5.3.2 Simulation Parameters and Inputs

The AC distribution network parameters are taken from a MATPOWER test case 'case85' [123] and the ULTDHC network parameters have been derived by normalising the AC line resistance values to obtain relative distances and scaling for a pipe pressure drop of 0.03 m$H_2O/100$ m at a base mass flow rate of 10 kg/s. Frictional losses in each substation are determined with the same head loss coefficient, $C_j = 5 \times 10^{-4}$ m$H_2O \cdot$ s/kg. Component model parameters are given in Table 5.1 and various operating limits for the district are given in Table 5.2.

Table 5.1: Component Model Coefficients

Parameter	Value[1]
Heat Pump COP	3.90
Heat Pump EER	2.10
Battery Cycle Efficiency	[0.68;0.81]
Battery Standby Loss Factor	2.50 $\times 10^{-4}$
Tank Standby Loss Factor	2.60 $\times 10^{-4}$
Borehole Standby Loss Factor	2.50 $\times 10^{-4}$
Circulation Pump Efficiency	0.49

[1] [a;b] - uniform random distribution.

Data to represent a day's active power and heating demands from the 83 buildings at 15 minute intervals (Figs. 5.4 and 5.5) have been assembled from an OpenEI dataset [124]. These data have been scaled so that network voltage and pressure constraints become active during simulation. For simplicity, the reactive power consumption at each node is assumed to be 0 p.u.; therefore reactive power is only supplied to balance power dissipated in network lines. Electricity purchase prices have been interpolated at 15 minute intervals from historic price data available from UK energy supplier Octopus Energy Ltd for their Agile Octopus tariff [116] (see the orange plot in Figs 5.6 and 5.7). Fixed prices are assumed for selling electricity and for battery degradation, at 1p/kWh and 3.15p/kWh, respectively. The penalty costs used to obtain exact solutions in the AC and ULTDHC networks are $\lambda^{\text{val}}_{\ell_{ij}} = 10$, $\lambda^{\text{val}}_{\Delta H_{ij}} = 100$ and $\lambda^{\text{val}}_{\text{pump}\Delta H_j} = 10$.

Table 5.2: District Parameters

Device Parameter	Value[1]	Units
AC Substation Capacity	3	MW
AC Voltage Limits	0.9 / 1.1	p.u.
ULTDHC Pipe Temperatures	16 / 20	°C
Plant Heat Input	1.60	MW
Plant Pump Max. Head Gain	50	mH_2O
Plant Pump Max. Mass Flow	250	kg/s
Borehole Storage Capacity	0.00 / 500	MWh
Borehole Heat Transfer Rate	-4.00 / 4.00	MW
Borehole Pump Head Gain	30	mH_2O
Battery Capacity Limits	[4.70;4.90] / [18.8;19.6]	kWh
Battery Charge Rate	[-12.5;-11.5] / [11.5;12.5]	kW
Tank Heat Capacity Limits	0.00 / 40.0	kWh
Tank Heat Transfer Rate	-20.0 / 20.0	kW
Building Pump Max. Head Gain	10	mH_2O

[1] $[a;b]$ - uniform random distribution.

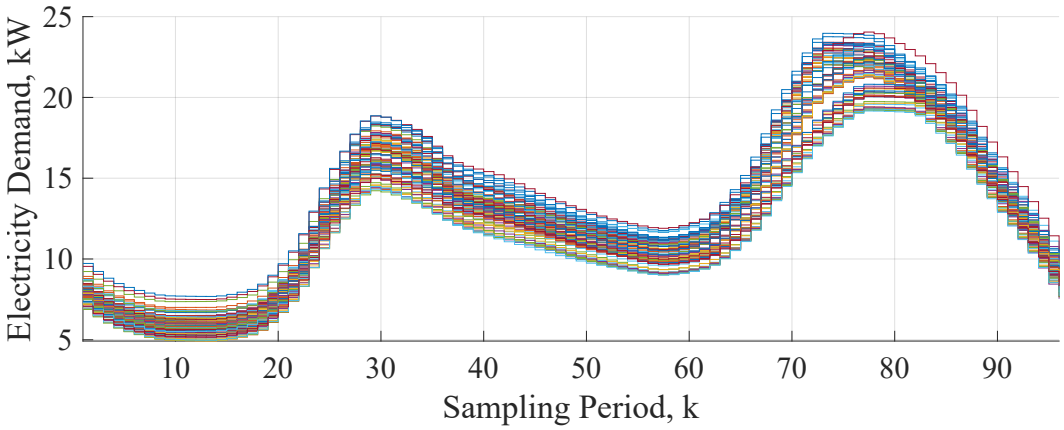

Figure 5.4: Electricity demand profiles used in simulations.

5.4 Results

The data described in Section 5.3.2 were used to run a simulation over 96 sampling periods of 15 minutes, with prediction horizon $H = 3$. The prediction horizon used, despite being very short, leads to unacceptably long computation times, which is why a longer horizon length was not simulated. The simulations were carried out using Gurobi [110] and YALMIP [106] in MATLAB [121] on a laptop with Intel Core i5-

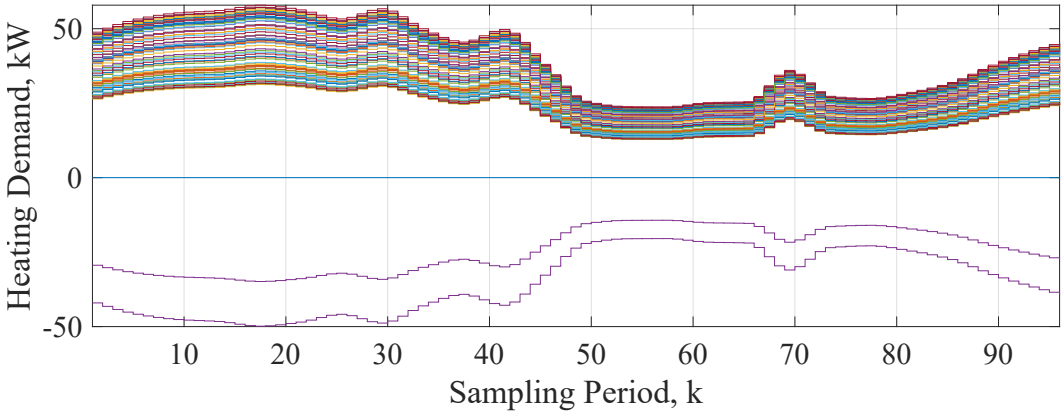

Figure 5.5: Heating demand profiles used in simulations.

6200U CPU @ 2.30GHz and 8 GB RAM. The default relative MIP gap tolerance of 1×10^{-4} was increased to a comparatively large value of 1×10^{-2}; this was necessary to speed up the already prohibitively long computation time of the controller in certain periods.

The electrical power and heat power supplied to all the buildings during the simulated day (Figs 5.6 and 5.7), is mostly consumed at periods of low electricity price. This shows that the controller is able to manipulate controllable devices in attempt to minimise the overall cost of the district. However, it is also apparent that the prediction horizon length is not long enough to deliver optimal control. The controller responds to a foreseen increase in the price of electricity in period $k = 62$ by increasing consumption of both electricity and heat to charge battery and thermal storage. This is enables a short term cost saving as the electricity and heat consumed in subsequent periods is temporarily reduced by discharging both types of storage. However, the price continues to rise whilst simultaneously the fixed demands for electricity and heat also rise, leaving the controller with no option but to purchase electricity and heat during the price peak because there is no stored power available. Clearly the prediction horizon length needs to be at least as long as the main price peak and preferably equal to cyclic patterns of price and energy use, i.e. one full day. Unfortunately, increases in the prediction horizon length are not possible as the time for computation with $H = 3$ is already prohibitive (Table 5.3). During one sampling instance the time taken to compute a control action was almost 1 hour, greatly exceeding the sampling interval of 15 minutes, and the standard deviation of over 7 minutes suggests poor consistency.

Although time consuming, the optimisation solutions that were returned by the controller were exact and ensured that the control actions were feasible for the global

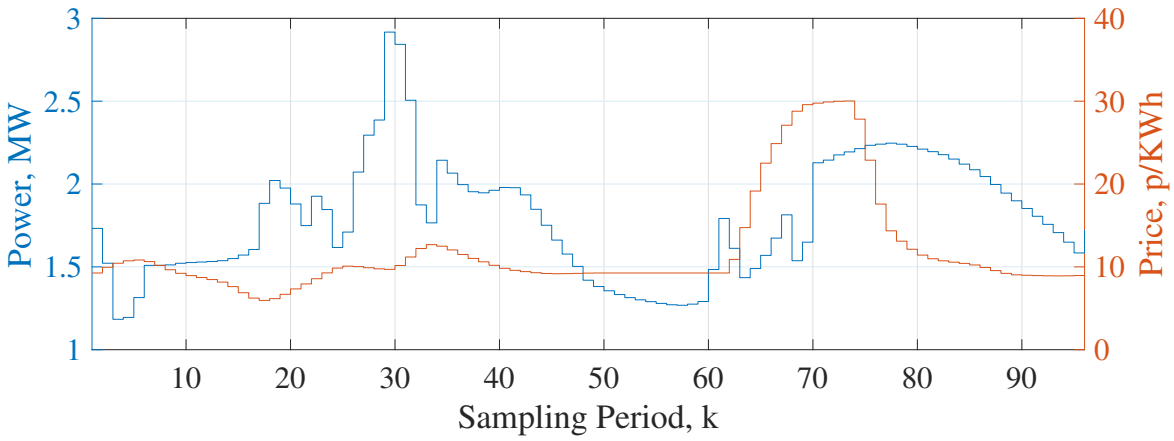

Figure 5.6: Total electrical power supplied to buildings.

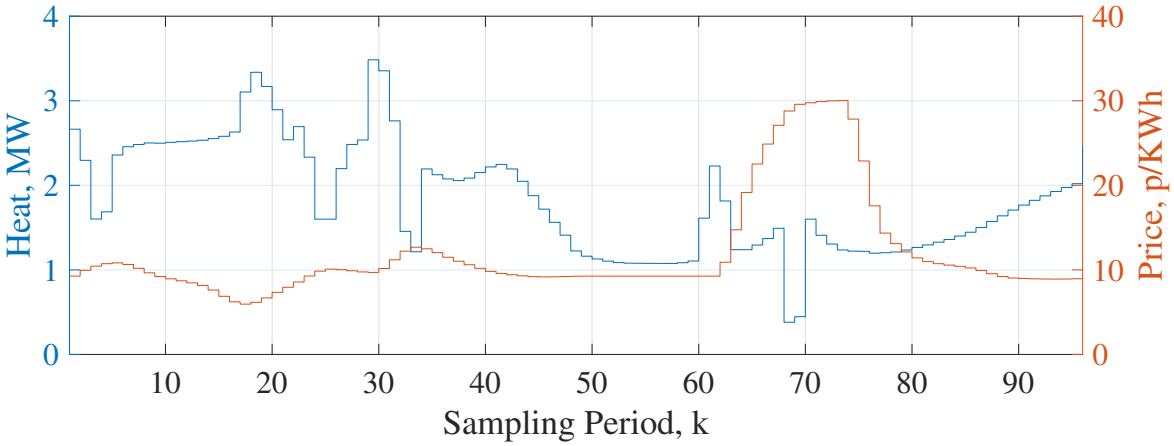

Figure 5.7: Total heat power supplied to buildings.

Table 5.3: Computational Performance over 96 Sampling Instances

	H = 3
Mean computation time, secs	153.88
Minimum computation time, secs	13.58
Maximum computation time, secs	3,354.40
Standard deviation of computation time, secs	464.57

system. This is demonstrated by the fact that, during the period of highest energy consumption, $k = 29$, both the nodal voltage and required pump head gain values were on or close to the operational limits, without exceeding them in any location (Figs. 5.8 and 5.9).

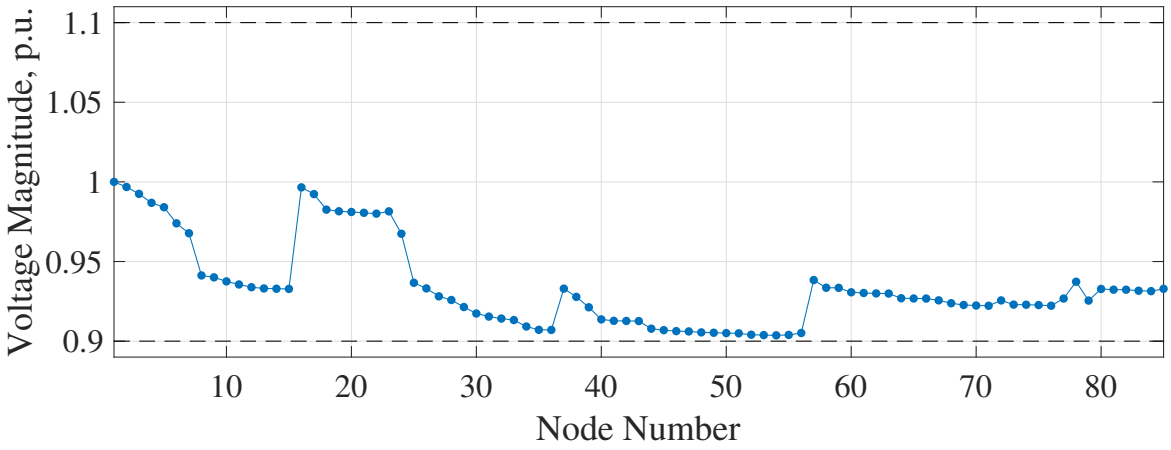

Figure 5.8: Voltage profile throughout AC network for sampling period $k = 29$. Dashed lines indicate voltage limits, as per Table 5.2.

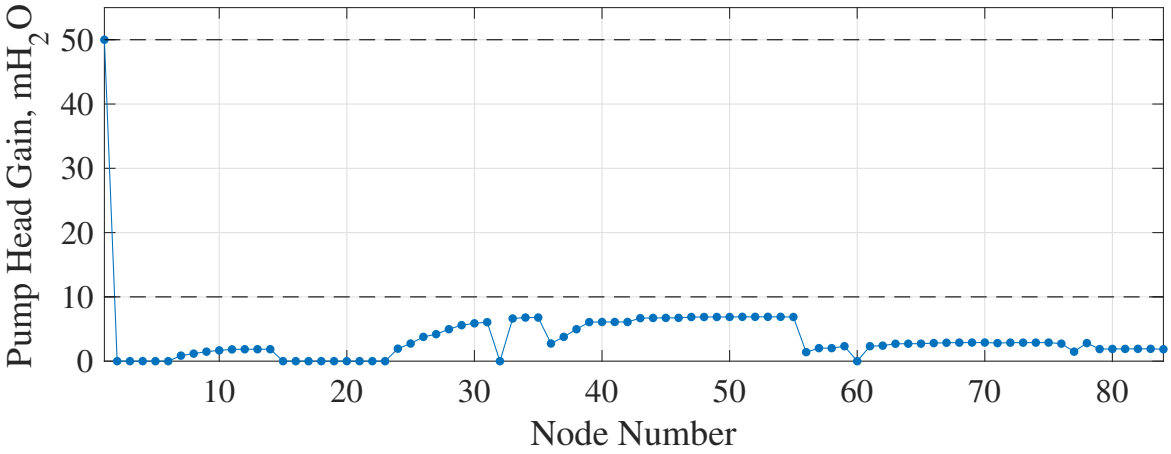

Figure 5.9: Pump pressure gain profile throughout ULTDHC network for sampling period $k = 29$. Dashed lines indicate limits on pump capacity, as per Table 5.2.

5.5 Conclusions

Three additional modules have been added to the multi-energy district control problem in this chapter, the AC and ULTDHC network modules together with the reversible variable-speed circulation pump module. There are several reasons for adding these modules:

- To improve the modelling accuracy of the AC network so that network voltage limits could be considered when determining control actions for a large district;
- To enable modelling of power consumption from variable speed pumps;
- To enable variable speed pump scheduling so that decentralised pump capacities are not exceeded and their interactions do not cause instabilities in regulatory feedback control loops.

Whilst the modules have achieved these aims, the number of binary variables and quadratic constraints introduced in each prevent efficient computation using an advanced commercial solver, evidenced by the excessively long computation times. This is despite reformulations to make the AC and ULTDHC network modules convex when integrality constraints are relaxed. Hence, if the benefits of these modules are to be realised in a real control application, the lengthy computation times must be addressed. In the following chapter a multi-agent control scheme is introduced to mitigate this problem.

Chapter 6

Multi-Agent Coordination Methods

6.1 Introduction

In the previous chapter, it was established that a single centralised controller would not be able to coordinate hybrid multi-energy systems in a large building district with multiple connecting networks. Another problem with this type of control structure is that, in the case of a commercial aggregator, it involves a violation of privacy and the need to take direct control of customer-owned distributed energy resources, neither of which are likely to be accepted by customers. Instead, a multi-agent control structure is needed which ensures that customer privacy and autonomy is maintained, whilst the burden of computation is shared amongst individual control agents. In this approach, building agents responsible for their own local system send non-sensitive energy demand data to an aggregator, which acts as a central coordinator performing limited calculations to ensure that any shared network constraints would not be violated by the aggregated energy demand. If shared constraints would be violated, the aggregator then sends updated price signals to the individual agents to encourage a particular behaviour, either to ensure network security within the district or to provide a flexibility service to support wider power system operation. This process is then repeated until shared network constraints are no longer violated, thereby coordinating the agents whilst preserving a degree of privacy and autonomy.

The available strategies to decompose large optimisation problems into smaller, more easily solved agent sub-problems, by solving the Lagrange dual, often rely on strong duality to ensure that the recovered solution to the original problem is optimal [125].

However, for non-convex, mixed-integer problems with non-zero duality gap, the recovered solution may be sub-optimal or even infeasible. Recently, this issue was addressed in [28] for dual decomposition of MILPs in which the problem is completely separable after the removal of global linear constraints. For problems of this structure, it was shown that a suitable amount of tightening of the global constraint enabled '*good*' feasible solutions to be found by using established methods to solve the dual problem, such as the subgradient method [126]. For high-level energy management control of complex energy systems which are subject to uncertainty, a 'good' feasible solution, as oppose to a globally optimal one, can be justified. The work in [28] was later extended with an algorithm for using the subgradient method with adaptive constraint tightening [27]. This algorithm reduces the conservatism introduced by the worst-case constraint tightening of [28] and in doing so increases the number of problems for which dual decomposition and constraint tightening might be applied. Proofs of finite-time convergence and performance guarantees for this algorithm are also provided in [27]. The first known application of the dual decomposition and constraint tightening technique of [27] within an MPC scheme was presented at the 29$^{\text{th}}$ Mediterranean Conference on Control and Automation (MED), Bari, Italy, 2021, by this author, for a case study considering 175 connected multi-energy buildings [32]. That work has since been developed and the results are presented in this chapter.

The relevant background to these previous works is presented in the following section. In Section 6.3, two alternative algorithms are presented that use well-known subgradient acceleration techniques, the *Classical Momentum* method and *Nesterov's Accelerated Gradient* method. Then, in Sections 6.5 and 6.6, these new algorithms are compared against that of [27] in two different case studies, the latter case study demonstrating the convergence and tuning difficulties when embedding the algorithm from [27] into a MPC scheme, which motivated the development of accelerated algorithms. The development of an MPC scheme with accelerated algorithms for multi-agent optimisation represents another contribution of this thesis.

6.2 Background

The background information presented in this section is an amalgamation of the theory presented in [27], [28]. It is intended to replicate the minimum prerequisites for

understanding the multi-agent method and does not contain any original contributions. The equations provided are taken almost verbatim from these sources, with some slight changes to notation and ordering which should facilitate understanding of the contributions made by each work.

The multi-agent method is applied to MILP problems with the following structure, which is separable after the removal of global coupling constraints [27]:

$$\begin{aligned} \min_{\boldsymbol{v}} \quad & \sum_{i \in M} \boldsymbol{c}_i^\top \boldsymbol{v}_i \\ \text{s.t.} \quad & \sum_{i \in M} A_i \boldsymbol{v}_i \leq \boldsymbol{b} \\ & \boldsymbol{v}_i \in \mathcal{V}_i, \quad \forall i \in M \end{aligned} \tag{$\mathcal{P}$}$$

in which $\boldsymbol{v}_i$ is the decision vector, $\boldsymbol{c}_i^\top \boldsymbol{v}_i$ is the local cost and $\mathcal{V}_i$ is the local constraint set of a subsystem i. Each mixed-integer polyhedral set $\mathcal{V}_i = \{\boldsymbol{v}_i \in \mathbb{R}^{r_i} \times \mathbb{Z}^{z_i} : D_i \boldsymbol{v}_i \leq \boldsymbol{d}_i\}$ is assumed to be non-empty and compact. Matrices $A_i \in \mathbb{R}^H \times \mathbb{R}^{r_i + z_i}$ and a single *resource* vector $\boldsymbol{b} \in \mathbb{R}^H$ define a global inequality constraint which is applied component-wise. By introducing a vector of Lagrange dual multipliers $\boldsymbol{\lambda} \in \mathbb{R}^H$ it is possible to derive the *dual problem*, ($\mathcal{D}$), of the primal problem ($\mathcal{P}$), in which the global constraint is added to the objective function:

$$\max_{\boldsymbol{\lambda} \geq 0} \quad -\boldsymbol{\lambda}^\top \boldsymbol{b} + \sum_{i \in M} \min_{\boldsymbol{v}_i \in V_i} \left(\boldsymbol{c}_i^\top + \boldsymbol{\lambda}^\top A_i \right) \boldsymbol{v}_i \tag{$\mathcal{D}$}$$

The inner minimisations within $\mathcal{D}$ are separable, lower-dimensional sub-problems associated with each subsystem i and may be solved in parallel by independent agents.

It is possible to solve $\mathcal{D}$ using a subgradient algorithm [126], in which candidate primal solutions $\boldsymbol{v}(\boldsymbol{\lambda})_i$ are determined for each inner minimisation problem over a series of iterations. If all the variables $\boldsymbol{v}_i$ in each local subsystem were continuous, then by averaging these tentative solutions across iterations, it would be possible to recover an optimal solution $\boldsymbol{v}(\boldsymbol{\lambda}^*)$ which is also an optimal solution of $\mathcal{P}$ [127]. However, in the mixed-integer case, the recovered solution would not satisfy the integrality condition and would therefore not be feasible for $\mathcal{P}$. What is actually recovered is a solution to the following problem, $\mathcal{P}_{\text{LP}}$:

$$\begin{aligned} \min_{\boldsymbol{v}} \quad & \sum_{i \in M} \boldsymbol{c}_i^\top \boldsymbol{v}_i \\ \text{s.t.} \quad & \sum_{i \in M} A_i \boldsymbol{v}_i \leq \boldsymbol{b} \\ & \boldsymbol{v}_i \in \text{conv}(V_i), \quad \forall i \in M \end{aligned} \tag{$\mathcal{P}_{\text{LP}}$}$$

where $\text{conv}(V_i)$ denotes the convex hull of V_i. This connection between the solution $\boldsymbol{v}^*_{\text{LP}}$ to $\mathcal{P}_{\text{LP}}$ and $\boldsymbol{v}(\boldsymbol{\lambda}^*)$ is exploited by the authors in [28]. They note that $(\boldsymbol{v}^*_{\text{LP}})_i \in V_i$ for at least $|M| - H$ sub-problems and $(\boldsymbol{v}^*_{\text{LP}})_i \in \text{conv}(V_i)$ for the remaining ones. They then prove the following proposition, transferring this useful property onto the inner solutions $\boldsymbol{v}(\boldsymbol{\lambda}^*)$.

Proposition 1. *(Relation between $\boldsymbol{v}^*_{LP}$ and $\boldsymbol{v}(\boldsymbol{\lambda}^*)$, Theorem 2.5, [28]). For $\boldsymbol{v}(\boldsymbol{\lambda}^*)_i \in \arg\min_{\boldsymbol{v}_i \in V_i} \left(\boldsymbol{c}_i^\top + \boldsymbol{\lambda}^\top A_i\right) \boldsymbol{v}_i$, $i \in M$, there exists $M_1 \subseteq M$, with $|M_1| \geq |M| - H$, such that $(\boldsymbol{v}^*_{LP})_i = \boldsymbol{v}_i(\boldsymbol{\lambda}^*)$*

This result is used to determine an amount of constraint tightening $\boldsymbol{\rho} \in \mathbb{R}^p$ in the following modified version of $\mathcal{P}$:

$$\begin{aligned} \min_{\boldsymbol{v}} \quad & \sum_{i \in M} \boldsymbol{c}_i^\top \boldsymbol{v}_i \\ \text{s.t.} \quad & \sum_{i \in M} A_i \boldsymbol{v}_i \leq \boldsymbol{b} - \boldsymbol{\rho} \\ & \boldsymbol{v}_i \in V_i, \quad \forall i \in M \end{aligned} \tag{$\overline{\mathcal{P}}$}$$

Let $\overline{\mathcal{D}}$ and $\overline{\mathcal{P}}_{\text{LP}}$ be defined similarly to $\mathcal{D}$ and $\mathcal{P}_{\text{LP}}$ but for the modified problem $\overline{\mathcal{P}}$.

Assumption 1. *(Existence and Uniqueness, [28]). Problems $\overline{\mathcal{D}}$ and $\overline{\mathcal{P}}_{LP}$ have unique solutions $\overline{\boldsymbol{\lambda}}^*$ and $\overline{\boldsymbol{v}}^*_{LP}$.*

Proposition 2. *(Feasible Solutions, Theorem 3.1 in [28]). If Assumption 1 holds then any primal solution $\boldsymbol{v}(\overline{\boldsymbol{\lambda}}^*)$ recovered when solving $\overline{\mathcal{D}}$ will be a feasible solution for $\mathcal{P}$, providing an appropriate $\boldsymbol{\rho}$ is used.*

If $\overline{\mathcal{P}}$ does not have a unique solution, then a small perturbation of the cost function coefficients can be incorporated to ensure the returned solution is unique and that Assumption 1 is fulfilled [28]. A worst-case contraction for the k-th element of $\boldsymbol{\rho}$ is given in (6.1). This means that in each row of the global constraint, the resource vector will be contracted by p times the largest possible consumption range of any subsystem [28].

$$[\boldsymbol{\rho}_{(1)}]_k = H \cdot \max_{i \in M} \left(\max_{\boldsymbol{v}_i \in V_i} A_i^k \boldsymbol{v}_i - \min_{\boldsymbol{v}_i \in V_i} A_i^k \boldsymbol{v}_i \right) \tag{6.1}$$

A less conservative contraction is given in (6.2), which contracts b by the p-largest possible consumption ranges of all subsystems, thus $\boldsymbol{\rho}_{(2)} \leq \boldsymbol{\rho}_{(1)}$ [27].

$$[\boldsymbol{\rho}_{(2)}]_k = \max_{\overline{M} \subseteq M,\, |\overline{M}| = H} \left\{ \sum_{i \in \overline{M}} \left(\max_{\boldsymbol{v}_i \in V_i} A_i^k \boldsymbol{v}_i - \min_{\boldsymbol{v}_i \in V_i} A_i^k \boldsymbol{v}_i \right) \right\} \tag{6.2}$$

An even less conservative contraction can be determined adaptively as per Algorithm 4, first proposed in [27]. In this algorithm the contraction is based on the p-largest consumption ranges determined up to the current iteration, j, of an iterative scheme. This approach is herein referred to as multi-agent dual decomposition and adaptive constraint tightening, which is shortened to simply *MA*.

Algorithm 4 MA algorithm from [27]

1: $\overline{\boldsymbol{s}}_i(0) = -\infty,\ i \in M$
2: $\underline{\boldsymbol{s}}_i(0) = +\infty,\ i \in M$
3: $j = 0$
4: **while** stopping criteria is not met **do**
5: **for** $i = 1$ to $|M|$ **do**
6: $\boldsymbol{v}_i(j+1) \leftarrow \arg\min_{\boldsymbol{v}_i \in V_i} (\boldsymbol{c}_i^\top + \boldsymbol{\lambda}(j)^\top A_i)\boldsymbol{v}_i$
7: **end for**
8: $\overline{\boldsymbol{s}}_i(j+1) = \max\{\overline{\boldsymbol{s}}_i(j), A_i\boldsymbol{v}_i(j+1)\},\ i \in M$
9: $\underline{\boldsymbol{s}}_i(j+1) = \min\{\underline{\boldsymbol{s}}_i(j), A_i\boldsymbol{v}_i(j+1)\},\ i \in M$
10: $\boldsymbol{\rho}_i(j+1) = \overline{\boldsymbol{s}}_i(j+1) - \underline{\boldsymbol{s}}_i(j+1),\ i \in M$
11: $\boldsymbol{\rho}(j+1) = \max\left\{\sum_{i \in \overline{M}, |\overline{M}| = H} \rho_i(j+1)\right\}$
12: $\nabla \boldsymbol{g}(j+1) = \sum_{i \in M} A_i\boldsymbol{v}_i(j+1) - \boldsymbol{b} + \boldsymbol{\rho}(j+1)$
13: $\boldsymbol{\lambda}(j+1) = [\boldsymbol{\lambda}(j) + \alpha(j)\nabla \boldsymbol{g}(j+1)]_+$
14: $j \leftarrow j + 1$
15: **end while**

MA is a variant of the subgradient algorithm, with steps 6 and 13 comprising the two main subgradient update steps. Step 6 may be carried out in parallel by individual agents and the output communicated to a central coordinator that is responsible for all remaining steps. In Step 13 the dual multiplier is updated, involving a step-length equal to $\alpha(j)$ and a projection onto the positive orthant, denoted by $[\cdot]_+$. The step-length sequence $\{\alpha(j)\}_{j \geq 0}$ is chosen so that $\alpha(j) \to 0$ and $\sum_{j=1}^{\infty} \alpha(j) = \infty$. A simple stopping criterion is that the original global constraint in $\mathcal{P}$ is satisfied for a number of consecutive iterations, e.g. 5 iterations.

Assumption 2. *(Boundedness). The polyhedral sets $V_i, i \in M$, in $\mathcal{P}$ are bounded.*

Under Assumption 2, the iterative sequence to determine $\boldsymbol{\rho}$ in Algorithm 4 converges in finite-time to some $\overline{\boldsymbol{\rho}}$, since it takes values from a finite-set and is monotonically

increasing [27]. Therefore the following proposition, an extension to Proposition 2, holds for Algorithm 4 (see [27] for detailed proofs).

Proposition 3. *(Finite-time Feasibility, Theorem 1 in [27]). Under Assumptions 1 and 2, there exists a finite iteration index J such that, for all $j \geq J$, $\boldsymbol{v}(j)$ is a feasible solution for $\mathcal{P}$, i.e., $\sum_{i \in M} A_i \boldsymbol{v}_i(j) \leq \boldsymbol{b}$, $j \geq J$ and $\boldsymbol{v}_i(j) \in V_i$, where $\boldsymbol{v}_i(j)$, $i \in M$ are computed by Algorithm 4.*

A finite-time optimality bound may be similarly defined [27]. First, for any iteration $j \geq 1$ in Algorithm 4, let

$$\phi = H \cdot \max_{i \in M} \left\{ \max_{r \leq j} \boldsymbol{c}_i^\top \boldsymbol{v}_i(r) - \min_{r \leq j} \boldsymbol{c}_i^\top \boldsymbol{v}_i(r) \right\} \tag{6.3}$$

Assumption 3. *(Slater). There exists a scalar $\zeta > 0$ and $\hat{\boldsymbol{v}}_i \in conv(V_i)$ for all $i \in M$ such that $\sum_{i \in M} A_i \hat{\boldsymbol{v}}_i \leq b - \overline{\boldsymbol{\rho}} - \zeta \left| M \right| \mathbb{1}$.*

Proposition 4. *(Performance Guarantee, Theorem 2 in [27]). Under assumptions 1-3, there exists a finite iteration index J such that, for all $j \geq J$, $\boldsymbol{v}(j)$ is a feasible solution for $\mathcal{P}$ that satisfies:*

$$\sum_{i \in M} \boldsymbol{c}_i^\top \boldsymbol{v}_i(j) - C_{\mathcal{P}^*} \leq \phi + \frac{||\overline{\boldsymbol{\rho}}||_\infty}{H\zeta} \phi \tag{6.4}$$

where $C_{\mathcal{P}^*}$ is the optimal cost of $\mathcal{P}$ and $\boldsymbol{v}_i(j)$, $i \in M$ are computed by Algorithm 4.

The MA method is an effective means to distribute the computational burden of large problems with the form of $\mathcal{P}$ over multiple agents. Furthermore, as the number of managed subsystems $|M| \to \infty$ for a fixed dimension H of the global constraint, the optimality gap to $C_{\mathcal{P}^*} \to 0$ [28]. However, whilst MA achieves these feasibility and performance guarantees in finite-time, the actual timescale for convergence may not always be considered of practical benefit, as shown in Sections 6.5 and 6.6. Moreover, tuning of MA by changing the step-length sequence can be difficult because the step-length sequence can either be tuned for large subgradients (relative to final optimal dual values), requiring small step-lengths, or small subgradients, requiring large step-lengths, but not both. Excessive oscillations occur if large step-lengths are used with large sub-gradient values, whereas asymptotic-like convergence may result if small step-lengths are used with small sub-gradients. This issue must be addressed in receding horizon control schemes since there is no time available for trial and error tuning at each sampling instance.

Algorithm 5 MA-CM algorithm

1: Steps 1 to 3 of Algorithm 4.
2: **while** stopping criteria not met **do**
3: Steps 5 to 12 of Algorithm 4.
4: $\boldsymbol{\lambda}(j+1) = [\boldsymbol{\lambda}(j) + \alpha \nabla \boldsymbol{g}(j+1) + \beta\,(\boldsymbol{\lambda}(j) - \boldsymbol{\lambda}(j-1))]_+$
5: $j \leftarrow j+1$
6: **end while**

In the following section improved algorithms are proposed with the intention of avoiding this problem, by accelerating convergence when using small step-lengths. The two acceleration methods are the well-known Classical Momentum method [128] and Nesterov's Accelerated Gradient method [129]. These methods are chosen over other acceleration methods because no prior knowledge of optimal converged values is required to determine the step-length at each iteration [128]. In Section 6.5, comparable performance of each algorithm is demonstrated for an electric vehicle (EV) charging case study, providing that algorithm parameters have been tuned effectively. Section 6.6 then demonstrates the superior performance of MA algorithm with accelerated gradients for model predictive control of connected multi-energy buildings, in which the presence of very small dual function subgradients slows down convergence at certain sampling instances.

6.3 Proposed Accelerated Algorithms

The alternatives to MA that are explored in the following sections are shown in Algorithms 5 and 6, which are herein referred to as MA with **C**lassical **M**omentum (MA-CM) and MA with **N**esterov's **A**ccelerated **G**radient (MA-NAG). In each algorithm, the dual update step is replaced by an accelerated dual update step and all duals are initialised with $\boldsymbol{\lambda}(0) = 0$. The momentum variable μ, which is used in MA-NAG, is also initialised with $\boldsymbol{\mu}(0) = 0$. It should be noted that the dual update for MA-NAG is only restricted to the positive orthant when updating $\boldsymbol{\lambda}$, not for the update of $\boldsymbol{\mu}$ (step 4 of Algorithm 6). This is to prevent the acceleration term exhibiting a bias towards positive subgradients. A feasible solution is found when all subgradients are non-positive, i.e. $\nabla \boldsymbol{g} \leq 0$.

Algorithm 6 MA-NAG algorithm

1: Steps 1 to 3 of Algorithm 4.
2: **while** stopping criteria not met **do**
3: Steps 5 to 12 of Algorithm 4.
4: $\boldsymbol{\mu}(j+1) = \boldsymbol{\lambda}(j) + \alpha \nabla \boldsymbol{g}(j+1)$
5: $\boldsymbol{\lambda}(j+1) = \left[\boldsymbol{\mu}(j+1) + \frac{j}{j+\beta}\left(\boldsymbol{\mu}(j+1) - \boldsymbol{\mu}(j)\right)\right]_+$
6: $j \leftarrow j+1$
7: **end while**

In each algorithm an additional tuning parameter is introduced, β, which must be determined a-priori. For MA-CM the value of β should be chosen within the interval $(0, 1)$ and requires a trial and error approach to determine a suitable value. When NAG is applied to problems such as ordinary differential equations which are convex and Lipschitz continuous, it is possible to determine values for α and β which guarantee convergence at a rate $\mathcal{O}(1/t^2)$ [129]. However, the dual problem $\overline{\mathcal{D}}$ does not exhibit these convenient properties and therefore requires a heuristic approach to determine these parameters. A value of $\beta = 3$ works well for MA-NAG in all the problems encountered, which constitutes a monotonically increasing series $\sum_{j=1}^{\infty} \frac{j}{j+\beta}$ in the interval [0.25,1). For both algorithms the initial value of α is chosen to be sufficiently small that large dual price oscillations do not occur, which can otherwise slow down convergence and cause the contraction $\boldsymbol{\rho}$ to be excessive, which would then lead to overly conservative constraint tightening.

6.4 Control Schemes

When using these algorithms in a MPC scheme, it is necessary to define new control algorithms for both individual agents and the central energy coordinator. An overview of the multi-agent control scheme (Fig. 6.1) illustrates the communication signals between N agents and the central energy coordinator; it should be noted that agents do not communicate with one another. Although a fully distributed scheme, in which agents only communicate with their nearest neighbours, may be preferable in some multi-agent control schemes, the central coordinator is utilised here so that it can perform optimal energy flow checks when detailed network modules are con-

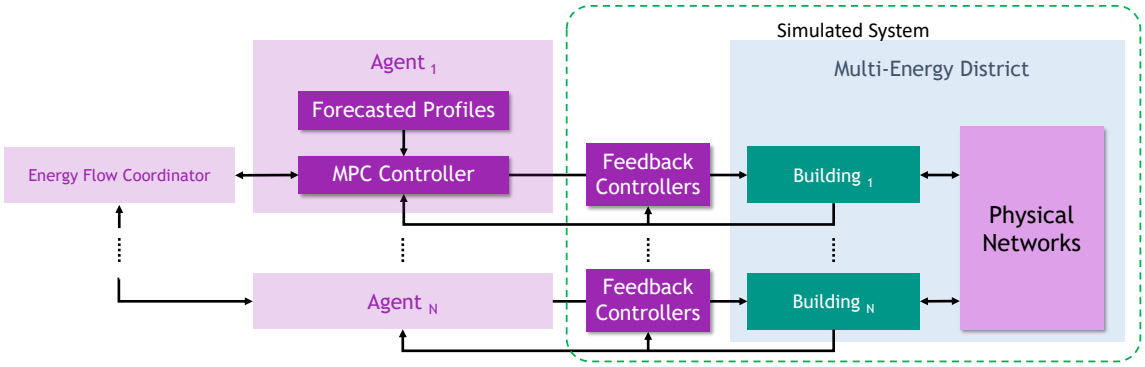

Figure 6.1: Illustration of the multi-agent district control scheme. Although only shown for Agent 1, all agents in the scheme receive forecasted data and utilise a controller.

sidered. The scheme is applied to the case study from Chapter 5 in the next chapter, which requires detailed network modelling.

Component modules aggregated at the building level provide the system models for individual agent MPC controllers. The optimisation problem for each agent controller $i \in M$ is to minimise the cost function given in 6.5, subject to the local system model of m_i aggregated components within a given building i.

$$J_{k,i} = \sum_{h=0}^{H-1} c_{k+h,i} + \boldsymbol{\lambda}^{\text{val}\,\top}_{k+h,\text{dual}} A_i \boldsymbol{v}_{k+h,i} \tag{6.5}$$

Solving the agent's optimisation problem provides a candidate solution vector $\boldsymbol{v}_{k,i}$ which is communicated to the central coordinator, as per Algorithm 7. The central coordinator then carries out Algorithm 8, 9 or 10 (depending on the selected method). Updated dual prices, $\boldsymbol{\lambda}^{\text{val}}_{\text{dual}}$, are then returned to the agent with an instruction to carry out the optimisation again, if the stopping criteria has not been met, or otherwise an instruction to continue, at which point the agent will implement the control actions based on the incumbent solution. This means that the agents are coordinated – dual prices are used to encourage globally feasible solutions and control actions are not implemented until a globally feasible solution has been found – but that they have autonomy over how they operate their local system in response to the combination of actual energy prices and imposed dual prices.

The dual update vectors $\boldsymbol{\lambda}^{\text{val}}_{\text{dual}}$ and $\boldsymbol{\mu}$ are initialised with all zero vectors only once before the control scheme is online. Once online, these vectors are warm started at each k, determined by applying a circular shift to the final vectors of the previous

Algorithm 7 Agent receding horizon scheme

1: $t = 0,\ \Delta t > 0$
2: Initialise $\boldsymbol{\lambda}_{\text{dual}}^{\text{val}}$ with zero vector, $\mathbf{0}^{H\times 1}$
3: **for** $k = 0, 1, 2, ...$ **do**
4: Update current system states, $\mathbf{x}_k$
5: Update price forecasts, $\boldsymbol{\lambda}_{k+h}^{\text{val}},\ h = 0, ..., H-1$
6: Update disturbance forecasts, $\mathbf{w}_{k+h},\ h = 0, ..., H-1$
7: Minimise the agent control objective (6.5)
8: Communicate candidate solution, $\boldsymbol{v}_i$, to the central coordinator
9: **Wait until** instruction received from central coordinator
10: **if** instruction == "re-optimise" **then**
11: Go to step 7
12: **end if**
13: Pass control inputs for next sampling interval, $\mathbf{u}_k$, to lower-level feedback controllers; discard $\mathbf{u}_{k+h},\ h = 1, ..., H-1$
14: **Wait until** $t = (k+1)\Delta t$
15: $k = k + 1$
16: **end for**

control instance (step 16 of Algorithm 8). The circular shift is described by multiplication with the matrix, $\boldsymbol{C}_{\text{shift}} = \begin{bmatrix} 0 & \mathbf{I} \\ 1 & 0 \end{bmatrix}$. After applying this shift, the final element of each vector is given a zero value. This is to reduce the number of algorithm iterations taken to find a feasible solution at each sampling instance. Algorithm iterations for a given control sampling instance are interrupted once a suitable stopping criteria has been met, e.g. that the incumbent agent solutions do not violate any global constraints. Since the primary aim of this chapter is to assess the functionality of the multi-agent algorithms, uncertainty is not considered; perfect forecasts are provided to the agent controllers.

In the following sections, the performance of the multi-agent optimisation algorithms and the multi-agent MPC schemes are compared in consecutive case studies.

Algorithm 8 Central coordination using MA method in receding horizon scheme

1: Initialise $\boldsymbol{\lambda}_{\text{dual}}^{\text{val}}$ with zero vector, $\mathbf{0}^{H\times 1}$
2: Initialise $\overline{\boldsymbol{s}}_i(0) = -\infty,\ i \in M$
3: Initialise $\underline{\boldsymbol{s}}_i(0) = +\infty,\ i \in M$
4: $j = 0$
5: **if** new candidate solutions, $\boldsymbol{v}_i$, received from all agents $i \in M$ **then**
6: $\quad \overline{\boldsymbol{s}}_i(j+1) = \max\left\{\overline{\boldsymbol{s}}_i(j), A_i\boldsymbol{v}_i(j+1)\right\},\ i \in M$
7: $\quad \underline{\boldsymbol{s}}_i(j+1) = \min\left\{\underline{\boldsymbol{s}}_i(j), A_i\boldsymbol{v}_i(j+1)\right\},\ i \in M$
8: $\quad \boldsymbol{\rho}_i(j+1) = \overline{\boldsymbol{s}}_i(j+1) - \underline{\boldsymbol{s}}_i(j+1),\ i \in M$
9: $\quad \boldsymbol{\rho}(j+1) = \max\left\{\sum_{i\in\overline{M},|\overline{M}|=H} \rho_i(j+1)\right\}$
10: $\quad \nabla \boldsymbol{g}(j+1) = \sum_{i\in M} A_i\boldsymbol{v}_i(j+1) - \boldsymbol{b} + \boldsymbol{\rho}(j+1)$
11: $\quad \boldsymbol{\lambda}_{\text{dual}}^{\text{val}}(j+1) = \left[\boldsymbol{\lambda}_{\text{dual}}^{\text{val}}(j) + \alpha(j)\nabla \boldsymbol{g}(j+1)\right]_+$
12: $\quad$ **if** stopping criteria not met **then**
13: $\quad\quad$ Broadcast $\boldsymbol{\lambda}_{\text{dual}}^{\text{val}}$ to agents $i \in M$ with instruction "re-optimise"
14: $\quad\quad j = j + 1$
15: $\quad$ **else**
16: $\quad\quad$ Shift algorithm parameter vector $\boldsymbol{\lambda}_{\text{dual}}^{\text{val}}$ by one time step
17: $\quad\quad$ Broadcast $\boldsymbol{\lambda}_{\text{dual}}^{\text{val}}$ to agents $i \in M$ with instruction "continue"
18: $\quad\quad \overline{\boldsymbol{s}}_i(0) = -\infty,\ i \in M$
19: $\quad\quad \underline{\boldsymbol{s}}_i(0) = +\infty,\ i \in M$
20: $\quad\quad j = 0$
21: $\quad$ **end if**
22: **end if**
23: Go to step 5

Algorithm 9 Central coordination using MA-CM method in receding horizon scheme

1: Steps 1 to 4 of Algorithm 8.
2: **if** new candidate solutions, $\boldsymbol{v}_i$, received from all agents $i \in M$ **then**
3: $\quad$ Steps 6 to 10 of Algorithm 8.
4: $\quad \boldsymbol{\lambda}_{\text{dual}}^{\text{val}}(j+1) = \left[\boldsymbol{\lambda}_{\text{dual}}^{\text{val}}(j) + \alpha\nabla \boldsymbol{g}(j+1) + \beta\left(\boldsymbol{\lambda}_{\text{dual}}^{\text{val}}(j) - \boldsymbol{\lambda}_{\text{dual}}^{\text{val}}(j-1)\right)\right]_+$
5: $\quad$ Steps 12 to 21 of Algorithm 8.
6: **end if**
7: Go to step 2

Algorithm 10 Central coordination using MA-NAG method in receding horizon scheme

1: Initialise $\boldsymbol{\mu}$ with zero vector, $\mathbf{0}^{H\times 1}$
2: Steps 1 to 4 of Algorithm 8.
3: **if** new candidate solutions, $\boldsymbol{v}_i$, received from all agents $i \in M$ **then**
4: Steps 6 to 10 of Algorithm 8.
5: $\boldsymbol{\mu}(j+1) = \boldsymbol{\lambda}^{\text{val}}_{\text{dual}}(j) + \alpha\nabla\boldsymbol{g}(j+1)$
6: $\boldsymbol{\lambda}^{\text{val}}_{\text{dual}}(j+1) = \left[\boldsymbol{\mu}(j+1) + \frac{j}{j+\beta}\left(\boldsymbol{\mu}(j+1) - \boldsymbol{\mu}(j)\right)\right]_+$
7: **if** stopping criteria not met **then**
8: Broadcast $\boldsymbol{\lambda}^{\text{val}}_{\text{dual}}$ to agents $i \in M$ with instruction "re-optimise"
9: $j = j + 1$
10: **else**
11: Shift algorithm parameter vectors $\boldsymbol{\lambda}^{\text{val}}_{\text{dual}}$ and $\boldsymbol{\mu}$ by one time step
12: Broadcast $\boldsymbol{\lambda}^{\text{val}}_{\text{dual}}$ to agents $i \in M$ with instruction "continue"
13: $\overline{\boldsymbol{s}}_i(0) = -\infty,\ i \in M$
14: $\underline{\boldsymbol{s}}_i(0) = +\infty,\ i \in M$
15: $j = 0$
16: **end if**
17: **end if**
18: Go to step 3

6.5 Case Study: Application to Optimal EV Charging

To provide a fair comparison between MA and the accelerated MA-CM and MA-NAG algorithms (Algorithms 4 - 6), each are applied to the plug-in electric vehicle (EV) charging problem described in [28], which was used to demonstrate the performance improvements of MA in [27]. In other words, the EV problem is an example of the type of problem for which the MA method was originally intended (although reference to MPC schemes is made in [27]). This problem considers m vehicles for which an optimal 24 hour charging schedule must be found to satisfy local constraints, such as EV battery limitations and a specified minimum final charge state, as well as a shared capacity limit for power supply in each time slot.

6.5.1 Simulation Inputs and Parameters

The 'charge-only' case in which EVs only import power from the network is considered, with the battery component module used to represent EVs. The problem was set-up with $m = 300$ and power capacity limit $b = 1.5m$, whilst all other inputs and parameters were randomly generated from uniform probability distributions, including the electricity price, as described in Table 1 of [28]. The step-length sequence used for all algorithms was either $\alpha = \sum_{j=1}^{j_{max}} 1 \times 10^{-5}/j$ or $\alpha = \sum_{j=1}^{j_{max}} 5 \times 10^{-6}/j$, where j is the iteration index and $j_{max} = 300$. For MA-CM, three values for β were explored, 0.5, 0.7 and 0.9, with $\beta = 0.5$ found to give the best performance for this problem, both in terms of optimality and number of iterations to convergence. The stopping criterion used in all cases was that the recovered primal solution was feasible for 5 consecutive iterations.

6.5.2 Results

The local minimisations carried out in step 7 of Algorithm 4 were solved using Gurobi [110] and YALMIP [106] in MATLAB [121] on a laptop with Intel Core i5-6200U CPU @ 2.30GHz and 8 GB RAM. The default settings for MILP problems were used in Gurobi. Across 50 independent simulations with randomly generated parameters, optimality of the solution was comparable across the three methods whenever convergence was achieved (Fig. 6.2), though did marginally favour MA with an initial $\alpha = 5 \times 10^{-6}$. It is clear that the MA algorithm is more sensitive to the choice of α than the other two methods, since when the initial value of α is halved from 1×10^{-5} to 5×10^{-6}, the number of iterations to convergence increase significantly for certain simulations, with three simulations failing to converge within the iteration limit (Fig. 6.3). In these simulations, the dual multipliers approach their optimal values too slowly, the effect of diminishing step-length causing convergence to appear asymptotic. For the two accelerated algorithms, on the other hand, the additional momentum terms used for the dual updates counteract the effect of diminishing step-length, accelerating duals to their optimum values when using either α sequence.

The EV charging problem highlights that MA requires some tuning to achieve a consistently fast convergence rate, which can be impractical if used within a receding horizon control scheme where system conditions are likely to change. In the follow-

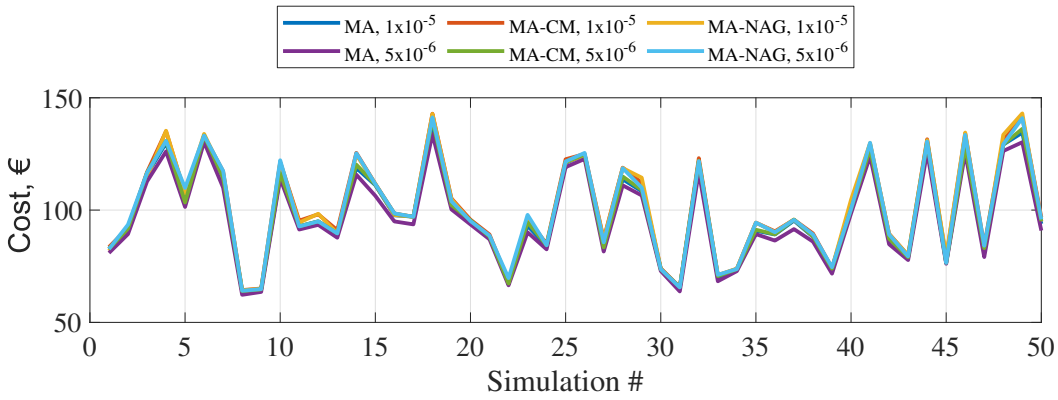

Figure 6.2: Overall cost of EV charging determined from 50 independent charge schedule optimisations, plotted for each algorithm and each initial step-length.

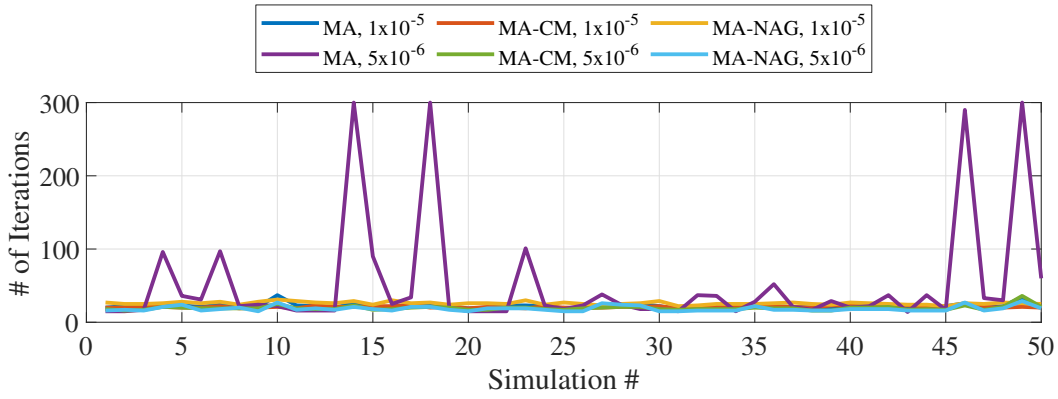

Figure 6.3: Number of iterations before convergence for 50 independent charge schedule optimisations, plotted for each algorithm and each initial step-length. Convergence was not achieved in instances where the maximum number of iterations, $j_{max} = 300$, is shown.

ing section another energy management problem is explored in which these difficulties become more apparent.

6.6 Case Study: Application to Multi-Energy Building Control

This case study is a development of research undertaken as part of this project which has already been published in conference proceedings [32]; for brevity, the prior case study description is not replicated here and the interested reader is referred to [32] for full details. The previous study demonstrated the application of Algorithm 8 for management of 175 connected multi-energy buildings with limited supply capacity of both electricity and gas. Each building was able to schedule it's own microturbine-driven combined heat and power unit (μ-CHP), heat pump and battery, providing

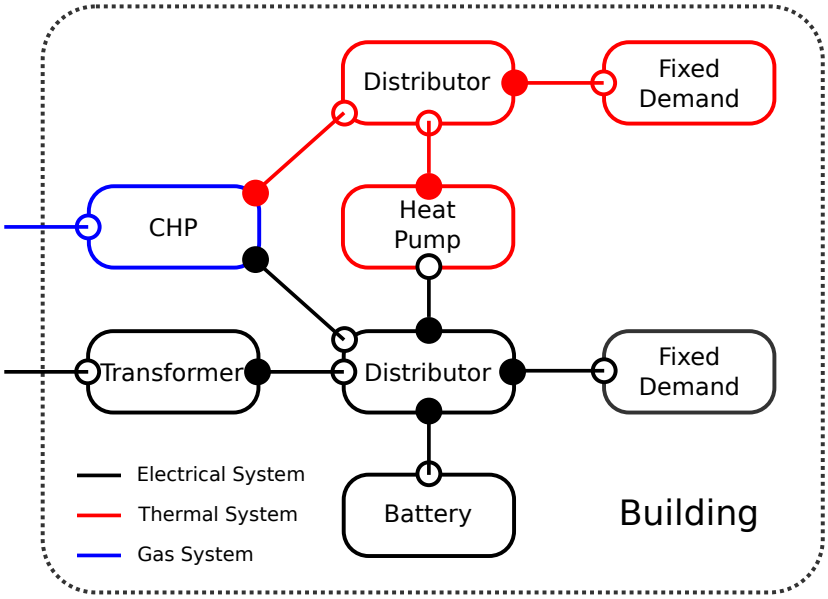

Figure 6.4: Illustration of aggregated building module.

some flexibility in electricity consumption (Fig. 6.4). Additional flexibility was made available to local agent controllers via pliable heating demands for each building, for which the consumption profile could be manipulated within four hour phases. The agents' objective was to minimise local costs, similarly to the previously discussed EV charging schedule problem, whilst ensuring that the gas and electricity consumed by all buildings did not exceed capacity limits of 500 kW for each network. A sampling interval of one hour was chosen and the prediction horizon length was $H = 24$. The MA based MPC scheme exhibited good performance against an equivalent centralised control scheme, with order of magnitude reductions in computation time for only a 3.7% increase in overall costs. However, subsequent work has highlighted that in situations for which there is less available flexibility and a shorter sampling period, such that the same prediction horizon length covers a shorter time span, the MA based scheme exhibits convergence issues.

To demonstrate these issues, the case study presented below lowers the capacity limit of the electricity network, removes the gas capacity constraint, increases the sampling frequency and removes the flexibility from pliable heating demands. The effect of these changes when determining dual prices is that very small subgradients are encountered in certain time periods, associated with small violations of shared constraints. Furthermore, at certain times such small subgradients are derived from agent candidate solutions which reside in steep-sided local minima. This situation requires large dual update step-lengths to quickly move away from these local minima and find a globally feasible solution, since the small subgradients depress the size

of dual updates. However, at other time periods the agent solutions reside in very shallow local minima, which requires small step-lengths to minimise dual multiplier oscillations which would otherwise slow down convergence to a feasible solution. It is therefore possible to demonstrate the difficulties in choosing a suitable step-length sequence for MA when embedded in an MPC scheme, unlike in the EV charging problem, in which only shallow local minima are encountered.

6.6.1 Control Problem

The objective function $J_{k,i}$ minimised by agent controller i at each time step consists of the economic cost to each building for importing, and revenue for exporting, power from/to the AC power network, the cost for importing gas, as well as the cost associated with battery degradation. A purchase and sale cost modifier is applied to the electricity transformer output variable, $y_{k,\text{tx,in}}$, with associated prices $\lambda^{\text{buy}}_{k,y_{\text{tx,in}}}$ and $\lambda^{\text{sell}}_{k,y_{\text{tx,in}}}$. A value cost modifier is applied to the CHP output variable, $y_{\text{chp,in}}$, with associated cost $\lambda^{\text{val}}_{k,y_{\text{tx,in}}}$. A battery degradation cost coefficient $\lambda^{\text{abs}}_{k,u_{\text{batt,chg}}}$ is applied to the battery by adding an absolute value cost modifier applied to $u_{k,\text{batt,chg}}$.

$$J_{k,i} = \sum_{h=0}^{H-1} c_{k+h,i} + \boldsymbol{\lambda}^{\text{val}\,\top}_{k+h,\text{dual}} A_i \boldsymbol{v}_{k+h,i} \tag{6.6}$$

$$c_{k+h,i} = (\lambda^{\text{buy}}_{k,y_{i,\text{tx,in}}} - \lambda^{\text{sell}}_{k,y_{i,\text{tx,in}}}) z_{k,y_{i,\text{tx,in}},\text{buy}} + \lambda^{\text{sell}}_{k,y_{i,\text{tx,in}}} \cdot y_{k,i,\text{tx,in}} + \lambda^{\text{val}}_{k,y_{i,\text{chp,in}}} \cdot y_{i,\text{k,chp,in}} + \lambda^{\text{abs}}_{k,u_{\text{batt}_i,\text{chg}}} \cdot z_{k,u_{\text{batt}_i,\text{chg}},\text{abs}} \tag{6.7}$$

$$\boldsymbol{\lambda}^{\text{val}\,\top}_{k+h,\text{dual}} A_i \boldsymbol{v}_{k+h,i} = \lambda^{\text{val}\,\top}_{k+h,\text{tx,in,dual}} \cdot y_{k,i,\text{tx,in}} \tag{6.8}$$

The agent control problem is formally stated as:

$$\min_{v_i} J_{k,i} = \sum_{h=0}^{H-1} c_{k+h,i} + \boldsymbol{\lambda}^{\text{val}\,\top}_{k+h,\text{dual}} A_i \boldsymbol{v}_{k+h,i} \tag{6.9}$$

$$\text{s.t. (3.1)-(3.4)} \;\forall\; m_i$$

for which the m_i aggregated components are shown in Fig. 6.4 and the specific constraints for these components are given in Chapter 3.

6.6.2 Simulation Inputs and Parameters

For the 175 buildings considered in this case study, the device conversion factors are given in Table 6.1 and key parameters are given in Table 6.2. The electricity supply capacity limit is nearly halved from the value in [32] to 260 kW. Fixed electricity and heating demands used in the simulation have been interpolated from hourly building data [124] to produce data at 15 minute sampling intervals (Figs. 6.5-6.6). Similarly, electricity purchase prices have been interpolated from those set on 1st February 2018 by UK energy supplier Octopus Energy Ltd for customers on its Agile Octopus tariff [116] (Fig. 6.7). Fixed prices are assumed for export of electricity to the external grid and purchasing of gas, at 1 p/kWh and 2.8 p/kWh respectively. A purchase and sale cost modifier is applied to the electricity network output variable, $y_{k,p_1,\text{elec}}$, with associated prices $\lambda^{\text{buy}}_{k,p_1,\text{elec}}$ and $\lambda^{\text{sell}}_{k,p_1,\text{elec}}$. A value cost modifier is applied to the gas network output variable $y_{k,p_1,\text{gas}}$, with associated cost $\lambda^{\text{val}}_{p_1,\text{gas}}$. A battery degradation cost coefficient $\lambda^{\text{abs}}_{\text{batt,chg}}$ is applied to each battery by adding an absolute value cost modifier applied to $u_{k,\text{batt,chg}}$; the value of $\lambda^{\text{abs}}_{\text{batt,chg}} = 3.15$ p/kWh is determined using the approach in [117].

For the MA MPC method, the step-length sequence takes the form $\sum_{j=1}^{j_{\max}} \alpha(j) = a/j$, where parameter a is varied to try and achieve consistent convergence to a feasible solution between agents. For both the MA-CM and MA-NAG MPC approaches, the step-length is kept constant at $\alpha = 3 \times 10^{-4}$ in every iteration, having been tuned to achieve the fastest convergence with minimal dual oscillations. For MA-CM, the value of β is varied in the range [0.5,0.99] to try and achieve fast convergence. The range of small, uniformly distributed random perturbations added to cost function coefficients is $[-5 \times 10^{-2}; 5 \times 10^{-2}]$. The prediction horizon length used in each simulation is $H = 24$, the duration of each simulation was a single day (96 $\times$ 15 minute sampling intervals) and the maximum number of algorithm iterations at each sampling instance was 500.

6.6.3 Results

The simulations were carried out using Gurobi [110] and YALMIP [106] in MATLAB [121] on a laptop with Intel Core i5-6200U CPU @ 2.30GHz and 8 GB RAM. The default settings for MILP problems were used in Gurobi.

Table 6.1: Device Conversion Factors

Conversion Factor	Device	Value[1]
η_{tx}	Transformer	0.98
COP	Heat Pump	3.90
$\eta_{\text{chp,heat}}$	CHP (heat)	[0.30;0.50]
$\eta_{\text{chp,elec}}$	CHP (electricity)	[0.23;0.43]
$\eta_{\text{batt,chg}}$	Battery (charging)	[0.85;0.95]
$\eta_{\text{batt,dchg}}$	Battery (discharging)	[0.80;0.90]

[1] $[a;b]$ - uniform random distribution.

Table 6.2: Simulation Parameters

Parameter	Value[1]	Units
Starting battery level	[1.2;2.6]	kWh
Minimum/maximum battery capacity	[1.0;1.4] / [4.0;5.6]	kWh
Minimum/maximum charge rate	[-3.0;-1.0] / [1.0;3.0]	kW
Standby discharge	0.9997	-
Minimum/maximum transformer capacity	-5 / 5	kW
Minimum/maximum μ-CHP fuel input	0 / 6	kW
Minimum/maximum heat pump output	0/20	kW

[1] $[a;b]$ - uniform random distribution.

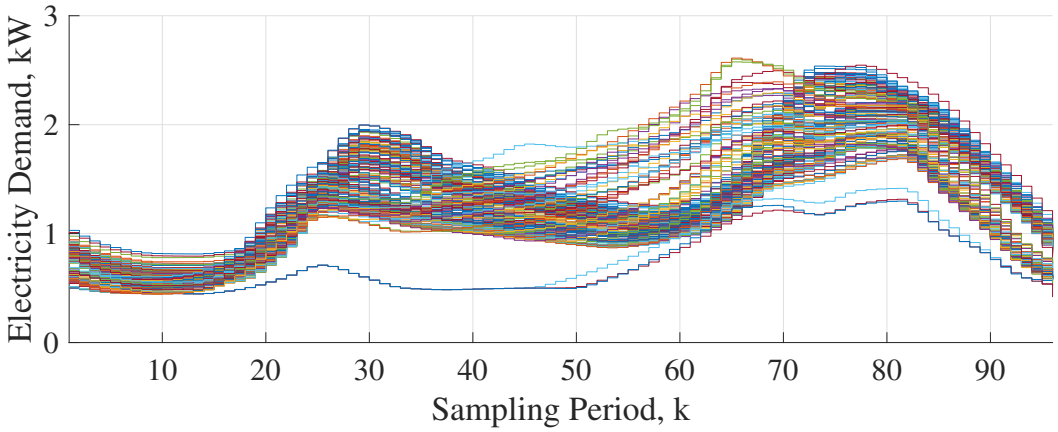

Figure 6.5: Electricity demand profiles used in simulations.

The MA method was used in a number of simulations, each with an increasing value of the step-length sequence parameter, a, from 0.001 up to 1. None of these simulations were able to be completed since for each value of a there was a sampling instance at which the MA algorithm failed to achieve the stopping criterion within

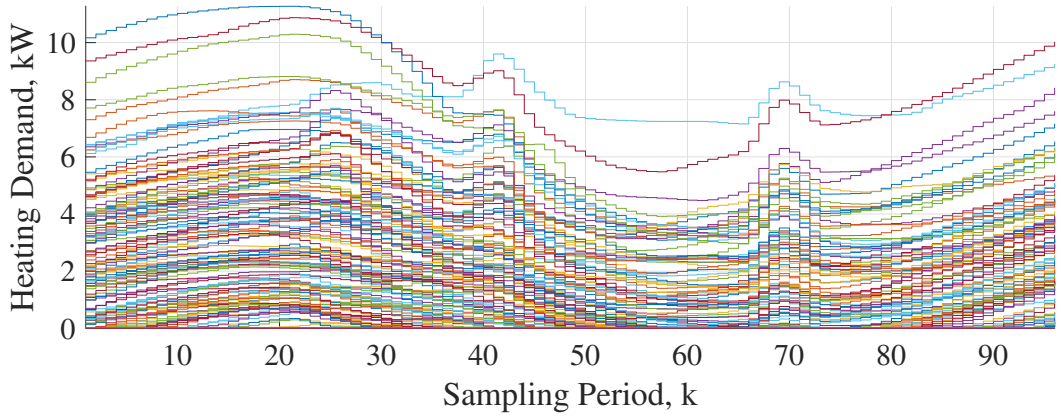

Figure 6.6: Heating demand profiles used in simulations.

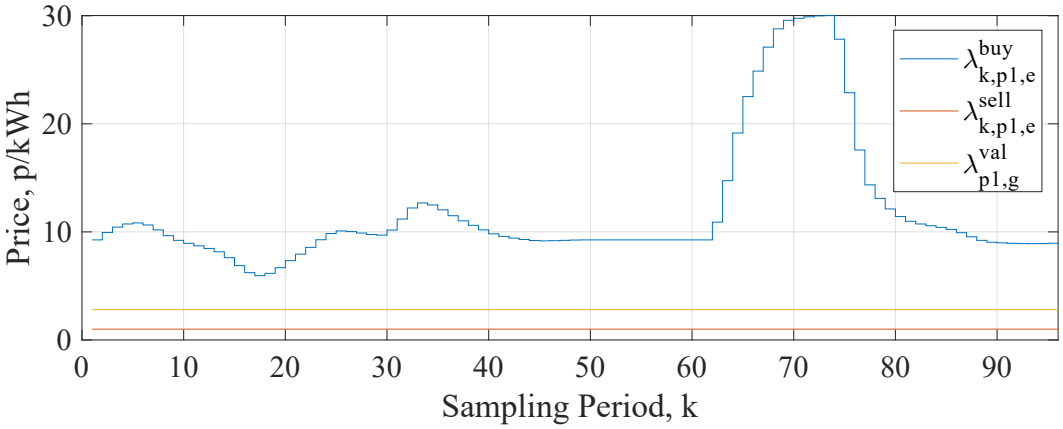

Figure 6.7: Price profiles used in simulations.

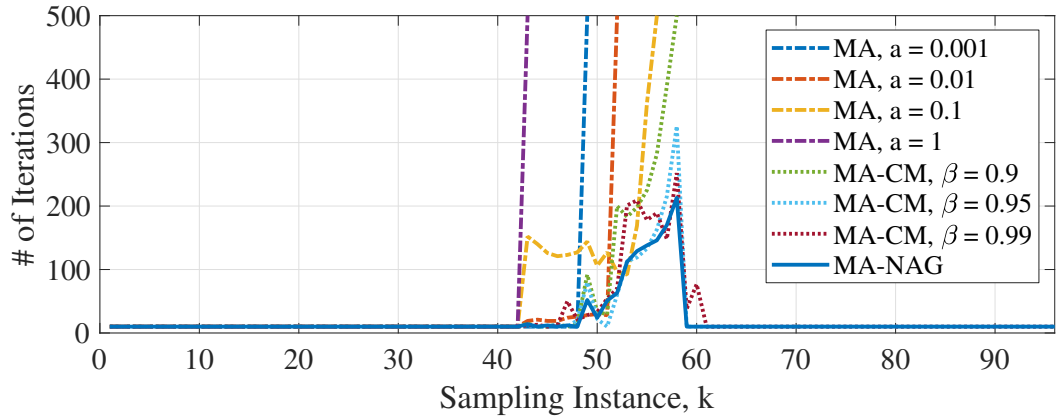

Figure 6.8: Number of iterations taken to compute a solution at each sampling instance. Simulations were terminated after reaching 500 iterations in any sampling instance. Note that for MA, only a small sample of the a values simulated are shown, although every attempt was unsuccessful.

the 500 iteration limit (see Fig. 6.8). On the other hand, convergence to a feasible solution within the iteration limit was possible at every sampling instance when using MA-CM or MA-NAG. However, tuning of β was needed for MA-CM and some simulations were not completed.

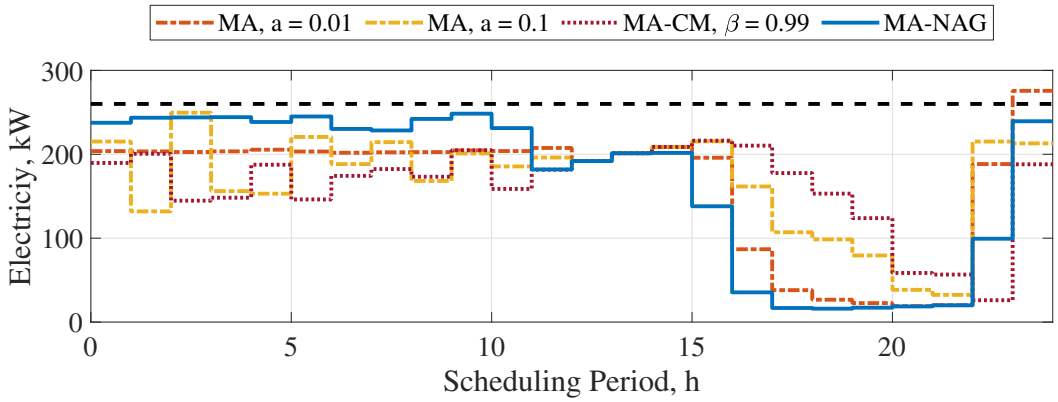

Figure 6.9: Total power consumption schedules at sampling instance $k = 52$. Capacity limit is exceeded by MA method with $a = 0.01$ in final scheduling period, $h = 23$, even after 1000 iterations.

It can be seen that MA with $a = 0.01$ reaches the stopping criterion with relatively few iterations early in the simulation but then at sampling instance $k = 52$ it reaches 500 iterations without obtaining a feasible solution. The reasons for this can be better understood by comparing the predicted schedule of total electricity consumption determined at the final iteration for this sampling instance (Fig. 6.9), together with the dual variable values at each iteration (Fig. 6.10), across different methods.

The capacity limit is violated in the final time period of the prediction schedule for MA with $a = 0.01$, indicating an infeasible solution, even though the simulation was actually allowed to proceed to 1000 iterations (Fig. 6.9). Across the different methods, the final values of the dual associated with this time period are: MA $(a = 0.01)$, $\lambda_{k+23} = 1.17$; MA $(a = 0.1)$, $\lambda_{k+23} = 5.93$; MA-CM $(\beta = 0.99)$, $\lambda_{k+23} = 6.62$; and MA-NAG, $\lambda_{k+23} = 2.68$.

Clearly for MA with $a = 0.01$, the value of this particular dual needs to be further increased, yet it increases in an apparently asymptotic manner and therefore a feasible solution is never obtained (Fig. 6.10a). In contrast, when the step-lengths are increased for MA with $a = 0.1$, the value of this dual variable increases quickly to a final value (Fig. 6.10b). However, this final value is much higher, due to large oscillations in other dual variables which result in excessive constraint tightening. Also, these high frequency oscillations prevent the stopping criterion from being satisfied until the 96$^{\text{th}}$ iteration, even though the duals oscillate around their final values from about the 40$^{\text{th}}$ iteration. This highlights the tuning problems encountered for MA with this type of problem, in which dual variable values increase at very different rates: it is difficult to find a step-length rule which increases duals with small sub-

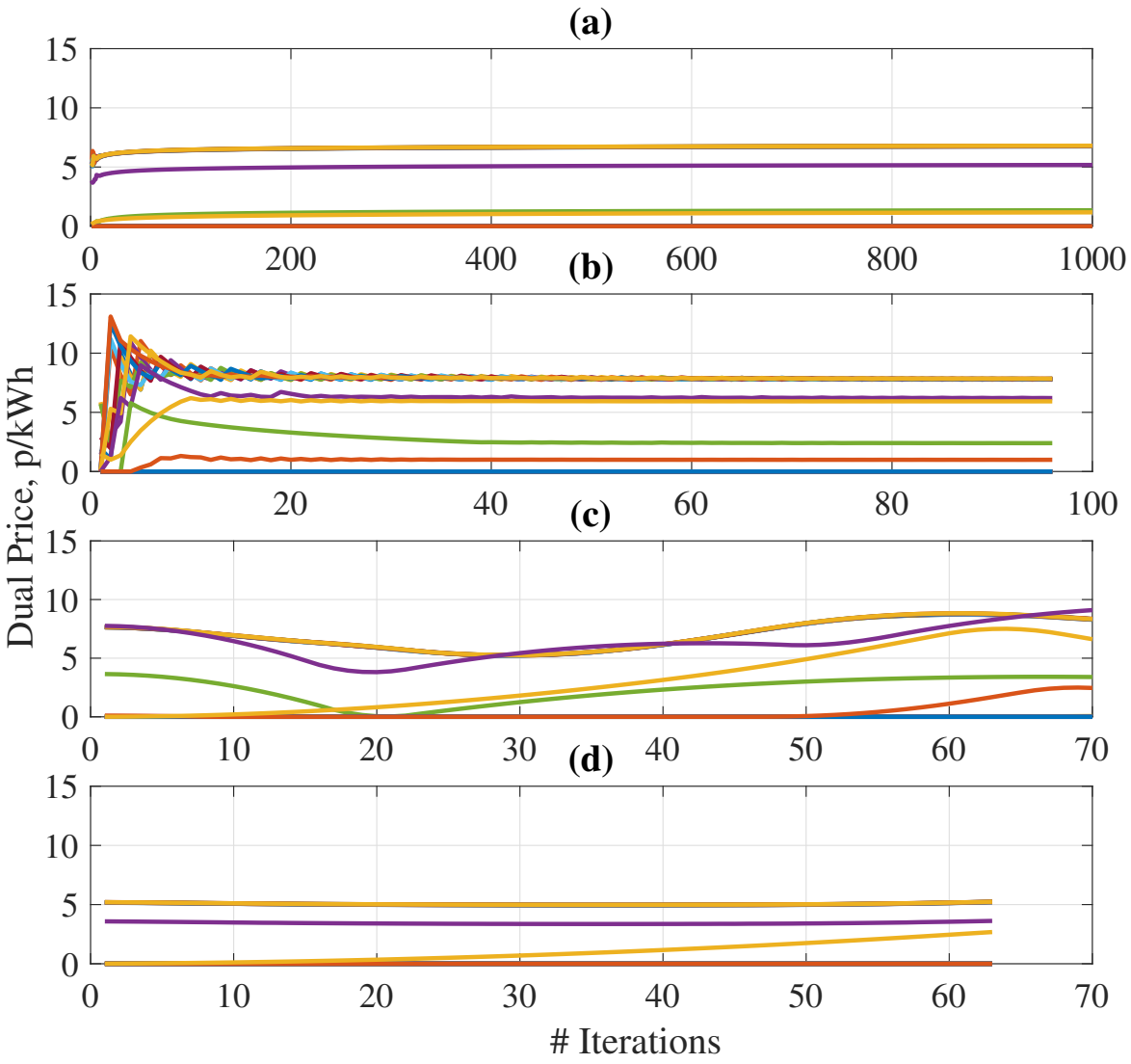

Figure 6.10: Dual variable value iterations at sampling instance $k = 52$ for (a) MA with $a = 0.01$, (b) MA with $a = 0.1$, (c) MA-CM with $\beta = 0.99$ and (d) MA-NAG.

gradients quickly, whilst not causing other duals with larger initial subgradients to excessively oscillate. It should be noted that only a subset of the a values used for MA are shown here and that despite time-consuming manual tuning, it was not possible to find an a value that resulted in feasible solutions in every sampling instance. Furthermore, the use of other nonsummable diminishing step-length rules were also unsuccessful, although an exhaustive search of step-length rules was not undertaken.

It was possible to achieve convergence to feasible solutions using a constant step-length for MA-CM and MA-NAG. This is because the added momentum terms accelerate duals to their final values, regardless of the step-length. A diminishing step-length rule was employed in the previous EV problem for a like-for-like comparison with MA and because convergence was relatively quick. However, for this problem a diminishing step-length only slows convergence because a relatively small initial

step-length is required to prevent high frequency dual value oscillations. Step-length tuning is therefore simple - the largest value is chosen which does not result in high frequency dual oscillations at any sampling instance.

Despite being the fastest MA-CM simulation to successfully converge in every sampling instance, MA-CM with $\beta = 0.99$ exhibits large slow oscillations in the dual values due to aggressive acceleration and subsequent overshoot (Fig. 6.10c). As a result, the schedule produced in Fig. 6.9 is overly conservative in periods $h = 0$ to 11 and consumes more electricity during the electricity price peak at $h = 16$ to 21. MA-NAG, on the other hand, requires less tuning and exhibits minimal dual oscillations (Fig. 6.10d), enabling the most optimal schedule to be found in the fewest iterations. Oscillations are dampened because in the MA-NAG method, acceleration is determined based on current subgradient values, whereas in MA-CM acceleration is based only on past dual values.

The actual computation times for MA-CM with $\beta = 0.99$ and MA-NAG are compared against a benchmark in Table 6.3. A (possibly sub-optimal) solution to the global MILP problem, without decomposition, provides the benchmark against which to compare the decentralised methods; this problem does not have tightened constraints and should therefore be less conservative. The overall costs for operating all buildings are also compared with the benchmark simulation (Table 6.4). It is clear that MA-NAG outperforms MA-CM in both aspects and also achieves comparable costs to the benchmark. The small increase in costs compared to the benchmark can be attributed to constraint tightening in periods of low electricity price, resulting in higher consumption of electricity during the price peak (Fig. 6.11). However, average computation times are greatly reduced when using both MA-CM and MA-NAG in comparison to the benchmark. Moreover, whereas the the benchmark method is likely to scale poorly, both MA-CM and MA-NAG should scale much more favourably due to the ability of agents to solve local sub-problems in parallel.

6.7 Conclusions

The capability to solve large MILP problems in a decentralised fashion is of significant benefit for advanced control of hybrid dynamical systems. Such systems are often modelled using a mixed logical dynamical (MLD) framework which involves

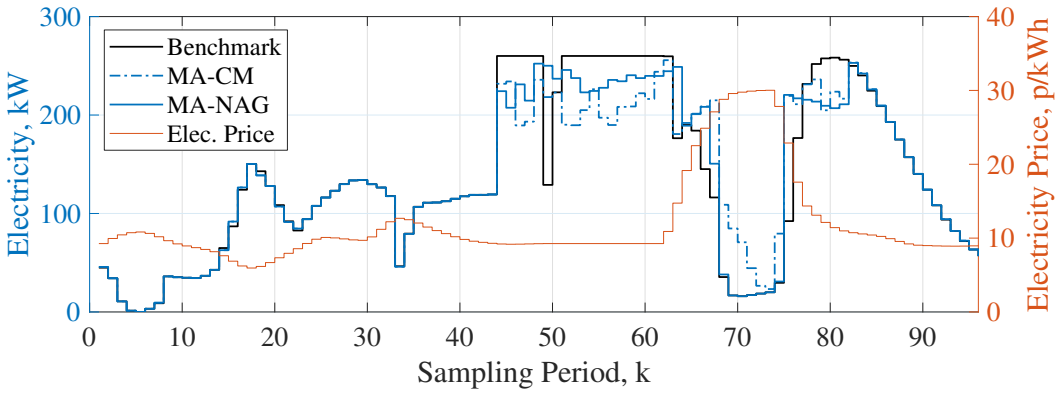

Figure 6.11: Comparison of total power consumption between centralised benchmark, MA-CM and MA-NAG methods.

Table 6.3: Computation Time

	Benchmark	MA-CM*	MA-NAG*
Mean comp. time, secs	6.53	0.76	0.61
Min. comp. time, secs	5.20	0.21	0.27
Max. comp. time, secs	8.69	7.67	6.09
Std. Dev. comp. time, secs	0.75	1.46	1.06

* - parallel computation time for all agents is assumed to be equal to the slowest agent; communication time between agents and coordinator is assumed to be insignificant.

Table 6.4: Overall Cost

	Benchmark	MA-CM	MA-NAG
Overall Cost, £	2,514	2,598 (+3.31%)	2,556 (+1.63%)

both continuous and discrete variables. Recent work has shown that decentralised optimisation of large MILPs is possible using dual decomposition and constraint tightening, achieving 'good' feasible solutions. An algorithm to exploit this finding and minimise the degree of constraint tightening was later developed and shown to provide finite-time feasibility and performance. However, in this chapter it has been shown by way of an illustrative case study that this method may exhibit impractically long convergence behaviour under certain possible conditions. Therefore, two new algorithms have been presented which accelerate convergence using Classical Momentum and Nesterov's Accelerated Gradient methods, respectively. In addition, a model predictive control implementation is presented which expands the use of

multi-agent MILP for use in control applications. Both novel algorithms introduced in this chapter outperform the inspiring algorithm in two case studies and are particularly effective for MPC, for which the minimal need for tuning is a considerable benefit. However, due to the need for tuning of a momentum parameter and overall inferior performance of the Classical Momentum algorithm, the algorithm with Nesterov's Accelerated Gradient method should be recommended for any MILP problem which would benefit from multi-agent computation.

In the following chapter, the computationally inefficient problem derived in the case study from Chapter 5 is solved using a modified form of the multi-agent MPC scheme with Nesterov's Accelerated Gradient, further demonstrating the utility of this approach.

Chapter 7

Multi-Agent Coordination of a Large-Scale Multi-Energy District

7.1 Introduction

In this chapter, the problematic case study of Chapter 5 is revisited to try and address the issues of prohibitive computation times when incorporating detailed models for reversible variable speed circulation pumps, an ULTDHC network and an AC network into a multi-energy district coordination problem. The **M**ulti-**A**gent dual decomposition and adaptive constraint tightening method with **N**esterov's **A**ccelerated **G**radient (MA-NAG) is applied for this purpose. The central coordinator in this application serves a dual purpose, to not only check global constraint violations and update dual prices but also to perform optimal energy flow checks to ensure that, for the power flows requested by agents, the supplied global constraints ensure feasibility. If there are any violations of network limits incurred by the combined agents' operating schedules then the global constraints are adjusted, causing associated changes to dual prices which should encourage feasible schedules. For this reason the central coordinator is referred to as an *energy flow coordinator* in this chapter.

In the following section, the MA-NAG based MPC scheme from Chapter 6 is extended to account for the new role of the energy flow coordinator. The notation is also made more explicit to improve clarity of the algorithms presented.

7.2 Control Scheme

Agent controllers in the MA-NAG MPC scheme only consider components which have been aggregated at the building scale, they do not individually consider network constraints. Coordination of agent controllers therefore requires the use of price signals to encourage energy schedules that do not violate network limits.

To achieve this, first an overall district problem is defined which comprises the set of all aggregated building modules, M, and has added shared capacity constraints to limit the consumption of energy from each network:

$$
\begin{aligned}
\min_{v_i} \quad & \sum_{h=0}^{H-1} \sum_{i \in M} c_{k+h,i} \\
\text{s.t.} \quad & \sum_{i \in M} \boldsymbol{y}^B_{m_i} \leq \overline{\boldsymbol{b}}_{\text{HC}}, \quad \sum_{i \in M} \boldsymbol{y}^B_{p_i} \leq \overline{\boldsymbol{b}}_{\text{AC}}, \\
\text{and} \quad & \boldsymbol{x}_{k+1,i} = \boldsymbol{A}_i \boldsymbol{x}_{k,i} + \boldsymbol{B}_{u,i} \boldsymbol{u}_{k,i} + \boldsymbol{B}_{d,i} \boldsymbol{\delta}_{k,i} + \boldsymbol{B}_{z,i} \boldsymbol{z}_{k,i} + \boldsymbol{B}_{w,i} \boldsymbol{w}_{k,i} \\
& \boldsymbol{y}_{k,i} = \boldsymbol{C} \boldsymbol{x}_{k,i} + \boldsymbol{D}_u \boldsymbol{u}_{k,i} + \boldsymbol{D}_d \boldsymbol{\delta}_{k,i} + \boldsymbol{D}_z \boldsymbol{z}_{k,i} + \boldsymbol{D}_w \boldsymbol{w}_{k,i} \\
& \boldsymbol{E}_d \boldsymbol{\delta}_{k,i} + \boldsymbol{E}_z \boldsymbol{z}_{k,i} \leq \boldsymbol{E}_u \boldsymbol{u}_{k,i} + \boldsymbol{E}_x \boldsymbol{x}_{k,i} + \boldsymbol{E}_w \boldsymbol{w}_{k,i} + \boldsymbol{E} \\
& y_{k,\text{snk}_j} = \gamma_{ij} \cdot y_{k,\text{src}_i} \\
& \forall\, k \in H,\ i \in M
\end{aligned}
\tag{$\mathcal{MAP}$}
$$

where H is the prediction horizon length, $\overline{\boldsymbol{b}}_{\text{HC}}$ is a $H \times 1$ vector of mass flow capacity limit for the ULTDHC network and $\overline{\boldsymbol{b}}_{\text{AC}}$ is a $H \times 1$ vector of power capacity limit for the electricity network. Since the building-side output variables which connect to network component output variables $\boldsymbol{y}_{m_i}$ and $\boldsymbol{y}_{p_i}$ could belong to any suitable building component (depending on the specific layout of the building), the generic $\boldsymbol{y}^B_{m_i}$ and $\boldsymbol{y}^B_{p_i}$are used to represent the connected outputs on the building side. The structure of ($\mathcal{MAP}$) is amenable to Lagrangian dual decomposition and the agent problems can therefore be solved in parallel, with the use of a central energy flow coordinator.

By introducing $H \times 1$ dual multiplier vectors $\boldsymbol{\lambda}^{\text{val}}_{\text{HC}}$ and $\boldsymbol{\lambda}^{\text{val}}_{\text{AC}}$, the *dual problem* ($\mathcal{D}$) of the primal problem ($\mathcal{MAP}$) can be derived, in which the shared constraints are added to the objective function:

$$
\begin{aligned}
\max_{\boldsymbol{\lambda}^{\text{val}}_{\text{HC}} \geq 0,\ \boldsymbol{\lambda}^{\text{val}}_{\text{AC}} \geq 0} \quad & -{\boldsymbol{\lambda}^{\text{val}}_{\text{HC}}}^{\top} \overline{\boldsymbol{b}}_{\text{HC}} - {\boldsymbol{\lambda}^{\text{val}}_{\text{AC}}}^{\top} \overline{\boldsymbol{b}}_{\text{AC}} \\
& + \sum_{i \in M} \min_{v_i} \left(\sum_{h=0}^{H-1} c_{k+h,i} + {\boldsymbol{\lambda}^{\text{val}}_{\text{HC}}}^{\top} \boldsymbol{y}^B_{m_i} + {\boldsymbol{\lambda}^{\text{val}}_{\text{AC}}}^{\top} \boldsymbol{y}^B_{p_i} \right)
\end{aligned}
\tag{$\mathcal{D}$}
$$

The inner minimisations within $\mathcal{D}$ are separable, lower dimensional sub-problems associated with each aggregated module i and may be solved in parallel. As in the previous chapter, Algorithm 12 provides a method to exploit this property and find a good feasible solution to ($\mathcal{MAP}$) by coordinating individual agent controllers.

The MA-NAG MPC scheme is extended in this section to include additional sub-routines, Algorithms 13 and 14, in which optimal energy flow problems are solved and the vectors $\boldsymbol{b}_{\text{HC}}$, $\boldsymbol{b}_{\text{AC}}$ and $\hat{\boldsymbol{y}}_{\text{cp}_i,\Delta H}$ are updated. The centralised energy flow co-ordinator carries out all steps in Algorithms 12, 13 and 14, whilst Algorithm 11 is carried out by each individual building agent. Therefore, the agents each solve their local optimisation problem ($\mathcal{AP}$) and the only optimisation problems solved by the coordinator are network optimal energy flow problems ($\mathcal{HC}$) and ($\mathcal{AC}$).

The inner minimisations of $\mathcal{D}$ become the local optimisation problems ($\mathcal{AP}$) of each agent $i \in M$:

$$\begin{aligned} \min_{v_i} \quad & \sum_{h=0}^{H-1} c_{k+h,i} + \boldsymbol{\lambda}_{\text{HC}}^{\text{val}\,\top} \boldsymbol{y}_{m_i}^{B} + \boldsymbol{\lambda}_{\text{AC}}^{\text{val}\,\top} \boldsymbol{y}_{p_i}^{B} \\ \text{s.t.} \quad & (3.1) - (3.3), (3.5) \text{ for aggregated module } i \end{aligned} \tag{$\mathcal{AP}$}$$

The energy flow problem for the ULTDHC network includes a nodal mass flow reference term in the cost function:

$$\begin{aligned} \min_{v} \quad & c_{k,\text{HC}} + \sum_{i \in M} \lambda_{k,m_i}^{\text{ref}} \cdot |y_{k,m_i} - r_{k,m_i}| \;\; \forall k \\ \text{s.t.} \quad & (3.1) - (3.5) \text{ for ULTDHC component} \end{aligned} \tag{$\mathcal{HC}$}$$

The cost function $c_{k,\text{HC}}$ is given in Section 3.6.3. The reference signal, r_{k,m_i}, for each nodal mass flow, y_{k,m_i}, is that determined by the agent controller located at node i, with an associated cost, $\lambda_{k,m_i}^{\text{ref}}$, that is much larger than other penalty terms in $c_{k,\text{HC}}$. Solving this problem determines a feasible energy flow solution with values of nodal mass flow which are of minimum absolute distance from the reference values. If the distance is non-zero ($|y_{k,m_i} - r_{k,m_i}| > 0$) for a given sampling instance k in the prediction horizon, then the value of $b_{k,\text{HC}}$ is updated to equal the sum of all mass flows determined in the energy flow solution, y_{k,m_i}; otherwise $b_{k,\text{HC}}$ remains unchanged (see Algorithm 13). This tightening of shared constraints, by reducing $b_{k,\text{HC}}$ for the affected sampling periods, increases the associated dual prices so that all agents are encouraged to shift their demand to alternative sampling intervals. The eventual result of this constraint tightening is that agents converge to local energy

schedules that do not violate network limits. At this point, the stopping criteria has been met and the coordinator allows agents to implement their incumbent solutions. A secondary purpose of solving ($\mathcal{HC}$) is that the required pump pressure gain at each node, $\hat{y}_{k,\text{cp}_i,\Delta H}$, can be communicated to individual agents and used to fix the value of $y_{k,\text{cp},\Delta H}$. Hence, the bilinear term in (3.69) is linearised at the determined feasible energy flow solution.

Similarly, the power flow problem solved by the energy flow coordinator for the AC distribution network includes a nodal power injection reference term in the cost function:

$$\begin{aligned} \min_{v} \quad & c_{k,\text{AC}} + \sum_{i \in M} \lambda^{\text{ref}}_{k,p_i} \cdot |y_{k,p_i} - r_{k,p_i}| \ \forall k \\ \text{s.t.} \quad & (3.1) - (3.5) \text{ for AC component} \end{aligned} \tag{$\mathcal{AC}$}$$

The cost function $c_{k,\text{AC}}$ is given in Section 3.6.2. The total capacity limit, $\boldsymbol{b}_{\text{AC}}$, for the AC network is similarly updated if $|y_{k,p_i} - r_{k,p_i}| > 0$, otherwise $\boldsymbol{b}_{\text{AC}}$ remains unchanged (see Algorithm 14).

In both Algorithm 11 and Algorithm 12, the dual update vectors $\boldsymbol{\lambda}^{\text{val}}_{\text{HC}}$, $\boldsymbol{\lambda}^{\text{val}}_{\text{AC}}$, $\boldsymbol{\mu}_{\text{HC}}$ and $\boldsymbol{\mu}_{\text{AC}}$ are initialised with all zero vectors only once before the control scheme is online. Once online, these vectors are warm started at each k, determined by applying a circular shift to the final vectors of the previous control instance (step 27 of Algorithm 12). The circular shift is represented by multiplication with the matrix, $\boldsymbol{C}_{\text{shift}} = \begin{bmatrix} 0 & \mathbf{I} \\ 1 & 0 \end{bmatrix}$. After applying this shift, the final element of each vector is given a zero value. This is to reduce the number of algorithm iterations taken to find a feasible solution at each sampling instance. Algorithm iterations for a given control sampling instance are interrupted once a suitable stopping criteria has been met, e.g. that the incumbent agent solutions do not violate any network constraints.

In the following case study section, the performance of the multi-agent scheme is compared against the equivalent centralised MPC scheme, achieved by employing a single controller to solve the global problem $\mathcal{MAP}$, as per Chapter 5. The centralised scheme provides a benchmark in terms of solution optimality, since the constraints do not need be tightened in the centralised scheme.

Algorithm 11 Agent receding horizon scheme

1: $t = 0,\ \Delta t > 0$
2: Initialise $\boldsymbol{\lambda}^{\text{val}}_{\text{HC}}$, $\boldsymbol{\lambda}^{\text{val}}_{\text{AC}}$ and $\boldsymbol{y}_{\text{cp}_i,\Delta H}(i \in M)$ with zero vector, $\mathbf{0}^{H\times 1}$
3: **for** $k = 0, 1, 2, ...$ **do**
4: Update current system states, $\mathbf{x}_k$
5: Update price forecasts, $\boldsymbol{\lambda}^{\text{val}}_{k+h},\ h = 0, ..., H-1$
6: Update disturbance forecasts, $\mathbf{w}_{k+h},\ h = 0, ..., H-1$
7: Solve local optimisation problem ($\mathcal{AP}$)
8: Communicate candidate solution, $\boldsymbol{v}_i$, to energy flow coordinator
9: Receive instruction from energy flow coordinator
10: **if** instruction == "re-optimise" **then**
11: Go to step 7
12: **end if**
13: Pass control inputs for next sampling interval, $\mathbf{u}_k$, to lower-level feedback controllers; discard $\mathbf{u}_{k+h},\ h = 1, ..., H-1$
14: **Wait until** $t = (k+1)\Delta t$
15: $k = k + 1$
16: **end for**

7.3 Case Study

The case study introduced in Chapter 5 is also used in this section, with identical inputs and system parameters for 84 buildings and a ULTDHC plant substation, connected by an AC network and ULTDHC network as per Fig. 5.1. Two main branches can be identified for each network, which split at node 8. Capacity constraints and associated dual multipliers were applied separately to the sets of nodes describing these branches, which each include the nodes preceding node 8. This is to avoid constraint violations on a given branch causing constraint tightening on unaffected branches. The stopping criteria for Algorithm 12 is that, for the current iteration, feasibility checks have been carried out without adjustment to any capacity constraints and that these constraints are satisfied for both networks. Algorithm parameters used for the multi-agent scheme during simulation were $\alpha_{\text{HC}} = 1 \times 10^{-4}$, $\alpha_{\text{AC}} = 1 \times 10^{-5}$ and $\beta = 3$.

The prediction horizon used for simulating the centralised scheme in Chapter 5 was $H = 3$ which, despite being very short, led to unacceptably long computation times.

Algorithm 12 Energy flow coordination

Initialise $\boldsymbol{\lambda}^{\text{val}}_{\text{HC}}$, $\boldsymbol{\lambda}^{\text{val}}_{\text{AC}}$, $\boldsymbol{\mu}_{\text{HC}}$ and $\boldsymbol{\mu}_{\text{AC}}$ with zero vector, $\mathbf{0}^{H\times 1}$
Initialise $\overline{\boldsymbol{s}}_{\text{HC}_i}(0) = \overline{\boldsymbol{s}}_{\text{AC}_i}(0) = -\infty^{H\times 1}, \quad i \in M$
Initialise $\underline{\boldsymbol{s}}_{\text{HC}_i}(0) = \underline{\boldsymbol{s}}_{\text{AC}_i}(0) = \infty^{H\times 1}, \quad i \in M$
$j = 0, n = 0$
if new candidate solutions, $\boldsymbol{v}_i$, received from all agents $i \in M$ **then**
    $\overline{\boldsymbol{s}}_{\text{HC}_i}(j+1) = \max\{\overline{\boldsymbol{s}}_{\text{HC}_i}(j), \boldsymbol{y}^B_{m_i}(j+1)\}, i \in M$
    $\underline{\boldsymbol{s}}_{\text{HC}_i}(j+1) = \min\{\underline{\boldsymbol{s}}_{\text{HC}_i}(j), \boldsymbol{y}^B_{m_i}(j+1)\}, i \in M$
    $\boldsymbol{\rho}_{\text{HC}_i}(j+1) = \overline{\boldsymbol{s}}_{\text{HC}_i}(j+1) - \underline{\boldsymbol{s}}_{\text{HC}_i}(j+1), i \in M$
    $\boldsymbol{\rho}_{\text{HC}}(j+1) = \max(\sum_{i\in\hat{M},|\hat{M}|=H} \rho_i(j+1))$
    Repeat 6 to 9 for AC network parameters.
    if $j < 2$ OR $\sum_{i\in M} \boldsymbol{y}^B_{m_i}(j+1) \leq \boldsymbol{b}_{\text{HC}}$ **then**
        Run Algorithm 13.
    end if
    if $j < 2$ OR $\sum_{i\in M} \boldsymbol{y}^B_{p_i}(j+1) \leq \boldsymbol{b}_{\text{AC}}$ **then**
        Run Algorithm 14.
    end if
    $\nabla \boldsymbol{g}_{\text{HC}}(j+1) = \sum_{i\in M} \boldsymbol{y}^B_{m_i}(j+1) - \boldsymbol{b}_{\text{HC}}(j+1) + \boldsymbol{\rho}_{\text{HC}}(j+1)$
    $\nabla \boldsymbol{g}_{\text{AC}}(j+1) = \sum_{i\in M} \boldsymbol{y}^B_{m_i}(j+1) - \boldsymbol{b}_{\text{AC}}(j+1) + \boldsymbol{\rho}_{\text{AC}}(j+1)$
    $\boldsymbol{\mu}_{\text{HC}}(j+1) = \boldsymbol{\lambda}_{\text{HC}}(j) + \alpha_{\text{HC}} \nabla \boldsymbol{g}_{\text{HC}}(j+1)$
    $\boldsymbol{\lambda}_{\text{HC}}(j+1) = \left[\boldsymbol{\mu}_{\text{HC}}(j+1) + \frac{n}{n+\beta}\left(\boldsymbol{\mu}_{\text{HC}}(j+1) - \boldsymbol{\mu}_{\text{HC}}(j)\right)\right]_+$
    $\boldsymbol{\mu}_{\text{AC}}(j+1) = \boldsymbol{\lambda}_{\text{AC}}(j) + \alpha_{\text{AC}} \nabla \boldsymbol{g}_{\text{AC}}(j+1)$
    $\boldsymbol{\lambda}_{\text{AC}}(j+1) = \left[\boldsymbol{\mu}_{\text{AC}}(j+1) + \frac{n}{n+\beta}\left(\boldsymbol{\mu}_{\text{AC}}(j+1) - \boldsymbol{\mu}_{\text{AC}}(j)\right)\right]_+$
    if stopping criteria not met **then**
        Broadcast $\boldsymbol{\lambda}^{\text{val}}_{\text{HC}}$, $\boldsymbol{\lambda}^{\text{val}}_{\text{AC}}$ and $\boldsymbol{y}_{\text{cp}_i,\Delta H}$ to agents $i \in M$ with instruction "re-optimise"
        $j = j + 1$
    else
        Shift algorithm parameter vectors $\boldsymbol{b}_{\text{HC}}$, $\boldsymbol{b}_{\text{AC}}$, $\boldsymbol{\lambda}^{\text{val}}_{\text{HC}}$, $\boldsymbol{\lambda}^{\text{val}}_{\text{AC}}$, $\boldsymbol{\mu}_{\text{HC}}$, $\boldsymbol{\mu}_{\text{AC}}$ and $\boldsymbol{y}_{\text{cp}_i,\Delta H}$ by one time step
        Broadcast $\boldsymbol{\lambda}^{\text{val}}_{\text{HC}}$, $\boldsymbol{\lambda}^{\text{val}}_{\text{AC}}$ and $\boldsymbol{y}_{\text{cp}_i,\Delta H}$ to agents $i \in M$ with instruction "continue"
        $\overline{\boldsymbol{s}}_{\text{HC}_i}(0) = \overline{\boldsymbol{s}}_{\text{AC}_i}(0) = -\infty^{H\times 1}, \quad i \in M$
        $\underline{\boldsymbol{s}}_{\text{HC}_i}(0) = \underline{\boldsymbol{s}}_{\text{AC}_i}(0) = \infty^{H\times 1}, \quad i \in M$
        $j = 0$
    end if
end if
Go to step 5

When simulating the multi-agent scheme, prediction horizons of $H = 3$ and $H = 24$ are used for both a direct comparison to the centralised benchmark and to demon-

Algorithm 13 Sub-routine for checking ULTDHC network solution feasibility

for $i = 1$ to $|M|$ **do**
  $\boldsymbol{r}_{m_i} = \boldsymbol{y}^B_{m_i}(j+1)$
end for
Solve ($\mathcal{HC}$)
for $i = 1$ to $|M|$ **do**
  $\hat{\boldsymbol{y}}_{\text{cp}_i,\Delta H} = \boldsymbol{y}_{\text{pump}\Delta H_i}$
  if $|y_{k,m_i} - r_{k,m_i}| > 0 \quad \forall k$ **then**
    $b_{k,\text{HC}} = \sum_{i \in M} y_{k,m_i}(j+1)$
  end if
end for
$n = 0$

Algorithm 14 Sub-routine for checking AC network solution feasibility

for $i = 1$ to $|M|$ **do**
  $\boldsymbol{r}_{p_i} = \boldsymbol{y}^B_{p_i}(j+1)$
end for
Solve ($\mathcal{AC}$)
for $i = 1$ to $|M|$ **do**
  if $|y_{k,p_i} - r_{k,m_i}| > 0 \quad \forall k$ **then**
    $b_{k,\text{AC}} = \sum_{i \in M} y_{k,p_i}(j+1)$
  end if
end for
$n = 0$

strate scalability to larger problems. The penalty costs used to obtain exact solutions in the AC and ULTDHC networks are $\lambda^{\text{val}}_{\ell_{ij}} = 0.1$, $\lambda^{\text{val}}_{\Delta H_{ij}} = 1$ and $\lambda^{\text{val}}_{\text{pump}\Delta H_j} = 0.1$.

7.3.1 Agent Control Problems

The objective function $J_{k,i}$ minimised by agent controller i at each time step varies between the plant substation at node 2 and the buildings at the remaining nodes. Hence, they are given separately below. For each building, the economic cost for importing, and revenue for exporting, power from/to the AC power network, as well as the cost associated with battery degradation is included in the objective function. The cost for purchasing power is the only economic term included for the plant substa-

tion objective function. A purchase and sale cost modifier is applied to the electricity distributor output variable, $y_{k,\text{snk}_{1,elec}}$, of all buildings, with associated prices $\lambda^{\text{buy}}_{k,y_{\text{snk}_1,\text{elec}}}$ and $\lambda^{\text{sell}}_{k,y_{\text{snk}_1,\text{elec}}}$. A value cost modifier is applied to the electricity distributor output variable, $y_{\text{snk}_{1,elec}}$, of the plant substation, with associated cost $\lambda^{\text{val}}_{k,y_{\text{snk}_1,\text{elec}}}$. A battery degradation cost coefficient $\lambda^{\text{abs}}_{k,u_{\text{batt,chg}}}$ is applied to all batteries by adding an absolute value cost modifier applied to $u_{k,\text{batt,chg}}$. The objective function for all agents includes dual variable terms associated with both the AC power and the ULTDHC networks.

The control objective for the plant substation agent is as follows:

$$J_{k,2} = \sum_{h=0}^{H-1} c_{k+h,2} + \boldsymbol{\lambda}^{\text{val}\,\top}_{k+h,\text{dual}} A_2 \boldsymbol{v}_{k+h,2} \tag{7.1}$$

$$c_{k+h,2} = \lambda^{\text{val}}_{k,y_{2,\text{snk}_1,\text{elec}}} \cdot y_{k,2,\text{snk}_{1,elec}} \tag{7.2}$$

$$\boldsymbol{\lambda}^{\text{val}\,\top}_{k+h,\text{dual}} A_2 \boldsymbol{v}_{k+h,2} = \lambda^{\text{val}}_{k,y_{\text{snk}_1,\text{elec,dual}}} \cdot y_{k,2,\text{snk}_{1,elec}} + \lambda^{\text{val}}_{k,y_{\text{vsp,in}}} \cdot y_{k,2,\text{vsp,in}} \tag{7.3}$$

Similarly, the control objective for the building agents is as follows:

$$J_{k,i\neq 1,2} = \sum_{h=0}^{H-1} c_{k+h,i\neq 1,2} + \boldsymbol{\lambda}^{\text{val}\,\top}_{k+h,\text{dual}} A_{i\neq 1,2} \boldsymbol{v}_{k+h,i\neq 1,2} \tag{7.4}$$

$$\begin{aligned} c_{k+h,i\neq 1,2} = {} & (\lambda^{\text{buy}}_{k,y_{i,\text{snk}_1,\text{elec}}} - \lambda^{\text{sell}}_{k,y_{i,\text{snk}_1,\text{elec}}}) z_{k,y_{i,\text{snk}_1,\text{elec}},\text{buy}} + \lambda^{\text{sell}}_{k,y_{i,\text{snk}_1,\text{elec}}} \cdot y_{k,i,\text{snk}_1,\text{elec}} \\ & + \lambda^{\text{abs}}_{k,u_{\text{batt}_i,\text{chg}}} \cdot z_{k,u_{\text{batt}_i,\text{chg}},\text{abs}} \end{aligned} \tag{7.5}$$

$$\boldsymbol{\lambda}^{\text{val}\,\top}_{k+h,\text{dual}} A_{i\neq 1,2} \boldsymbol{v}_{k+h,i\neq 1,2} = \lambda^{\text{val}}_{k,y_{\text{snk}_1,\text{elec,dual}}} \cdot y_{k,i,\text{snk}_{1,elec}} + \lambda^{\text{val}}_{k,y_{\text{vsp,in}}} \cdot y_{k,i,\text{vsp,in}} \tag{7.6}$$

The control problem for each agent is formally stated as:

$$\begin{aligned} \min_{v_i} J_{k,i} &= \sum_{h=0}^{H-1} c_{k+h,i} + \boldsymbol{\lambda}^{\text{val}\,\top}_{k+h,\text{dual}} A_i \boldsymbol{v}_{k+h,i} \\ \text{s.t. } & (3.1)\text{-}(3.4)\ \forall\ m_i \end{aligned} \tag{7.7}$$

for which the m_i aggregated components are shown in Figs. 5.2 and 5.3, and the specific constraints for these components are given in Chapter 3.

7.4 Results

The simulations were carried out using Gurobi [110] and YALMIP [106] in MATLAB [121] on a laptop with Intel Core i5-6200U CPU @ 2.30GHz and 8 GB RAM. There is little difference in the actions determined by the two schemes for a prediction

horizon of $H = 3$, when comparing the total electrical and heat power supplied to the buildings (Figs. 7.1 and 7.2). This is also reflected in the very similar overall costs to plant and building owners when using each scheme (Table 7.1). However, there is a marked difference in the computational performance (Table 7.2), with a single optimisation problem in the centralised scheme taking as long as 55 minutes to solve and an average computation time of over 2.5 minutes, whereas the multi-agent equivalent scheme takes no longer than 1.01 seconds.

As expected, when the prediction horizon is increased to $H = 24$ and $H = 48$, the agent controllers consume energy more strategically. Greater amounts of energy are consumed during periods of lower electricity purchase price and less is consumed during price peaks. This results in a slight reduction in cost versus the centralised benchmark. However, the main benefit of this multi-agent scheme is that, despite a sixteen-fold increase in the problem size, the computation time remains several orders of magnitude faster than the centralised scheme. It may also be noted that, as in Chapter 4, there is a point at which increases in the prediction horizon length provides little benefit for this particular study, based on the marginal decrease in costs when increasing H from 24 to 48. Finally, whilst agents did often generate energy schedules which, according to detailed energy flow analysis, initially violated network constraints, it was always possible to coordinate their actions to find feasible alternatives. The case study therefore demonstrates the capability of the multi-agent control scheme to coordinate a multi-energy district without neglecting local network constraints.

In order to give greater confidence that MA-NAG can produce consistently good computational performance, a longer simulation was undertaken consisting of 2,016 sampling intervals of 15 minutes, i.e. a simulation length of 21 days, with $H = 24$, a prediction horizon of 4 hours. This was not carried out for the benchmark scheme, due to the excessively slow computation time already highlighted, and therefore cost comparisons cannot be made. However, it is clear from the number of algorithm iterations for this extended dataset that the computational performance remains consistent (Fig. 7.3). The mean number of iterations was 6.58 and the minimum number was 2. The maximum number of iterations was 165, with more iterations occurring at the start of each day at around 4.00 am, 4 hours before the morning electricity and heating load peaks, the time when both networks are most congested.

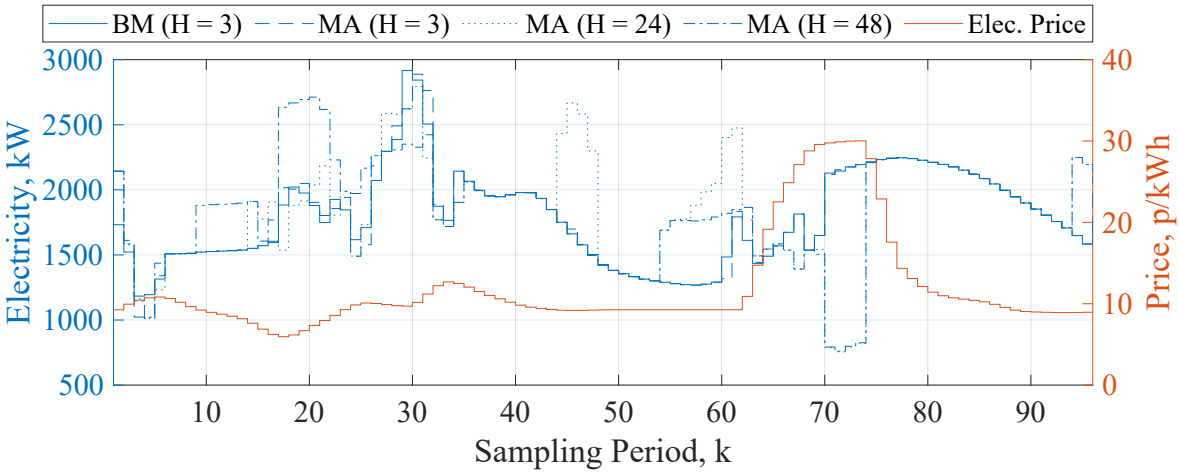

Figure 7.1: Total electrical power supplied to buildings under benchmark (BM) and multi-agent NAG (MA) schemes.

Table 7.1: Overall Cost for Purchase/Sale of Electricity and Battery Usage over 24 Hour Period

	Benchmark	Multi-Agent		
	H = 3	H = 3	H = 24	H = 48
Overall Cost, £	5,247	5,265 (+0.3%)	5,121 (-2.4%)	5,102 (-2.8%)

Despite these impressive results for the control of this multi-energy district, there are some limitations to the control scheme. Whilst the energy flow coordinator performs a vital role in validating the combined operating schedules of agents in the district, much like the 'independent platform' in [45], it does have the potential to become a bottleneck within the scheme. This could take place either as a result of increases to the geographical scale of the district, since the sizes of optimal energy flow problems solved by the coordinator are directly proportional to the size of the networks, or due to the communication burden as every agent must communicate with the energy flow coordinator. On the other hand, there is an upper limit to the size of networks that may be considered, as pointed out in [92]. Another limitation is that the energy flow coordinator represents a single point of failure for the scheme, something which could also be said of a centralised scheme but might be avoided with a fully distributed scheme; this should be the subject of further research into multi-agent multi-energy district coordination schemes.

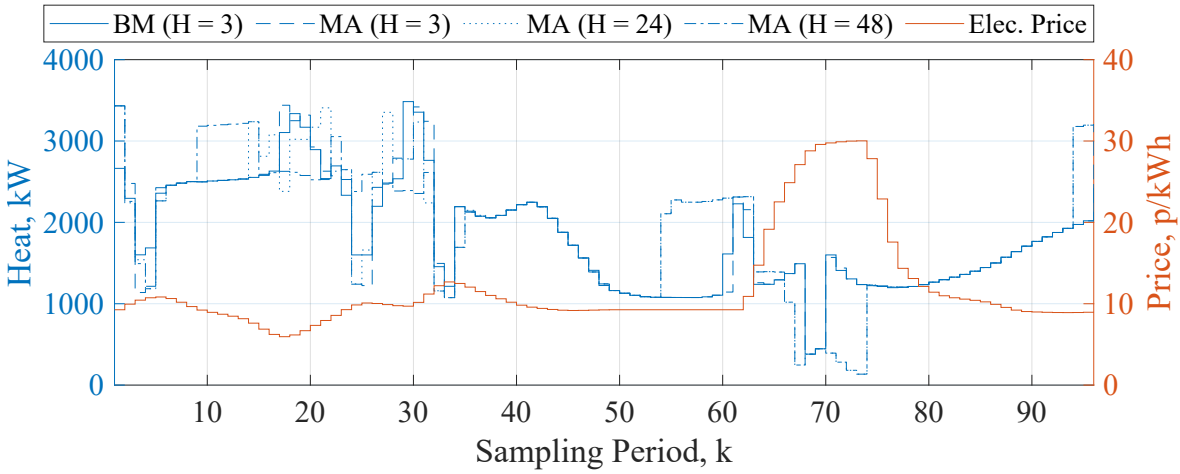

Figure 7.2: Total heat power supplied to buildings under benchmark (BM) and multi-agent NAG (MA) schemes.

Table 7.2: Computational Performance over 96 Sampling Instances

	Benchmark	Multi-Agent*		
	H = 3	H = 3	H = 24	H = 48
Mean computation time, secs	153.88	0.19	2.82	2.37
Min. computation time, secs	13.58	0.13	1.39	0.31
Max. computation time, secs	3,354.40	1.01	35.43	60.21
Std. dev. computation time, secs	464.57	0.10	3.09	7.22
Mean Algorithm Iterations	-	2.95	7.81	6.92
Max. Algorithm Iterations	-	65	121	160

* - parallel computation time for all agents is assumed to be equal to the slowest agent; communication time between agents and coordinator is assumed to be insignificant. Computation time includes that of the energy flow coordinator.

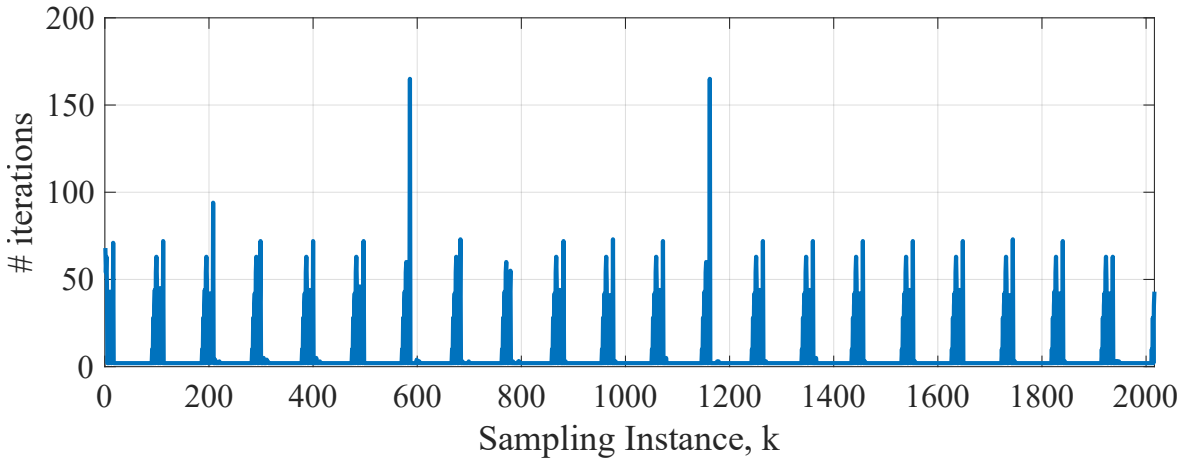

Figure 7.3: Required number of iterations at each sampling instance for an extended three week simulation, $H = 24$.

7.5 Conclusions

In this final results chapter, the contributions of Chapters 5 and 6, namely the ULT-DHC modelling modules and the accelerated multi-agent optimisation algorithm MANAG, have been combined and extended to produce an effective means to coordinate large district energy systems comprising hybrid dynamical systems. The introduction of the energy flow coordinator has enabled consideration of non-linear flow physics in multiple district energy networks, whilst keeping the overall problem tractable. It has also been possible to separate the security of these networks from the operation of energy systems in individual buildings, ensuring that a commercial aggregator can coordinate a district without raising privacy concerns. However, some limitations have also been identified in relation to this centralised coordinator, since it represents a potential single point of failure and could incur high computation and communication burdens. These and other areas for improvement will be discussed further in the following chapter.

Chapter 8

Conclusion and Future Work

8.1 Introduction

In the introductory chapter to this thesis, a central motivation for the research was articulated by the following quote from [24]:

'*...it is critical to represent multi-energy system and network models as relevant optimisation and control tasks and uncover intrinsic convexity structures that lead to computationally efficient distributed solutions*'.

The reason that this has been identified as such a critical research area, is due to the significant potential benefits afforded by multi-energy system modelling and control in real world applications, which has been the main focus of the project. In power system operations, commercial multi-energy aggregators, responsible for managing large portfolios of distributed resources in support of a net-zero energy system, require tools to optimise the coordination of these resources via online control. The aim is that these tools not only support secure operation of the energy system, they also maximise social benefit, utilising the full flexibility of 'behind the meter' assets to lower costs for consumers, all while maintaining the privacy and independence of individual stakeholders.

The objectives of the project are centered on delivery of such a tool, including the establishment of a general optimisation modelling framework and the addition of computationally efficient models of relevant distributed energy resources and supply networks. A final objective was to incorporate a decentralised control architecture which would allow the tool to be scalable and ensure privacy.

A review of the relevant literature identified several specific research gaps which needed to be addressed in order to achieve these objectives. A discussion of how well these aims, objectives and gaps have been addressed follows in the next section, before future research directions are suggested in the final section.

8.2 Conclusion

The first step in this project was to establish a general multi-energy systems modelling and control framework which could be developed to incorporate detailed networks models. Initially the framework introduced in [30] was used, since it was intended to be technology agnostic and therefore could, in theory, represent any arbitrary system. However, this approach involved representing devices in an abstract way, which could become confusing, and also required development to represent devices such as circulation pumps and WSHPs. Despite updating the method to allow modelling of these devices in [29], it was decided that the potential for confusion outweighed the benefits of generality, especially when considering that there is only a limited number of different types of energy device.

Instead, the framework first introduced in [26] was adopted and presented in Chapter 3. Rather than use HYSDEL to implement this framework, as in [26], an object-oriented programming solution was created based on the open-source optimisation software parser, YALMIP [106]. The newly developed software uses classes, methods and inheritance to enable the rapid development of large system models, by connecting up individual pre-defined device modules to form larger, aggregated modules. Each module inherits a basic set of methods or 'modifiers' which can alter the behaviour of the device, or add specific cost objectives related to the device, when activated by an end-user.

The general constraints of the framework in [26] were updated to include quadratic inequality constraints, which could easily be handled within the software implementation, and the useful flexible prosumer models from [30] were also incorporated into the framework. At this point, the objective of establishing a general multi-energy optimisation modelling framework for optimisation and control had been met. Furthermore, the framework was structured to allow further modules to be easily defined

and incorporated, so that both network energy flow models and additional device models could be added.

Initially, a simple network power balance module was demonstrated in Chapter 4, which enabled bi-directional exchange of power between a small number of buildings but did not allow power losses or changes in pressure and voltage to be modelled. Alongside this, modules for reversible WSHPs and fixed speed circulation pumps were also employed, enabling ULTDHC substations to be modelled. With the addition of these three modules it was possible to generate an MPC scheme for an integrated district with couplings between gas, electricity and ULTDHC networks, addressing the second research gap. This was also compared against a simple rule-based controller, demonstrating the economic advantage of using MPC.

Noting the issues of scalability with this centralised scheme using a single controller, it was demonstrated that the prediction horizon could be reduced by almost half without impacting economic performance. This could be exploited for managing the computational burden of the scheme but does not fully address the problem of scalability.

This is borne out by the case study presented in Chapter 5, in which modules for optimal energy flow modelling of AC power and ULTDHC networks were included in the control problem. These modules, together with a reversible, variable speed circulation pump module, increased the number of binary variables in the control problem significantly and also added non-linear constraints, giving a MISOCP problem. As a result, even though the prediction horizon was reduced to $H = 3$, which reduced the ability of the scheme to plan effectively, it took as long as 55 minutes to compute a solution when using a single controller. This meant that the controller could not provide control actions in the time required, preventing its use for practical applications. On the other hand, this case study did demonstrate that it is possible to model mass and energy flows in bi-directional ULTDHC networks, such that pumps may be dispatched and globally feasible control actions can be found for a large multi-energy district.

As a first step towards reducing the computation time of MPC schemes incorporating these modules, the scalability of MILP based MPC schemes using dual decomposition and constraint tightening methods was then addressed. Existing techniques were tested in a case study using multi-agent MPC to coordinate many multi-energy build-

ings and flexible demands in [29], for which the performance was considerably better than a centralised equivalent. However, in Chapter 6 it was shown that, under certain circumstances which could easily be encountered in a flexible energy system, the scheme exhibited poor convergence. This was because algorithm parameters needed time-consuming re-tuning as the system evolved, something which is impractical for online control. Therefore, two accelerated algorithms were proposed and shown to be both more robust and capable of achieving faster convergence without re-tuning.

Finally, in Chapter 7, an MISOCP based multi-agent MPC scheme was presented, building on the contributions of both Chapters 5 and 6. This scheme separated the global MISOCP problem for an entire multi-energy district into 85 local agent MILP problems and two central optimal energy flow problems, carried out as feasibility checks by a central energy flow coordinator. The iterative scheme, in which a set of dualised, linear global constraints are progressively updated to prevent network violations by the collective actions of agents, consistently returned feasible control actions. Computation times were reduced by two orders of magnitude in comparison to the centralised equivalent scheme, despite using a prediction horizon of $H = 48$, a sixteen-fold increase in the problem size. Owing to this increase in prediction horizon length, the multi-agent scheme outperformed the centralised scheme, which was used as a benchmark since the larger feasible region for the centralised scheme permits a lower optimality bound.

Based on these findings, the objectives and research gaps have been successfully addressed through a series of original contributions to this research area. However, there are some limitations to the work carried out and there are several suggestions to improve this research through further studies in the following section.

8.3 Further Research

Throughout this project the presence of uncertainty in forecasting has been acknowledged but not addressed, since achieving control of large scale multi-energy systems without considering uncertainty was a considerable challenge in itself. However, depending on the capability of forecasting methods, robustness against uncertainty should be built into the control scheme to some extent. Examples of optimisation schemes which addressed uncertainty in the literature often exhibited higher com-

putational burden and this is likely to be the case if considered for the final MISOCP based multi-agent scheme. On the other hand, the fact that forecasts are only considered by the individual agents, which compute solutions in parallel, may indicate that the scheme could handle the added problem complexity; however, research would have to be undertaken to demonstrate if this was indeed the case.

Another limitation to the presented work, is that the use of a centralised energy flow coordinator necessarily introduces a single point of failure and a communication burden which will require ever greater bandwidth as more agents are added. A potential solution is to employ a fully distributed scheme, in which agents only communicate with their nearest neighbours. The multi-agent dual decomposition and constraint tightening method [27], which inspired the work in Chapters 6 and 7, has been implemented as a fully distributed scheme in [130]. However, this was for an MILP problem; the inclusion of quadratic network constraints changes the problem structure and such an approach may not be applicable when networks are modelled. This would need to be confirmed through further research.

Finally, whilst the methods in this thesis have been shown to be effective in a basic simulation environment, where there is no transient behaviour in the system and no prediction model error, to fully validate the proposed control scheme would require application to a dynamic simulation model. It would then be possible to empirically assess the stability and robustness of the scheme in situations where the system behaviour is different from that expected by the prediction model. Due to the non-convex nature of the prediction model and the multiple physical environments being considered, it is not thought to be possible to determine stability and robustness analytically.

References

[1] Intergovernmental Panel on Climate Change IPCC, *IPCC press release AR6 - Climate change widespread, rapid, and intensifying*, 2021.

[2] Intergovernmental Panel on Climate Change IPCC, *Climate Change 2021: The Physical Science Basis. Contribution of Working Group I to the Sixth Assessment Report of the Intergovernmental Panel on Climate Change. Summary for Policymakers*, 2021.

[3] United Nations, "Adoption of the Paris Agreement," *Conference of the Parties on its twenty-first session*, vol. 21932, no. December, p. 32, 2015, ISSN: 1098-6596. DOI: FCCC/CP/2015/L.9/Rev.1. arXiv: arXiv:1011.1669v3. [Online]. Available: http://unfccc.int/resource/docs/2015/cop21/eng/l09r01.pdf.

[4] IEA, *World Energy Outlook 2020*, 2020.

[5] G. Strbac, D. Papadaskalopoulos, N. Chrysanthopoulos, *et al.*, "Decarbonization of Electricity Systems in Europe: Market Design Challenges," *IEEE Power and Energy Magazine*, 2021.

[6] A. Lever, H. Evans, M. Ravishankar, *et al.*, "Flexibility in Great Britain," *Imperial College London Consultants and The Carbon Trust*, p. 201, 2021.

[7] G. Strbac, M. Aunedi, D. Papadaskalopoulos, and D. Pudjianto, "Modelling Requirements for Least-Cost and Market-Driven Whole-System Analysis," *IET Special Interest Publication for the Council for Science and Technology on "Modelling Requirements of the GB Power System Resilience during the transition to Low Carbon Energy"*, pp. 1–18, 2015.

[8] B. M. Weedy, B. J. Cory, N. Jenkins, J. B. Ekanayake, and G. Strbac, *Electric Power Systems, 5th Edition — Wiley*. Wiley, 2012, vol. 14, p. 512, ISBN: 978-0-470-68268-5. [Online]. Available: https://www.wiley.com/en-us/Electric+Power+Systems%2C+5th+Edition-p-9780470682685.

[9] F. Teng, M. Aunedi, and G. Strbac, "Benefits of flexibility from smart electrified transportation and heating in the future UK electricity system," *Applied Energy*, vol. 167, pp. 420–431, Apr. 2016, ISSN: 0306-2619. DOI: 10.1016/J.APENERGY.2015.10.028.

[10] N. Hosseinzadeh, A. Aziz, A. Mahmud, and A. Gargoom, "Voltage Stability of Power Systems with Renewable-Energy Inverter-Based Generators : A Review," 2021.

[11] J. Hossain and H. R. Pota, *Robust Control for Grid Voltage Stability : High Penetration of Renewable Energy*. Springer, 2014, p. 311, ISBN: 9789812871152.

[12] P. Siano, "Demand response and smart grids—A survey," *Renewable and Sustainable Energy Reviews*, vol. 30, pp. 461–478, 2013. DOI: 10.1016/j.rser.2013.10.022. [Online]. Available: https://ac.els-cdn.com/S1364032113007211/1-s2.0-S1364032113007211-main.pdf?_tid=885f5432-a5b8-4fd6-9005-ad569dd3da1b&acdnat=1525355478_4fe30d5c65943d081259f3a80f

[13] P. Mancarella, "MES (multi-energy systems): An overview of concepts and evaluation models," *Energy*, vol. 65, pp. 1–17, 2014, ISSN: 03605442. DOI: 10.1016/j.energy.2013.10.041.

[14] N. Daina, A. Sivakumar, and J. W. Polak, "Electric vehicle charging choices: Modelling and implications for smart charging services," *Transportation Research Part C: Emerging Technologies*, vol. 81, pp. 36–56, 2017, ISSN: 0968-090X. DOI: https://doi.org/10.1016/j.trc.2017.05.006. [Online]. Available: https://www.sciencedirect.com/science/article/pii/S0968090X17301365.

[15] S. Mal, A. Chattopadhyay, A. Yang, and R. Gadh, "Electric vehicle smart charging and vehicle-to-grid operation," *International Journal of Parallel, Emergent and Distributed Systems*, vol. 28, no. 3, pp. 249–265, 2013. DOI: 10.1080/17445760.2012.663757. [Online]. Available: https://doi.org/10.1080/17445760.2012.663757.

[16] M. Royapoor, M. Pazhoohesh, P. J. Davison, C. Patsios, and S. Walker, "Building as a virtual power plant, magnitude and persistence of deferrable loads and human comfort implications," *Energy and Buildings*, vol. 213, p. 109 794, 2020, ISSN: 0378-7788. DOI: https://doi.org/10.1016/j.enbuild.2020.109794. [Online]. Available: https://www.sciencedirect.com/science/article/pii/S0378778819328956.

[17] D. Wang, S. Parkinson, W. Miao, H. Jia, C. Crawford, and N. Djilali, "Online voltage security assessment considering comfort-constrained demand response control of distributed heat pump systems," *Applied Energy*, vol. 96, pp. 104–114, 2012, Smart Grids, ISSN: 0306-2619. DOI: https://doi.org/10.1016/j.apenergy.2011.12.005. [Online]. Available: https://www.sciencedirect.com/science/article/pii/S0306261911007999.

[18] A. Vandermeulen, B. van der Heijde, and L. Helsen, "Controlling district heating and cooling networks to unlock flexibility: A review," *Energy*, vol. 151, pp. 103–115, 2018, ISSN: 03605442. DOI: 10.1016/j.energy.2018.03.034. [Online]. Available: https://doi.org/10.1016/j.energy.2018.03.034.

[19] S. Buffa, M. Cozzini, M. D'Antoni, M. Baratieri, and R. Fedrizzi, "5th generation district heating and cooling systems: A review of existing cases in Europe," *Renewable and Sustainable Energy Reviews*, vol. 104, pp. 504–522, Apr. 2019, ISSN: 1364-0321. DOI: 10.1016/J.RSER.2018.12.059.

[20] D. Sanders, A. Hart, M. Ravishankar, *et al.*, "An analysis of electricity system flexibility for Great Britain," *Imperial College London Consultants and The Carbon Trust*, no. November, 2016. [Online]. Available: https://www.gov.uk/government/uploads/system/uploads/attachment_data/file/568982/An_analysis_of_electricity_flexibility_for_Great_Britain.pdf.

[21] N. Good, E. A. Martínez Cesena, and P. Mancarella, "Ten questions concerning smart districts," 2017. DOI: 10.1016/j.buildenv.2017.03.037.

[22] L. Gkatzikis, I. Koutsopoulos, and T. Salonidis, "The role of aggregators in smart grid demand response markets," *IEEE Journal on Selected Areas in Communications*, vol. 31, no. 7, pp. 1247–1257, 2013, ISSN: 07338716. DOI: 10.1109/JSAC.2013.130708.

[23] S. Frank and S. Rebennack, "IIE Transactions An introduction to optimal power flow: Theory, formulation, and examples An introduction to optimal power flow: Theory, formulation, and examples," 2016, ISSN: 1545-8830. DOI: 10.1080/0740817X.2016.1189626.

[24] E. Dall'Anese, P. Mancarella, and A. Monti, "Unlocking Flexibility: Integrated Optimization and Control of Multienergy Systems," *IEEE Power and Energy Magazine*, vol. 15, no. 1, pp. 43–52, 2017, ISSN: 15407977. DOI: 10.1109/MPE.2016.2625218.

[25] A. Parisio, E. Rikos, and L. Glielmo, "A model predictive control approach to microgrid operation optimization," *IEEE Transactions on Control Systems Technology*, vol. 22, no. 5, pp. 1813–1827, 2014, ISSN: 10636536. DOI: 10.1109/TCST.2013.2295737.

[26] A. Moser, D. Muschick, M. Gölles, *et al.*, "A MILP-based modular energy management system for urban multi-energy systems: Performance and sensitivity analysis," *Applied Energy*, 2020, ISSN: 03062619. DOI: 10.1016/j.apenergy.2019.114342.

[27] A. Falsone, K. Margellos, and M. Prandini, "A decentralized approach to multi-agent MILPs: Finite-time feasibility and performance guarantees," *Automatica*, vol. 103, pp. 141–150, 2019, ISSN: 00051098. DOI: 10.1016/j.automatica.2019.01.009. arXiv: 1706.08788.

[28] R. Vujanic, P. Mohajerin Esfahani, P. J. Goulart, S. Mariéthoz, and M. Morari, "A decomposition method for large scale MILPs, with performance guarantees and a power system application," *Automatica*, vol. 67, pp. 144–156, 2016, ISSN: 00051098. DOI: 10.1016/j.automatica.2016.01.006. arXiv: 1411.1973.

[29] M. Taylor, S. Long, O. Marjanovic, and A. Parisio, "Model Predictive Control of Smart Districts with Fifth Generation Heating and Cooling Networks," *IEEE Transactions on Energy Conversion*, pp. 1–11, 2021, ISSN: 0885-8969. DOI: 10.1109/tec.2021.3082405.

[30] S. Long, O. Marjanovic, and A. Parisio, "Generalised control-oriented modelling framework for multi-energy systems," *Applied Energy*, vol. 235, pp. 320–331, Feb. 2019, ISSN: 03062619. DOI: 10.1016/j.apenergy.2018.10.074.

[31] A. Bemporad and M. Morari, "Control of systems integrating logic, dynamics, and constraints," *Automatica*, vol. 35, no. 3, pp. 407–427, 1999, ISSN: 00051098. DOI: 10.1016/S0005-1098(98)00178-2.

[32] M. Taylor, O. Marjanovic, and A. Parisio, "Decentralised Predictive Control of Multi-Energy Resources in Buildings," in *2021 29th Mediterranean Conference on Control and Automation (MED)*, Bari, Puglia, Italy, 2021, pp. 39–44, ISBN: 9780738110981.

[33] M. Taylor, O. Marjanovic, and A. Parisio, "Decentralised supervisory control of networked multi-energy buildings," *Manuscript in preparation*, 2023.

[34] A. Parisio, C. Del Vecchio, and A. Vaccaro, "A robust optimization approach to energy hub management," *International Journal of Electrical Power & Energy Systems*, vol. 42, no. 1, pp. 98–104, 2012, ISSN: 01420615. DOI: 10.1016/j.ijepes.2012.03.015. [Online]. Available: http://linkinghub.elsevier.com/retrieve/pii/S0142061512000701.

[35] H. Shi, N. Blaauwbroek, P. H. Nguyen, and R. I. Kamphuis, "Energy management in Multi-Commodity Smart Energy Systems with a greedy approach," *Applied Energy*, vol. 167, pp. 385–396, Apr. 2016, ISSN: 0306-2619. DOI: 10.1016/J.APENERGY.2015.11.101.

[36] A. Parisio, C. Wiezorek, T. Kyntäjä, J. Elo, K. Strunz, and K. H. Johansson, "Cooperative MPC-Based Energy Management for Networked Microgrids," *IEEE Transactions on Smart Grid*, vol. 8, no. 6, pp. 3066–3074, 2017, ISSN: 19493053. DOI: 10.1109/TSG.2017.2726941.

[37] W. Gu, Z. Wang, Z. Wu, Z. Luo, Y. Tang, and J. Wang, "An Online Optimal Dispatch Schedule for CCHP Microgrids Based on Model Predictive Control," *IEEE Transactions on Smart Grid*, vol. 8, no. 5, pp. 2332–2342, 2017, ISSN: 19493053. DOI: 10.1109/TSG.2016.2523504.

[38] A. Anvari-Moghaddam, A. Rahimi-Kian, M. S. Mirian, and J. M. Guerrero, "A multi-agent based energy management solution for integrated buildings and microgrid system," *Applied Energy*, vol. 203, pp. 41–56, Oct. 2017, ISSN: 0306-2619. DOI: 10.1016/J.APENERGY.2017.06.007.

[39] E. A. Cesena and P. Mancarella, "Energy Systems Integration in Smart Districts: Robust Optimisation of Multi-Energy Flows in Integrated Electricity, Heat and Gas Networks," *IEEE Transactions on Smart Grid*, 2018, ISSN: 19493053. DOI: 10.1109/TSG.2018.2828146.

[40] J. Iria and F. Soares, "Real-time provision of multiple electricity market products by an aggregator of prosumers," *Applied Energy*, vol. 255, p. 113 792, Dec. 2019, ISSN: 0306-2619. DOI: 10.1016/J.APENERGY.2019.113792.

[41] D. Ioli, A. Falsone, A. V. Papadopoulos, and M. Prandini, "A compositional modeling framework for the optimal energy management of a district network," *Journal of Process Control*, vol. 74, pp. 160–176, Feb. 2019, ISSN: 0959-1524. DOI: 10.1016/J.JPROCONT.2017.10.005.

[42] T. Pippia, J. Sijs, and B. De Schutter, "A Single-Level Rule-Based Model Predictive Control Approach for Energy Management of Grid-Connected Microgrids," *IEEE Transactions on Control Systems Technology*, pp. 1–13, 2019, ISSN: 1063-6536. DOI: 10.1109/tcst.2019.2945023.

[43] N. Good and P. Mancarella, "Flexibility in Multi-Energy Communities with Electrical and Thermal Storage: A Stochastic, Robust Approach for Multi-Service Demand Response," *IEEE Transactions on Smart Grid*, vol. 10, no. 1, pp. 503–513, Jan. 2019. DOI: 10.1109/TSG.2017.2745559.

[44] R. Jing, M. N. Xie, F. X. Wang, and L. X. Chen, "Fair P2P energy trading between residential and commercial multi-energy systems enabling integrated demand-side management," *Applied Energy*, vol. 262, p. 114 551, Mar. 2020, ISSN: 0306-2619. DOI: 10.1016/J.APENERGY.2020.114551.

[45] A. Coelho, J. Iria, and F. Soares, "Network-secure bidding optimization of aggregators of multi-energy systems in electricity, gas, and carbon markets," *Applied Energy*, vol. 301, p. 117 460, Nov. 2021, ISSN: 0306-2619. DOI: 10.1016/J.APENERGY.2021.117460.

[46] G. Yuan, Y. Gao, and B. Ye, "Optimal dispatching strategy and real-time pricing for multi-regional integrated energy systems based on demand response," *Renewable Energy*, vol. 179, pp. 1424–1446, Dec. 2021, ISSN: 0960-1481. DOI: 10.1016/J.RENENE.2021.07.036.

[47] H. Zakernezhad, M. S. Nazar, M. Shafie-khah, and J. P. Catalão, "Optimal resilient operation of multi-carrier energy systems in electricity markets considering distributed energy resource aggregators," *Applied Energy*, vol. 299, p. 117 271, Oct. 2021, ISSN: 0306-2619. DOI: 10.1016/J.APENERGY.2021.117271.

[48] L. M. P. Ghilardi, A. F. Castelli, L. Moretti, M. Morini, and E. Martelli, "Co-optimization of multi-energy system operation, district heating/cooling network and thermal comfort management for buildings," *Applied Energy*, vol. 302, p. 117 480, Nov. 2021, ISSN: 0306-2619. DOI: 10.1016/J.APENERGY.2021.117480.

[49] M. Wirtz, L. Neumaier, P. Remmen, and D. Müller, "Temperature control in 5th generation district heating and cooling networks : An MILP-based operation optimization," *Applied Energy*, vol. 288, no. January, p. 116 608, 2021, ISSN: 0306-2619. DOI: 10.1016/j.apenergy.2021.116608.

[50] *HYSDEL - Hybrid System DEscription Language*. [Online]. Available: http://people.ee.ethz.ch/%7B~%7Dcohysys/hysdel/ (visited on 10/22/2021).

[51] M. Geidl and G. Andersson, "Optimal power flow of multiple energy carriers," *IEEE Transactions on Power Systems*, vol. 22, no. 1, pp. 145–155, 2007, ISSN: 08858950. DOI: 10.1109/TPWRS.2006.888988.

[52] M. Geidl, G. Koeppel, P. Favre-Perrod, B. Klöckl, G. Andersson, and K. Fröhlich, *Energy hubs for the future*, 2007. DOI: 10.1109/MPAE.2007.264850. [Online]. Available: http://ieeexplore.ieee.org/stamp/stamp.jsp?arnumber=4042137%20http://ieeexplore.ieee.org.bdigital.udistrital.edu.co:8080/stamp/stamp.jsp?tp=%7B%5C&%7Darnumber=8009655%20http://ieeexplore.ieee.org/stamp/stamp.jsp?arnumber=5736181.

[53] K. Qu, T. Yu, L. Huang, B. Yang, and X. Zhang, "Decentralized optimal multi-energy flow of large-scale integrated energy systems in a carbon trading market," *Energy*, vol. 149, pp. 779–791, Apr. 2018, ISSN: 0360-5442. DOI: 10.1016/J.ENERGY.2018.02.083.

[54] G. T. Ayele, P. Haurant, B. Laumert, and B. Lacarrière, "An extended energy hub approach for load flow analysis of highly coupled district energy networks: Illustration with electricity and heating," *Applied Energy*, vol. 212, pp. 850–867, Feb. 2018, ISSN: 03062619. DOI: 10.1016/j.apenergy.2017.12.090.

[55] T. Ma, J. Wu, L. Hao, and D. Li, "Energy flow matrix modeling and optimal operation analysis of multi energy systems based on graph theory," *Applied Thermal Engineering*, vol. 146, pp. 648–663, Jan. 2019, ISSN: 1359-4311. DOI: 10.1016/J.APPLTHERMALENG.2018.10.022.

[56] Y. Li, H. Zhang, X. Liang, and B. Huang, "Event-Triggered-Based Distributed Cooperative Energy Management for Multienergy Systems," *IEEE Transactions on Industrial Informatics*, vol. 15, no. 4, pp. 2008–2022, Apr. 2019. DOI: 10.1109/TII.2018.2862436.

[57] J. Wasilewski, "Integrated modeling of microgrid for steady-state analysis using modified concept of multi-carrier energy hub," *International Journal of Electrical Power and Energy Systems*, vol. 73, pp. 891–898, 2015. DOI: 10.1016/j.ijepes.2015.06.022. [Online]. Available: https://ac.els-cdn.com/S0142061515002781/1-s2.0-S0142061515002781-main.pdf?%7B%

5C_%7Dtid=621415dc-ec85-11e7-a20f-00000aab0f02%7B%5C&%7Dacdnat=1514544508%7B%5C_%7Db6bfddd2286ad7ffa416120ecc55e5ff.

[58] A. Osiadacz, *Simulation and Analysis of Gas Networks*. London: E. & F.N. Spon Ltd, 1987, ISBN: 0 419 12480 2.

[59] M. Pirouti, "Modelling and analysis of a district heating network," p. 121, 2013. [Online]. Available: http://orca.cf.ac.uk/45201/1/Marouf.Pirouti%7B%5C_%7DPhD%20Thesis.pdf%20https://orca.cf.ac.uk/45201/1/Marouf.Pirouti%7B%5C_%7DPhD%20Thesis.pdf%7B%5C%%7D0Ahttp://orca.cf.ac.uk/45201/%7B%5C%%7D0Ahttp://orca.cf.ac.uk/45201/1/Marouf.Pirouti%7B%5C_%7DPhD%20Thesis.pdf%7B%5C%%7D0Ahttp://orca.cf.ac.uk/45201/.

[60] L. Gan, N. Li, U. Topcu, and S. H. Low, "Exact Convex Relaxation of Optimal Power Flow in Radial Networks," *IEEE Transactions on Automatic Control*, vol. 60, no. 1, pp. 72–87, 2015, ISSN: 00189286. DOI: 10.1109/TAC.2014.2332712.

[61] M. K. Singh and V. Kekatos, "Optimal Scheduling of Water Distribution Systems," *IEEE Transactions on Control of Network Systems*, vol. 7, no. 2, pp. 711–723, Jun. 2020, ISSN: 2325-5870. DOI: 10.1109/TCNS.2019.2939651.

[62] S. Huang, W. Tang, Q. Wu, and C. Li, "Network constrained economic dispatch of integrated heat and electricity systems through mixed integer conic programming," *Energy*, vol. 179, pp. 464–474, 2019, ISSN: 03605442. DOI: 10.1016/j.energy.2019.05.041. [Online]. Available: https://doi.org/10.1016/j.energy.2019.05.041.

[63] D. Xu, Q. Wu, B. Zhou, C. Li, L. Bai, and S. Huang, "Distributed Multi-Energy Operation of Coupled Electricity, Heating, and Natural Gas Networks," *IEEE Transactions on Sustainable Energy*, vol. 11, no. 4, pp. 2457–2469, 2020, ISSN: 19493037. DOI: 10.1109/TSTE.2019.2961432.

[64] Y. Zhou, M. Shahidehpour, Z. Wei, Z. Li, G. Sun, and S. Chen, "Distributionally Robust Unit Commitment in Coordinated Electricity and District Heating Networks," *IEEE Transactions on Power Systems*, vol. 35, no. 3, pp. 2155–2166, 2020, ISSN: 15580679. DOI: 10.1109/TPWRS.2019.2950987.

[65] Y. Cao, W. Wei, L. Wu, S. Mei, M. Shahidehpour, and Z. Li, "Decentralized Operation of Interdependent Power Distribution Network and District Heating Network: A Market-Driven Approach," *IEEE Transactions on Smart Grid*, vol. PP, no. c, p. 1, 2018, ISSN: 19493053. DOI: 10.1109/TSG.2018.2880909.

[66] S. Yao, W. Gu, S. Lu, *et al.*, "Dynamic optimal energy flow in the heat and electricity integrated energy system," *IEEE Transactions on Sustainable Energy*, vol. 12, no. 1, pp. 179–190, 2021, ISSN: 19493037. DOI: 10.1109/TSTE.2020.2988682.

[67] K. Lygnerud and S. Werner, "Annex TS2 Implementation of Low-Temperature District Heating Systems, Final Report," IEA-DHC, Tech. Rep., 2021.

[68] H. Lund, S. Werner, R. Wiltshire, *et al.*, "4th Generation District Heating (4GDH). Integrating smart thermal grids into future sustainable energy systems.," *Energy*, vol. 68, pp. 1–11, 2014, ISSN: 03605442. DOI: 10.1016/j.energy.2014.02.089. [Online]. Available: http://dx.doi.org/10.1016/j.energy.2014.02.089.

[69] *File:Generations of district heating systems EN.svg - Wikimedia Commons*. [Online]. Available: https://commons.wikimedia.org/wiki/File:Generations%7B%5C_%7Dof%7B%5C_%7Ddistrict%7B%5C_%7Dheating%7B%5C_%7Dsystems%7B%5C_%7DEN.svg (visited on 01/09/2022).

[70] H. Lund, P. A. Østergaard, T. B. Nielsen, *et al.*, "Perspectives on fourth and fifth generation district heating," *Energy*, vol. 227, pp. 147–159, Jul. 2021, ISSN: 0360-5442. DOI: 10.1016/J.ENERGY.2021.120520.

[71] O. Gudmundsson, R. R. Schmidt, A. Dyrelund, and J. E. Thorsen, "Economic comparison of 4GDH and 5GDH systems – Using a case study," *Energy*, vol. 238, p. 121 613, Jan. 2022, ISSN: 0360-5442. DOI: 10.1016/J.ENERGY.2021.121613.

[72] F. Bünning, M. Wetter, M. Fuchs, and D. Müller, "Bidirectional low temperature district energy systems with agent-based control: Performance comparison and operation optimization," *Applied Energy*, vol. 209, no. November 2017, pp. 502–515, 2018, ISSN: 03062619. DOI: 10.1016/j.apenergy.2017.10.072.

[73] R. Verhoeven, E. Willems, V. Harcouët-Menou, *et al.*, "Minewater 2.0 project in Heerlen the Netherlands: Transformation of a geothermal mine water pilot project into a full scale hybrid sustainable energy infrastructure for heating and cooling," in *Energy Procedia*, 2014. DOI: 10.1016/j.egypro.2014.01.158.

[74] N. Vetterli, M. Sulzer, and U. P. Menti, "Energy monitoring of a low temperature heating and cooling district network," *Energy Procedia*, vol. 122, pp. 62–67, Sep. 2017, ISSN: 1876-6102. DOI: 10.1016/J.EGYPRO.2017.07.289.

[75] ETH Zurich, *The energy of tomorrow: Anergy Grid Campus Hönggerberg-a dynamic underground storage system*, 2020. [Online]. Available: https://ethz.ch/content/dam/ethz/main/eth-zurich/nachhaltigkeit/Dokumente/Anergienetz/200129%7B%5C_%7DAnergienetz%7B%5C_%7DA4%7B%5C_%7D6s%7B%5C_%7DEinzel%7B%5C_%7DEN%7B%5C_%7DRZ.pdf (visited on 12/07/2021).

[76] M. Wetter and J. Hu, "Quayside Energy Systems Analysis," Lawrence Berkeley National Laboratory, Tech. Rep., 2019.

[77] A. Prasanna, V. Dorer, and N. Vetterli, "Optimisation of a district energy system with a low temperature network," *Energy*, vol. 137, pp. 632–648, Oct. 2017, ISSN: 03605442. DOI: 10.1016/j.energy.2017.03.137.

[78] T. Sommer, M. Sulzer, M. Wetter, A. Sotnikov, S. Mennel, and C. Stettler, "The reservoir network: A new network topology for district heating and cooling," *Energy*, vol. 199, p. 117 418, 2020, ISSN: 03605442. DOI: 10.1016/j.energy.2020.117418.

[79] L. Moretti, E. Martelli, and G. Manzolini, "An efficient robust optimization model for the unit commitment and dispatch of multi-energy systems and microgrids," *Applied Energy*, vol. 261, p. 113 859, Mar. 2020, ISSN: 0306-2619. DOI: 10.1016/J.APENERGY.2019.113859.

[80] C. Wang, W. Wei, J. Wang, L. Bai, Y. Liang, and T. Bi, "Convex Optimization Based Distributed Optimal Gas-Power Flow Calculation," *IEEE Transactions on Sustainable Energy*, vol. 9, no. 3, pp. 1145–1156, 2018, ISSN: 19493029. DOI: 10.1109/TSTE.2017.2771954.

[81] B. Hu, Y. Tie, C. Shao, *et al.*, "A hierarchical transactive energy management framework for optimizing the reserve profile in district energy systems," *CSEE*

Journal of Power and Energy Systems, 2021. DOI: 10.17775/cseejpes.2020.06410.

[82] X. Liu, J. Wu, N. Jenkins, and A. Bagdanavicius, "Combined analysis of electricity and heat networks," *Applied Energy*, vol. 162, pp. 1238–1250, Jan. 2016, ISSN: 03062619. DOI: 10.1016/j.apenergy.2015.01.102. [Online]. Available: http://linkinghub.elsevier.com/retrieve/pii/S0306261915001385.

[83] X. Liu and P. Mancarella, "Modelling, assessment and Sankey diagrams of integrated electricity-heat-gas networks in multi-vector district energy systems," *Applied Energy*, vol. 167, pp. 336–352, Apr. 2016, ISSN: 0306-2619. DOI: 10.1016/J.APENERGY.2015.08.089. [Online]. Available: https://www.sciencedirect.com/science/article/pii/S0306261915010259.

[84] M. Moeini-Aghtaie, A. Abbaspour, M. Fotuhi-Firuzabad, and E. Hajipour, "A decomposed solution to multiple-energy carriers optimal power flow," *IEEE Transactions on Power Systems*, vol. 29, no. 2, pp. 707–716, 2014, ISSN: 08858950. DOI: 10.1109/TPWRS.2013.2283259.

[85] C. Shao, X. Wang, M. Shahidehpour, X. Wang, and B. Wang, "An MILP-Based Optimal Power Flow in Multicarrier Energy Systems," *IEEE Transactions on Sustainable Energy*, vol. 8, no. 1, pp. 239–248, 2017, ISSN: 19493029. DOI: 10.1109/TSTE.2016.2595486.

[86] S. Chen, Z. Wei, G. Sun, D. Wang, and H. Zang, "Steady state and transient simulation for electricity-gas integrated energy systems by using convex optimisation," *IET Generation, Transmission and Distribution*, vol. 12, no. 9, pp. 2199–2206, 2018, ISSN: 17518687. DOI: 10.1049/iet-gtd.2017.1318.

[87] A. Shabanpour-Haghighi and A. R. Seifi, "Simultaneous integrated optimal energy flow of electricity, gas, and heat," *Energy Conversion and Management*, vol. 101, pp. 579–591, Sep. 2015, ISSN: 0196-8904. DOI: 10.1016/J.ENCONMAN.2015.06.002.

[88] E. F. Camacho and C. Bordons, *Model Predictive Control*. 2007, p. 405, ISBN: 9781852336943. DOI: 10.1007/978-0-85729-398-5. arXiv: arXiv:1011.1669v3. [Online]. Available: https://link.springer.com/content/pdf/10.1007%2F978-0-85729-398-5.pdf.

[89] D. E. Seborg, T. F. Edgar, D. A. Mellichamp, and F. J. Doyle, *Process dynamics and control*, 3rd. Wiley, 2010.

[90] Liuping Wang, *Model Predictive Control: Design and implementation using MATLAB*. 2009, pp. 25–26, ISBN: 9781848823303. DOI: 10.1109/acc.2009.5159781. arXiv: arXiv:1011.1669v3. [Online]. Available: https://link.springer.com/content/pdf/10.1007%2F978-1-84882-331-0.pdf.

[91] J. M. Maciejowski, *Predictive Control: With Constraints*. 2002, p. 331, ISBN: 0201398230. [Online]. Available: http://books.google.com/books?id=HV_Y58c7KiwC&pgis=1.

[92] Y. Liu, N. Yu, W. Wang, *et al.*, "Coordinating the operations of smart buildings in smart grids," *Applied Energy*, vol. 228, no. April, pp. 2510–2525, 2018, ISSN: 03062619. DOI: 10.1016/j.apenergy.2018.07.089. [Online]. Available: https://doi.org/10.1016/j.apenergy.2018.07.089.

[93] M. Petrollese, L. Valverde, D. Cocco, G. Cau, and J. Guerra, "Real-time integration of optimal generation scheduling with MPC for the energy management of a renewable hydrogen-based microgrid," *Applied Energy*, vol. 166, pp. 96–106, Mar. 2016, ISSN: 03062619. DOI: 10.1016/j.apenergy.2016.01.014. [Online]. Available: http://www.sciencedirect.com.manchester.idm.oclc.org/science/article/pii/S0306261916000337.

[94] J. Reynolds, M. W. Ahmad, Y. Rezgui, and J. L. Hippolyte, "Operational supply and demand optimisation of a multi-vector district energy system using artificial neural networks and a genetic algorithm," *Applied Energy*, vol. 235, pp. 699–713, Feb. 2019, ISSN: 0306-2619. DOI: 10.1016/J.APENERGY.2018.11.001.

[95] P. Velarde, L. Valverde, J. M. Maestre, C. Ocampo-Martinez, and C. Bordons, "On the comparison of stochastic model predictive control strategies applied to a hydrogen-based microgrid," *Journal of Power Sources*, vol. 343, pp. 161–173, Mar. 2017, ISSN: 03787753. DOI: 10.1016/j.jpowsour.2017.01.015. [Online]. Available: http://www.sciencedirect.com.manchester.idm.oclc.org/science/article/pii/S0378775317300150.

[96] J. Iria, F. Soares, and M. Matos, "Optimal bidding strategy for an aggregator of prosumers in energy and secondary reserve markets," *Applied Energy*, vol. 238, pp. 1361–1372, Mar. 2019, ISSN: 0306-2619. DOI: 10.1016/J.APENERGY.2019.01.191.

[97] J. M. Maestre and R. R. Negenborn, "Distributed Model Predictive Control Made Easy," *Intelligent Systems, Control and Automation: Science and Engineering*, Intelligent Systems, Control and Automation: Science and Engineering, vol. 69, J. M. Maestre and R. R. Negenborn, Eds., 2014, ISSN: 22138994. DOI: 10.1007/978-94-007-7006-5. [Online]. Available: http://link.springer.com/10.1007/978-94-007-7006-5.

[98] M. Arnold, R. R. Negenborn, G. Andersson, and B. De Schutter, "Distributed Predictive Control for Energy Hub Coordination in Coupled Electricity and Gas Networks," in *Intelligent Infrastructures*, vol. 42, Springer, 2010, pp. 235–273, ISBN: 978-90-481-3597-4. DOI: 10.1007/978-90-481-3598-1_10. [Online]. Available: http://www.dcsc.tudelft.nl/%7B~%7Dbdeschutter/pub/rep/09%7B%5C_%7D050.pdf%20http://link.springer.com/10.1007/978-90-481-3598-1%7B%5C_%7D10.

[99] D. Xu, B. Zhou, K. W. Chan, *et al.*, "Distributed multienergy coordination of multimicrogrids with biogas-solar-wind renewables," *IEEE Transactions on Industrial Informatics*, vol. 15, no. 6, pp. 3254–3266, 2019, ISSN: 15513203. DOI: 10.1109/TII.2018.2877143.

[100] R. Verschae, H. Kawashima, T. Kato, and T. Matsuyama, "Coordinated energy management for inter-community imbalance minimization," *Renewable Energy*, vol. 87, pp. 922–935, 2016, ISSN: 18790682. DOI: 10.1016/j.renene.2015.07.039. [Online]. Available: http://dx.doi.org/10.1016/j.renene.2015.07.039.

[101] R. Halvgaard, L. Vandenberghe, N. K. Poulsen, H. Madsen, and J. B. Jørgensen, "Distributed Model Predictive Control for Smart Energy Systems," *IEEE Transactions on Smart Grid*, vol. 7, no. 3, pp. 1675–1682, 2016, ISSN: 19493053. DOI: 10.1109/TSG.2016.2526077. arXiv: 1508.00794.

[102] R. M. Hermans, A. Jokić, M. Lazar, *et al.*, "Assessment of non-centralised model predictive control techniques for electrical power networks," *International Journal of Control*, vol. 85, no. 8, pp. 1162–1177, 2012, ISSN: 1366-5820. DOI: 10.1080/00207179.2012.679972. [Online]. Available: https://www.tandfonline.com/action/journalInformation?journalCode=tcon20.

[103] W. Zhong, K. Xie, Y. Liu, C. Yang, and S. Xie, "Auction Mechanisms for Energy Trading in Multi-Energy Systems," *IEEE Transactions on Industrial Informat-*

ics, vol. 14, no. 4, pp. 1511–1521, Apr. 2018. DOI: 10.1109/TII.2017.2787751.

[104] A. Sheikhi, M. Rayati, and A. M. Ranjbar, "Demand side management for a residential customer in multi-energy systems," *Sustainable Cities and Society*, vol. 22, pp. 63–77, Apr. 2016, ISSN: 2210-6707. DOI: 10.1016/J.SCS.2016.01.010.

[105] Y. Ye, Y. Ye, D. Qiu, X. Wu, G. Strbac, and J. Ward, "Model-Free Real-Time Autonomous Control for a Residential Multi-Energy System Using Deep Reinforcement Learning," *IEEE Transactions on Smart Grid*, vol. 11, no. 4, pp. 3068–3082, Jul. 2020. DOI: 10.1109/TSG.2020.2976771.

[106] J. Löfberg, "Yalmip : A toolbox for modeling and optimization in matlab," in *In Proceedings of the CACSD Conference*, Taipei, Taiwan, 2004.

[107] G. Bonvin, S. Demassey, C. Le Pape, N. Maïzi, V. Mazauric, and A. Samperio, "A convex mathematical program for pump scheduling in a class of branched water networks," *Applied Energy*, 2017, ISSN: 03062619. DOI: 10.1016/j.apenergy.2015.12.090.

[108] D. Verleye and E.-H. Aghezzaf, "Optimising production and distribution operations in large water supply networks: A piecewise linear optimisation approach," *International Journal of Production Research*, vol. 51, no. 23-24, pp. 7170–7189, Nov. 2013, ISSN: 0020-7543. DOI: 10.1080/00207543.2013.850550. [Online]. Available: http://www.tandfonline.com/doi/full/10.1080/00207543.2013.850550.

[109] B. Geiler, O. Kolb, J. Lang, G. Leugering, A. Martin, and A. Morsi, "Mixed integer linear models for the optimization of dynamical transport networks," *Mathematical Methods of Operations Research*, vol. 73, no. 3, pp. 339–362, 2011, ISSN: 14325217. DOI: 10.1007/s00186-011-0354-5.

[110] Gurobi Optimization LLC, *Gurobi Optimizer Reference Manual*, 2021. [Online]. Available: https://www.gurobi.com.

[111] J. Skaf and S. P. Boyd, "Design of affine controllers via convex optimization," *IEEE Transactions on Automatic Control*, vol. 55, no. 11, pp. 2476–2487, 2010, ISSN: 00189286. DOI: 10.1109/TAC.2010.2046053.

[112] S. Long, O. Marjanovic, and A. Parisio, "Demand smoothing in multi-energy systems using model predictive control," in *2018 IEEE PES Innovative Smart Grid Technologies Conference Europe (ISGT-Europe)*, 2018, pp. 1–6. DOI: 10.1109/ISGTEurope.2018.8571560.

[113] H. Abdi, S. Derafshi Beigvand, and L. Scala, "A review of optimal power flow studies applied to smart grids and microgrids," *Renewable and Sustainable Energy Reviews*, vol. 71, pp. 742–766, 2017. DOI: 10.1016/j.rser.2016.12.102. [Online]. Available: http://dx.doi.org/10.1016/j.rser.2016.12.102.

[114] Q. Wu, H. Ren, W. Gao, and J. Ren, "Benefit allocation for distributed energy network participants applying game theory based solutions," *Energy*, vol. 119, pp. 384–391, 2017, ISSN: 03605442. DOI: 10.1016/j.energy.2016.12.088.

[115] Grundfos, *TP 80-240/2 Performance Curve*. [Online]. Available: https://product-selection.grundfos.com.

[116] Octopus Energy Ltd, *Agile Octopus rates*. [Online]. Available: https://s3-eu-west-1.amazonaws.com/octoenergy-production-statics/data/agile-rates/agile_rates.2018-12-20.xlsx (visited on 02/04/2020).

[117] Y. Shi, B. Xu, D. Wang, and B. Zhang, "Using Battery Storage for Peak Shaving and Frequency Regulation: Joint Optimization for Superlinear Gains," *IEEE Transactions on Power Systems*, vol. 33, no. 3, pp. 2882–2894, 2018, ISSN: 08858950. DOI: 10.1109/TPWRS.2017.2749512. arXiv: 1702.08065.

[118] J. Salpakari and P. Lund, "Optimal and rule-based control strategies for energy flexibility in buildings with PV," *Applied Energy*, vol. 161, pp. 425–436, 2016, ISSN: 03062619. DOI: 10.1016/j.apenergy.2015.10.036. [Online]. Available: http://dx.doi.org/10.1016/j.apenergy.2015.10.036.

[119] J. B. Almada, R. P. Leão, R. F. Sampaio, and G. C. Barroso, "A centralized and heuristic approach for energy management of an AC microgrid," *Renewable and Sustainable Energy Reviews*, vol. 60, pp. 1396–1404, 2016, ISSN: 18790690. DOI: 10.1016/j.rser.2016.03.002. [Online]. Available: http://dx.doi.org/10.1016/j.rser.2016.03.002.

[120] IBM Corporation, *ILOG CPLEX Optimization Studio*, 2019. [Online]. Available: www.cplex.com.

[121] The MathWorks Inc., *MATLAB & Simulink*. [Online]. Available: https://uk.mathworks.com/products/matlab.html.

[122] "Natural Gas Flow Solvers Using Convex Relaxation," *IEEE Transactions on Control of Network Systems*, vol. 7, no. 3, pp. 1283–1295, Sep. 2020. DOI: 10.1109/TCNS.2020.2972593.

[123] R. D. Zimmerman and C. E. Murillo-Sanchez, "MATPOWER manual," pp. 0–249, 2020. [Online]. Available: https://matpower.org/docs/MATPOWER-manual.pdf.

[124] U.S. Department of Energy, *Commercial reference buildings*, 2016.

[125] S. Boyd and L. Vandenberghe, *Convex Optimization*. Cambridge University Press, 2004, ISBN: 9780521833783. [Online]. Available: http://stanford.edu/%7B~%7Dboyd/cvxbook/%7B%5C%%7D5Cnhttp://stanford.edu/%7B~%7Dboyd/cvxbook/bv%7B%5C_%7Dcvxbook.pdf.

[126] N. Z. Shor, *Minimization Methods for Non-Differentiable Functions* (Springer Series in Computational Mathematics September 2013). Berlin, Heidelberg: Springer Berlin Heidelberg, 1985, vol. 3, pp. 22–47, ISBN: 978-3-642-82120-2. DOI: 10.1007/978-3-642-82118-9. arXiv: arXiv:1011.1669v3.

[127] K. M. Anstreicher and L. A. Wolsey, "Two "well-known" properties of subgradient optimization," *Mathematical Programming*, vol. 120, no. 1 SPEC. ISS. Pp. 213–220, 2009, ISSN: 00255610. DOI: 10.1007/s10107-007-0148-y.

[128] S. Boyd and A. Mutapcic, *Subgradient Methods*, 2008.

[129] Y. Nesterov, "A method for solving a convex programming problem with convergence rate o (1/k2)," in *Soviet Mathematics. Doklady*, vol. 27, 1983, pp. 367–372.

[130] A. Falsone, K. Margellos, and M. Prandini, "A Distributed Iterative Algorithm for Multi-Agent MILPs: Finite-Time Feasibility and Performance Characterization," *IEEE Control Systems Letters*, vol. 2, no. 4, pp. 563–568, 2018, ISSN: 24751456. DOI: 10.1109/LCSYS.2018.2844353.

[131] J. Nocedal and S. J. Wright, "Numerical optimization," *Springer Series in Operations Research and Financial Engineering*, Springer Series in Operations Research and Financial Engineering, pp. 1–664, 2006, ISSN: 21971773. DOI: 10.1201/b19115-11. [Online]. Available: http://link.springer.com/10.1007/978-0-387-40065-5.

[132] C. A. Floudas, “Nonlinear and mixed-integer optimization : fundamentals and applications,” p. 462, 1995.

Appendix A

Preliminaries in Mathematical Optimisation

Expressed simply, mathematical optimisation is the minimisation or maximisation of some objective function $f(\boldsymbol{x})$, where $\boldsymbol{x}$ is a set of undetermined decision variables. Constrained optimisation, which is the subject of this discussion, also involves restricting the values of decision variables by adding equality and inequality constraints. In general form, a constrained optimisation problem can be written as [131]:

$$\begin{aligned} \boldsymbol{x}^* = \quad & \arg\min_{\boldsymbol{x}} f(\boldsymbol{x}) \\ \text{subject to} \quad & c_i(\boldsymbol{x}) = 0, \quad \forall i \in \mathcal{E} \\ & c_i(\boldsymbol{x}) \leq 0, \quad \forall i \in \mathcal{I} \end{aligned} \tag{A.1}$$

where $\mathcal{E}$ and $\mathcal{I}$ are the index sets of the equality and inequality constraints, respectively. For maximisation problems, the objective function can simply be replaced with $-f(\boldsymbol{x})$.

The optimal solution of (A.1) is the vector of decision variable values, denoted $\boldsymbol{x}^*$, for which the value of $f(\boldsymbol{x})$ is minimised. The equality and inequality constraint sets restrict the search for $\boldsymbol{x}^*$ to a *feasible region* of interest, such that candidate solutions are either optimal and feasible or sub-optimal and feasible. This is illustrated with

the following example:

$$\begin{aligned} \min_{x_1,x_2} \quad & f(x) = x_1 + x_2 \\ \text{subject to} \quad & -2x_1 + x_2 \leq 0 \\ & 1.5 \leq x_1 \leq 5 \\ & 2 \leq x_2 \leq 10 \end{aligned} \tag{A.2}$$

Since there are only two decision variables in this problem, x_1 and x_2, it can be solved graphically by plotting all the inequality constraints and objective function contours, as in Fig. A.1. Given that the objective is to minimise the sum of x_1 and x_2, it can be seen intuitively that the optimal solution is $x_1^* = 1.5$ and $x_2^* = 3$, for which the objective function value is $f(x^*) = 4.5$.

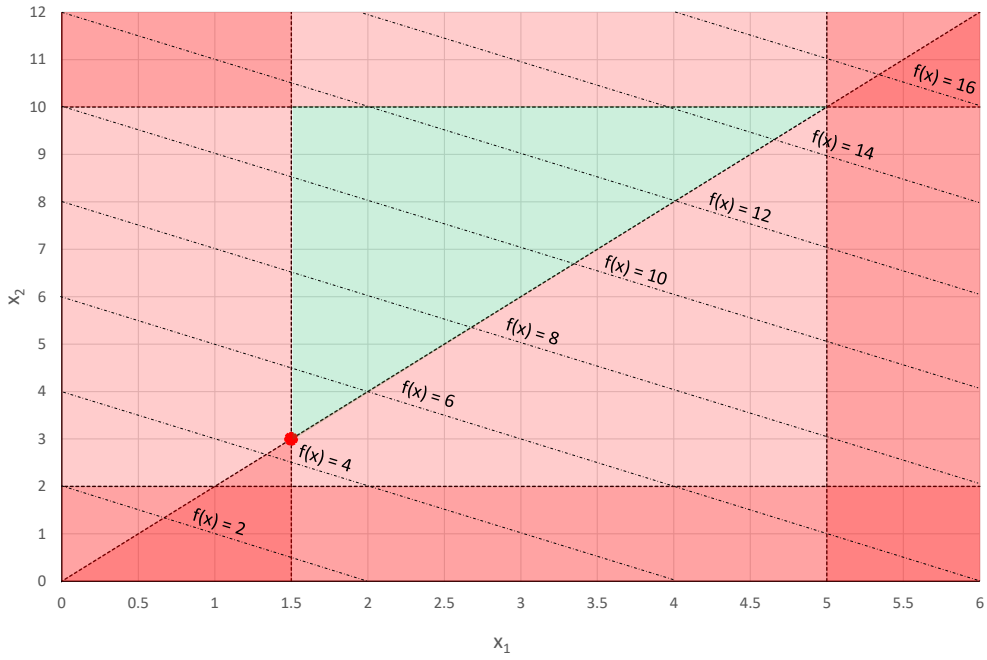

Figure A.1: Graphical illustration of the simple optimisation problem in (A.1). The green shaded area is the feasible region, the red shaded area is the infeasible region and the red circle indicates the optimal point.

This is an example of a linear programming (LP) problem, since the objective function and all constraints are linear. All LP problems are *convex*, meaning that for any two feasible points, a straight line segment between these points must reside wholly within the feasible region [125]. Quadratic programming (QP) problems, involving a quadratic objective function and linear or quadratic inequalities, are also convex if

this property holds. Non-linear programming (NLP) problems, involving non-linear equalities or higher-order inequalities, are often not convex. The importance of convexity is associated with the ease in which a problem can be solved using numerical methods. If a problem can be formulated as a convex optimisation, the unique global optimum can be found very quickly using computationally efficient algorithms, such as the simplex method or interior point methods [131]. However, if a problem is non-linear and non-convex, then there are no effective methods to solve it without compromising efficiency or optimality [125].

Another class of non-convex problems is that of mixed-integer programming (MIP) problems, for which some of the decision variables are restricted to discrete integer values:

$$\begin{aligned} \min_{\boldsymbol{x},\boldsymbol{y}} \quad & f(\boldsymbol{x},\boldsymbol{y}) \\ \text{subject to} \quad & c_i(\boldsymbol{x},\boldsymbol{y}) = 0, \quad \forall i \in \mathcal{E} \\ & c_i(\boldsymbol{x},\boldsymbol{y}) \leq 0, \quad \forall i \in \mathcal{I} \\ & \boldsymbol{x} \in \mathbb{R},\ \boldsymbol{y} \in \mathbb{Z} \end{aligned} \tag{A.3}$$

Even for the simplest sub-class of MIP problems, i.e. mixed-integer LP (MILP) problems with $\boldsymbol{y} \in \{0,1\}$, finding an optimal solution can be very difficult and such problems are known to have computational complexity that is NP-Hard. A brute-force approach to solving such an MILP problem would be to enumerate all possible combinations of 0 or 1 for each decision variable in $\boldsymbol{y}$ and solve a separate convex LP problem for each combination. The complexity of this approach grows exponentially with the number of binary variables, such that to solve a problem with n_y binary variables would result in the requirement to solve 2^{n_y} LP problems [132]. Fortunately, there are MIP solvers available, e.g. [110], [120], which offer heuristic approaches to drastically reduce the computation time for many MILP problems, e.g. using a branch-and-bound algorithm with cutting planes to reduce the search space. However, even with computationally efficient MIP solvers, the combinatorial explosion that occurs as n_y increases can still cause particularly large MILP problems to be intractable. On the other hand, in comparison to similarly sized non-convex NLP problems, especially those with integrality constraints, i.e. mixed-integer NLP (MINLP) problems, MILP problems can still be solved much more efficiently.

Appendix B

Connection Coefficients

Connections between component modules' sink and source ports, as outlined in Section 3.2, are modelled as constraints which define the flow of energy between connected ports:

$$y_{k,\text{snk}_j} = \gamma_{ij} \cdot y_{k,\text{src}_i} \tag{B.1}$$

Since it may be necessary to model linear losses, convert units or consider different physical flows of interest when moving between different modules, the connection coefficient γ_{ij} can take various forms. Some examples encountered in this thesis are given below.

Table B.1: Connection Coefficient Examples

Description	Source Type	Sink Type	γ_{ij} Value	Units
Linear loss	Real Power (kW)	Real Power (kW)	< 1	-
Scaling	Mass Flow (kg/s)	Mass Flow (100 kg/s)	$\frac{1}{100}$	-
Unit conversion	Real Power (kW)	Real Power (p.u.)	$\frac{1}{S_{base}}$	$\frac{p.u.}{kW}$
Quantity conversion	Heat (kW)	Mass Flow (kg/s)	$\frac{1}{C_p \Delta T}$	$\frac{kg \cdot K}{kJ \cdot K}$

Appendix C

Logical Constraints

As shown in [25], [31], it is possible to cast logical statements as a system of mixed-integer linear constraints. This methodology is utilised in several models that are presented in the main thesis but presenting these logical constraints each time can both negatively impact model readability and involve much repetition. Instead the mixed-integer linear constraints representing various logical statements are explained here in general form and only specific logical statements are presented in the main thesis chapters.

C.1 Logical Indicators

Binary indicator variables, δ, are used extensively in this thesis and in the literature [25], [26], [30], since they can be used to define if...then type conditions based on the value of a given variable or function, $f(k)$. Here a binary indicator is defined to indicate whether a given function is positive:

$$f(k) \geq 0 \iff \delta = 1$$

$$\text{is true if and only if } \begin{cases} -m\delta & \leq f(k) - m \\ -(M+\varepsilon)\delta & \leq -f(k) - \varepsilon \end{cases} \tag{C.1}$$

where $f(k)$ is upper and lower bounded by M and m, respectively, and ε is a small tolerance (typically the machine precision) needed to transform a constraint of the form $y > 0$ into $y \geq 0$, since MILP solvers can only handle nonstrict inequalities [25].

It can be shown that if, $\delta = 0$, the constraints in (C.1) are equivalent to $-m \leq f(k) \leq -\varepsilon$, whereas if $\delta = 1$, they are equivalent to $0 \leq f(k) \leq M$, thereby satisfying the logical statement.

C.2 Conditional Activation of Terms

If a given variable or function, $f(k)$, within a constraint or cost function, must only be considered under a certain condition indicated by δ, then it could simply be replaced by $\delta f(k)$ in the constraint. However, this introduces a non-linearity which should ideally be avoided to improve computational efficiency. Instead it is possible to 'hide' this product by defining an auxiliary variable, $y = \delta f(k)$, which may be expressed using mixed-integer linear inequalities. Having already defined δ using (C.1), it then follows that:

$$y = \delta f(k)$$

$$\text{is equivalent to } \begin{cases} y \geq m\delta \\ y \leq M\delta \\ y \geq f(k) - M(1-\delta) \\ y \leq f(k) - m(1-\delta) \end{cases} \tag{C.2}$$

In this case, when $\delta = 0$, the first two constraints are equivalent to $y = 0$ whilst the latter two satisfied trivially. When $\delta = 1$, the first two constraints are satisfied trivially whilst the latter two are equivalent to $y = f(k)$.

C.3 Sign Function

Where it is necessary to express a constraint $g(k) = \text{sign}(f(k))h(k)$, in which $\text{sign}(f(k))$ returns the sign of a given function $f(k)$ and $h(k)$ is a positively valued function, this constraint must be formulated as mixed-integer inequalities. Having first defined δ using (C.1), it then follows that:

$$f(k) \geq 0 \implies g(k) = h(k)$$

$$f(k) \leq 0 \implies g(k) = -h(k)$$

where $0 \leq h(k) \leq M$

$$\text{is equivalent to } \begin{cases} g(k) \geq h(k) - 2M(1-\delta) \\ g(k) \leq h(k) \\ g(k) \geq -h(k) \\ g(k) \leq -h(k) + 2M\delta \end{cases} \tag{C.3}$$

where $g(k)$ is a function upper and lower bounded by M and $-M$, respectively. Here, when $\delta = 0$, the first two constraints are satisfied trivially whilst the latter two are equivalent to $g(k) = -h(k)$. Similarly, when $\delta = 1$, the first two constraints are equivalent to $g(k) = h(k)$ whilst the latter two are satisfied trivially.

C.4 Absolute Value Cost Function Terms

The absolute value of a given function or variable, $f(k)$, can be replaced within a linear cost function by introducing an auxiliary variable, $y = |f(k)|$. Provided that a minimisation problem is being considered and the cost function is strictly increasing in y, it follows that:

$y = |f(k)|$

$$\text{is equivalent to } \begin{cases} y \geq f(k) \\ y \geq -f(k) \end{cases} \tag{C.4}$$

This simple reformulation ensures that y is equal to whichever is the greater of $f(k)$ or $-f(k)$.

Appendix D

Additional Flexible Demand Models

Constraints for flexible demand modules which are not used in the thesis are presented here for information. The following constraints, repeated from Chapter 3, are common to all flexible demand types:

$$y_{k,n} = \sum_{i=1}^{N_n^{ph}} u_{k,n,i}, \quad \forall k, n \tag{D.1}$$

$$\underline{u}_{k,n,i}\delta^p_{k,n,i} \leq u_{k,n,i} \leq \overline{u}_{k,n,i}\delta^p_{k,n,i}, \quad \forall k, n, i \tag{D.2}$$

$$\delta^p_{k,n,i} + \delta^c_{k,n,i} \leq 1, \quad \forall k, n, i \tag{D.3}$$

$$\delta^p_{k-1,n,i} - \delta^p_{k,n,i} \leq \delta^c_{k,n,i}, \quad \forall k, n, i \tag{D.4}$$

$$\delta^c_{k-1,n,i} \leq \delta^c_{k,n,i}, \quad \forall k, n, i \tag{D.5}$$

$$\delta^p_{k,n,i} \leq \delta^c_{k,n,i-1}, \quad \forall k, n, i \in \{2 : N_n^{ph}\} \tag{D.6}$$

D.1 Shiftable Demand Module

A shiftable demand must complete a number of phases within the cycle duration but does not have a fixed start time. The specific constraints for a shiftable demand are as follows:

$$\sum_{k=1}^{N_{\text{shift}}^{\text{rem}}} u_{k,\text{shift},i} = E_{\text{shift},i}, \quad \forall i \tag{D.7}$$

$$\sum_{k=1}^{H} \delta^p_{k,\text{shift},i} = 1, \quad \forall i \tag{D.8}$$

$$\delta^c_{k,\text{shift},i-1} = \delta^p_{k,\text{shift},i} + \delta^c_{k,\text{shift},i} \quad \forall k, n, i \in \{2 : N_{\text{shift}}^{ph}\} \tag{D.9}$$

$$\delta^{p}_{k,\text{shift},i} \leq T^{\text{pref}}_{k,\text{shift}}, \quad \forall i, k \tag{D.10}$$

where $N^{\text{rem}}_{\text{shift}}$ is the number of remaining periods within which all demand phases must be satisfied, H is the prediction horizon and $\boldsymbol{T}^{\text{pref}}_{\text{shift}}$ is a user-defined vector of time preferences, i.e. $T^{\text{pref}}_{k,\text{shift}} = 1$ if and only if a demand can be processed during period k. These constraints ensure that: the nominal amount of energy is delivered within the cycle time, preventing the demand start from being shifted indefinitely (D.7); each phase is only processed over one time period (D.8); each phase starts immediately after the preceding phase (D.9); and that phases can only be processed at times preferred by the user (D.10).

When this module is used as part of a receding horizon control scheme, the constants $E_{\text{shift},i}, N^{\text{rem}}_{\text{shift}}$ and $\boldsymbol{T}^{\text{pref}}_{\text{shift}}$ need to be updated between each call to the optimisation solver. A programmable logic controller (PLC) can fulfil this updating role, performing the following assignments at the end of each time period:

$$E_{\text{shift},i} = E_{\text{shift},i} - u_{k,\text{shift},i}, \quad \forall i \tag{D.11}$$

$$N^{\text{rem}}_{\text{shift}} = N^{\text{rem}}_{\text{shift}} - 1 \tag{D.12}$$

$$T^{\text{pref}}_{k} = T^{\text{pref}}_{k+1}, \quad \forall k \in \{1 : H-1\} \tag{D.13}$$

$$T^{\text{pref}}_{H} = 1 \tag{D.14}$$

The PLC would also reset all values to their defaults upon completion of the demand cycle.

D.2 Adjustable Demand Module

An adjustable demand is able to vary energy consumption above or below the nominal amount in each phase. The specific constraints for an adjustable demand are as follows:

$$u_{k,\text{adj},i} = z^{\text{base}}_{k,\text{adj},i} + z^{+}_{k,\text{adj},i} - z^{-}_{k,\text{adj},i}, \quad \forall i \tag{D.15}$$

$$\sum_{k=1}^{H} z^{\text{base}}_{k,\text{adj},i} = E_{\text{adj},i}, \quad \forall i \tag{D.16}$$

$$\underline{z}^{+}_{k,\text{adj},i}\delta^{+}_{k,\text{adj},i} \leq z^{+}_{k,\text{adj},i} \leq \overline{z}^{+}_{k,\text{adj},i}\delta^{+}_{k,\text{adj},i}, \quad \forall k, i \tag{D.17}$$

$$\underline{z}^{-}_{k,\text{adj},i}\delta^{-}_{k,\text{adj},i} \leq z^{-}_{k,\text{adj},i} \leq \overline{z}^{-}_{k,\text{adj},i}\delta^{-}_{k,\text{adj},i}, \quad \forall k, i \tag{D.18}$$

$$\delta^{+}_{k,\text{adj},i} + \delta^{-}_{k,\text{adj},i} \leq 1, \quad \forall k, i \tag{D.19}$$

$$0 \leq z^{+}_{k,\text{adj},i} \leq \overline{z}^{+}_{k,\text{adj},i}\delta^{p}_{k,\text{adj},i}, \quad \forall k,i \tag{D.20}$$

$$0 \leq z^{-}_{k,\text{adj},i} \leq \overline{z}^{-}_{k,\text{adj},i}\delta^{p}_{k,\text{adj},i}, \quad \forall k,i \tag{D.21}$$

$$\sum_{k=1}^{H} \delta^{p}_{k,\text{adj},i} = 1, \quad \forall i \tag{D.22}$$

$$\delta^{p}_{k_c,\text{adj},1} = 1 \tag{D.23}$$

$$\delta^{c}_{k,\text{adj},i-1} = \delta^{p}_{k,\text{adj},i} + \delta^{c}_{k,\text{adj},i} \quad \forall k,n,i \in \{2 : N^{ph}_{\text{adj}}\} \tag{D.24}$$

where $z^{\text{base}}_{k,\text{adj},i}$ is the baseline consumption, $z^{+}_{k,\text{adj},i}$ is a positive adjustment above the baseline consumption and $z^{-}_{k,\text{adj},i}$ is a negative adjustment below the baseline energy consumption. These constraints ensure that: the nominal energy consumption of each demand phase can be adjusted up or down within defined limits (D.15)-(D.19); adjustments are positive only when a given phase is processing (D.20),(D.21); each phase is only processed over one time period (D.22); the demand commences at a given time period k_c (D.23); and each phase starts immediately after the preceding phase (D.24).

Only the nominal energy consumption, $E_{\text{adj},i}$, must be repeatedly updated in a receding horizon control scheme, therefore a PLC can simply iterate through the nominal energy consumption profile at the end of each time period.

D.3 Interruptible Demand Module

An interruptible demand can have interruptions between each phase, the length of which are limited within a given range. The specific constraints for an interruptible demand are as follows:

$$\sum_{k=1}^{H} u_{k,\text{int},i} = E_{\text{int},i}, \quad \forall i \tag{D.25}$$

$$\sum_{k=1}^{H} \delta^{p}_{k,\text{int},i} = 1, \quad \forall i \tag{D.26}$$

$$\underline{N}^{w}_{\text{int},i} \leq \sum_{k=1}^{H} \delta^{w}_{k,\text{int},i} \leq \overline{N}^{w}_{\text{int},i} \tag{D.27}$$

$$\delta^{w}_{k,\text{int},i} = \delta^{c}_{k,\text{int},i-1} - (\delta^{p}_{k,\text{int},i} + \delta^{c}_{k,\text{int},i}) \quad \forall k,n,i \in \{2 : N^{ph}_{\text{int}}\} \tag{D.28}$$

$$\delta^{p}_{k,\text{int},i} \leq T^{\text{pref}}_{k,\text{int}}, \quad \forall i,k \tag{D.29}$$

$$\delta^{p}_{k_c,\text{adj},1} = 1 \tag{D.30}$$

where $\underline{N}^{w}_{\text{int},i}$ and $\overline{N}^{w}_{\text{int},i}$ are the minimum and maximum number of periods for which a phase can wait after the preceding phase has been completed. These constraints ensure that: the nominal amount of energy is consumed in each phase within the prediction horizon (D.25); each phase is only processed over one time period (D.26); the waiting period before any given phase must be completed within a given range of time periods (D.27),(D.28); phases can only be processed at times preferred by the user (D.29); and the demand commences at a given time period k_c (D.30).

In a receding horizon control scheme, the constants $E_{\text{int},i}, \underline{N}^{p}_{\text{int},i}$ and $\overline{N}^{p}_{\text{int},i}$ need to be updated between each call to the optimisation solver. A PLC would perform the following assignments at the end of each time period:

$$E_{\text{int},i} = E_{\text{int},i} - u_{k,\text{int},i}, \quad \forall i \tag{D.31}$$

$$\underline{N}^{w}_{\text{int},i} = \begin{cases} \underline{N}^{w}_{\text{int},i}, & \text{if } \delta^{w}_{k,\text{int},i} = 0 \\ \underline{N}^{w}_{\text{int},i} - 1, & \text{if } \delta^{w}_{k,\text{int},i} = 1 \wedge \underline{N}^{w}_{\text{int},i} > 0 \\ 0, & \text{otherwise} \end{cases} \tag{D.32}$$

$$\overline{N}^{w}_{\text{int},i} = \begin{cases} \overline{N}^{w}_{\text{int},i}, & \text{if } \delta^{w}_{k,\text{int},i} = 0 \\ \overline{N}^{w}_{\text{int},i} - 1, & \text{if } \delta^{w}_{k,\text{int},i} = 1 \wedge \overline{N}^{w}_{\text{int},i} > 0 \\ 0, & \text{otherwise} \end{cases} \tag{D.33}$$

The PLC would also reset all values to their defaults upon completion of the demand cycle.